THE UNIVERSITY OF CHICAGO

# CHEMICAL PROBES FOR CONTROLLING BACTERIAL TRANSCRIPTION, INDUCING MITOCHONDRIAL PERMEABILIZATION, AND STUDYING CELLULAR OXIDATION STATE

A DISSERTATION SUBMITTED TO

THE FACULTY OF THE DIVISION OF THE PHYSICAL SCIENCES

IN CADIDACY FOR THE DEGREE OF

DOCTOR OF PHILOSOPHY

DEPARTMENT OF CHEMISTRY

BY

ANTHONY M. MARTINEZ

CHICAGO, ILLINOIS

JUNE 2016

*I dedicate this to my grandmother, who even in times of hardship was there to support me, and my mother, who gave me a reason to pursue science.*

## TABLE OF CONTENTS

## LIST OF TABLES

## LIST OF FIGURES

## LIST OF SCHEMES

# CHAPTER I

# DEVELOPMENT OF STREPTOLYDIGIN ANALOGS FOR THE TREATMENT OF CLOSTRIDIUM DIFFICILE INFECTION

*This chapter describes our efforts toward the synthesis and biological characterization of a group of rationally designed streptolydigin analogs, which elucidated the structure-activity relationships of streptolydigin and inhibited growth of Clostridium difficile. The discussion begins with an overview of bacterial RNA polymerase and challenges in its use as a target of antibiotics. The chapter continues with an overview of C. difficile, discussing both its relevance and current therapies aimed at combating C. difficile infection. Next, this chapter reviews our laboratory's synthetic efforts toward streptolydigin's synthesis (a natural product with bacterial RNAP inhibitory activity), and the use of those methods to build a group of unique molecules, which displayed interesting antimicrobial activity. The chapter concludes with our efforts toward evaluating the analogs' biological and biochemical activities, and a brief discussion of their in vitro and in vivo evaluation.*

## I.1. Introduction

The development of novel antibiotic agents is a core challenge facing researchers today. Currently, the majority of frontline therapeutics hails from the heyday of antibiotic discovery, between 1940 and 1960.[1] Nearly all antibiotics used today were either discovered during this period, or are closely related analogs. In the face of constant bacterial evolution, the rise of antibiotic resistance is demanding urgent intervention. However, the low probability of identifying new leads against a background of known compounds has forced antibiotic developers to seek alternative methods for identifying ways to battle infectious disease. While new platforms for antibiotic discovery are being investigated, researchers have turned their eyes back to previously made antibiotics, in the hopes of making these agents more effective, or to re-develop them using today's standards.[2] One such class of molecules are tetramic acid-based bacterial RNA polymerase inhibitors, which our group has studied extensively.

Tetramic acid (i.e. pyrrolidine-2,4-dione) containing natural products have been shown to display wide ranging biological activity. Compounded by their synthetic complexity, a resurgence of interest in these natural products has led to a steady increase in reports focused on their synthesis and bioactivities.[3,4] Recent synthetic developments in the Kozmin laboratory have provided access to streptolydigin (**1,** Figure I.1), a complex, tetramic acid containing, natural product with significant antimicrobial activity.[5] Streptolydigin's activity arises from its ability to lock bacterial RNA polymerase in an inactive conformer, shutting down transcription, and leading to bacterial cell death. These efforts have enabled the synthesis and biological

characterization of a variety of unique analogs; to both characterize the structural connections between the natural product and its bioactivity, as well as to develop novel antibacterial agents.

### *I.1.1. RNA Polymerases - Effective Targets for Treating Bacterial Infections*

RNA Polymerases (RNAP), are essential enzymes that are responsible for transcription, or the production of RNA from a DNA or RNA template.[6] Bacterial RNAP represents an attractive target for treating bacterial infections, due to its inactivation leading to a bacterial cell death. Also, despite having many structural and functional similarities, eukaryotic RNAP shares little sequence homology with the bacterial forms, reducing the side effects of treatment with bacterial RNAP modulators.[7] Rifamycin antibiotics, which are well characterized bacterial RNAP inhibitors, display broad-spectrum antibacterial activity, but have little to no effect in eukaryotes.

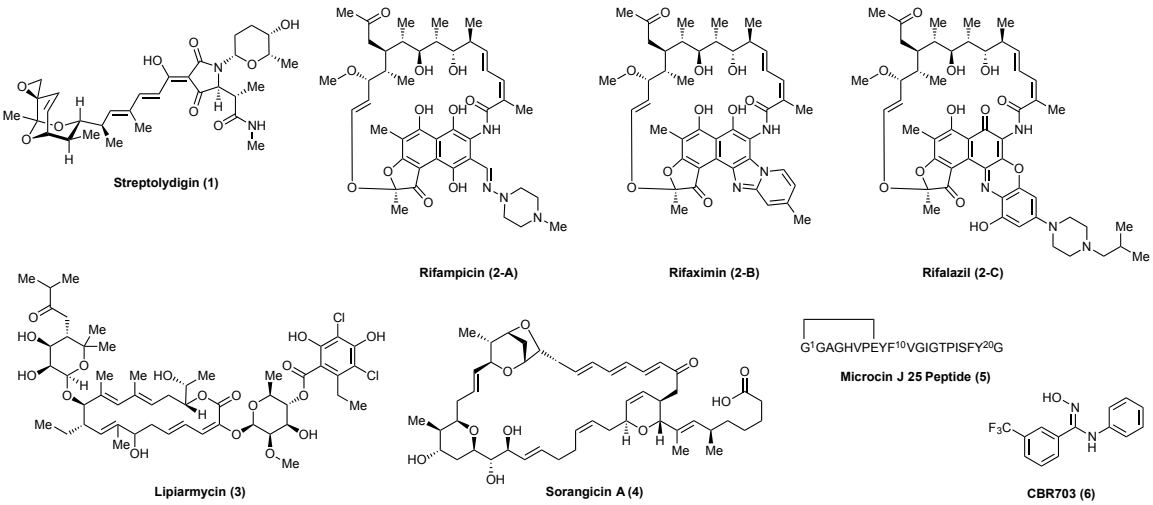


**Figure I.1:** Bacterial RNA polymerase inhibitors

Prokaryotic RNAP is comprised of three major subunits: **α2**, **β**, and **β'**, as well as a **σ**-factor, that is required for specific recognition of the promoter site and initiation of transcription.[6] The relationship between these subunits plays an enormous role in fine tuning gene expression, especially in organisms with complex genomes.[8] **β** and **β'** are composed of conserved and dispensable regions, and form an internal DNA channel approximately 10-12 angstroms wide. The RNAP active center is located on the back wall of this channel. These subunits are often the target of transcription effectors, including ansamycins (**2** A-C), lipiarmycin (**3**), sorangicin A (**4**), microcins (**5**), and the CBR703 series (**6**) (Figure I.1), with many having overlapping binding sites.

One of the largest challenges in the development of bacterial RNAP inhibitors is the rapid onset of resistance.[9] Although several classes of bacterial RNAP inhibitors act via unique mechanisms (e.g. lipiarmycin specifically blocks initiation, and is the only compound whose activity is modulated by the **σ**-factor), their overlapping binding sites are cause for concern. Resistance is often conveyed by facile substitutions of the amino acid residues at the rifamycin-binding site, limiting many of the aforementioned molecules to use in combination therapy or clinical emergencies. Spontaneous mutations in the *rpoB* and *rpoC* genes, which code for the **β** and **β'** subunits, respectively, are quite common and can lead to the onset of resistance. In fact, 95% of all organisms identified as resistant to anti-tuberculosis drugs, have been shown to exhibit the same mechanism of rifamycin-resistance, or mutation in the *rpoB* or *rpoC* genes.[6] Therefore, there is great need for the development of novel antibacterial agents, which target bacterial RNAP by alternative mechanisms, or bind to RNAP at alternative sites.

### *I.1.2. Isolation and Biological Evaluation of Streptolydigin*

Streptolydigin (**1**), also known as portamycin, was isolated from the culture broth of *Streptomyces lydicus* in 1956 by the Upjohn Company,[10] and was shown to display broad spectrum antibiotic activity.[11,12] The strength of streptolydigin's effect varied between different bacterial strains, with significantly pronounced inhibitory activity against *Clostridium*, *Mycobacterium,* and *Streptococcus* species (MIC values 0.04 - 1.56, 6.25 - 25, and 0.19 - 12.5 μg/mL, respectively). Streptolydigin (**1**) displayed significant potency in assays against the clinically relevant, pathogenic *Clostridia* strains *C. novyi* and *C. botulinum,* with MIC values of 0.04 and 3.1 μg/mL, respectively, and was also shown to be essentially inactive against most fungal strains tested, with MIC values significantly higher than those determined for bacteria (>1000 μg/mL). Streptolydigin (**1**) exhibited low toxicity to mammals with maximum tolerated doses reaching 1800 mg/kg/day of free acid in mice, when administered orally, and a maximum tolerated dose of 500 mg/kg/day when administered subcutaneously.[12]

Streptolydigin (**1**) inhibits initiation, elongation, and pyrophosphorolysis by bacterial RNAP[13], but does not affect eukaryotic RNAP-I, RNAP-II, or RNAP-III. As mentioned previously, the lack of activity in eukaryotes is due to the lack of sequence homology between bacterial and eukaryotic RNAPs. In addition to its broad-spectrum antibiotic activity and the lack of cross reactivity between eukaryotic and bacterial RNAPs, streptolydigin (**1**) also shows a different structural mechanism than other inhibitors of transcription. Streptolydigin (**1**) binds to a site adjacent to, but not overlapping, the RNAP active center, stabilizing an RNAP-active-center conformational state with a straight-bridge-helix, effectively locking the RNAP in an inactive conformer.

Therefore, streptolydigin (**1**) exhibits only limited cross resistance with rifamycins, and little to no cross-resistance with other characterized inhibitors of bacterial RNAP.[14] Due to initial reports of streptolydigin's activity against *Clostridia* strains, as well as its unique mechanism of RNAP inhibition, this class of antibiotics is ideally suited for development for the treatment of *Clostridium difficile*.

### *I.1.3. Clostridium Difficile – A Rapidly Rising Clinical Problem*

*Clostridium difficile* is an anaerobic, gram-positive, spore-forming, toxin-producing bacillus that is transmitted between humans via the fecal-oral route, and can only successfully colonize the human gut if the normal microbiota is disturbed or absent.[15] Therefore, colonization of the human gut is intimately connected to antimicrobial therapy, and is particularly relevant following administration of an antimicrobial regime during hospitalization. *Clostridium difficile* infections (CDIs) are particularly challenging to treat, as the design and analysis of interventions are complicated by the location of initial infection. Infectious outcomes of hospitalized patients are statistically non-independent, as they share health care providers, a common environment, and a host of other factors.[16]

CDIs have become a significantly larger problem in recent history. In 2011, 453,000 cases of CDI were reported, with approximately 29,000 deaths caused due to infection.[17] In addition to the toll on human health, nosocomial *C. difficile* infections result in a larger than four-fold increase in the cost of hospitalizations,[16] and increase annual health expenditures by approximately $1.5 billion in the United States.[18]

The rise in frequency and severity of CDIs has largely been attributed to the emergence of a "hypervirulent" strain, the North American pulsed-field gel electrophoresis type 1 (NAP1) strain.[19] This rise has also been compounded by the general aging of the population, as well as the ubiquitous overuse of antibiotics.[20] Successful colonization of the human gut results in colonocyte death, loss of intestinal barrier function, and neutrophillic colitis, and is the result of toxin-inactivation of the Rho family of guanosine triphosphatases.[17] Most CDIs respond to initial treatment and symptoms are resolved within three to five days.[21] However, CDIs that do not respond to initial treatments, or recurrent CDIs, are of the greatest concern, and result in sharp increases in mortality rates. Treatment of the first recurrent CDI is only successful in 50% of patients,[22] and subsequent infections are even more challenging to cure, often leading to the necessity of fecal microbial transplantations.[23]

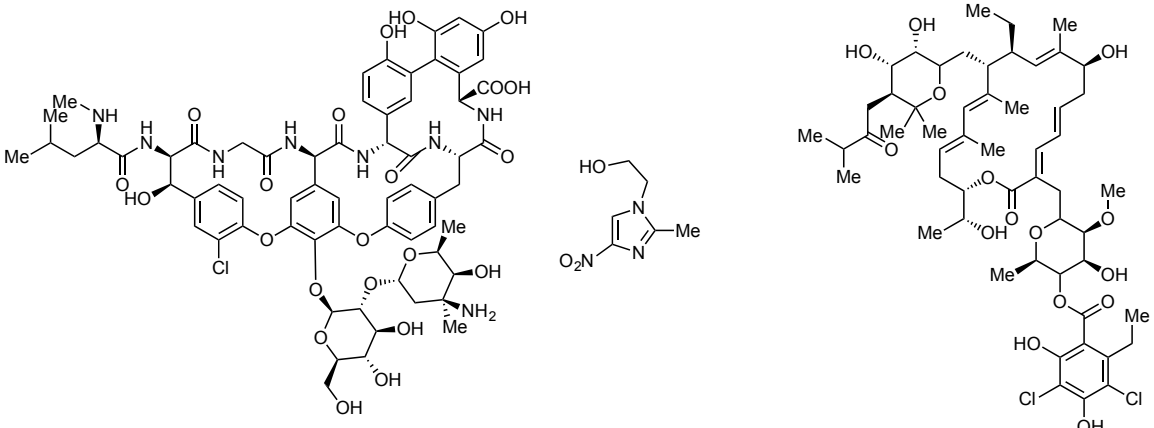


**Figure I.2**: Current CDI treatments.

Current treatments for CDIs are quite limited (Figure I.2). Orally administered vancomycin (**7**) and metronidazole (**8**) have been mainstays of *C. difficile* treatment since

the 1970s,[17] but the rise of the NAP1 strain has led to a sharp increase in the total number of infections, as well as the rates of clinical failure.[24] The recent FDA approval of fidaxomicin (**9**) has provided an alternative method of treating CDIs and has been shown to decrease the rates of recurrence in most cases from 25% to 15%.[25] However, the increase in patient benefit is lost when infections are associated with NAP1, and the prohibitive cost of fidaxomicin limit its clinical utility (~$340/day).

Taken together, the recent rise in NAP1-caused CDIs, the increase in clinical failure using currently available frontline therapeutics, and the prohibitive cost of new therapies demand the development of novel *C. difficile*-active antibiotics, which target clinically validated targets by alternative mechanisms.

### I.2. Synthesis of Streptolydigin

Despite streptolydigin's attractive antibacterial profile, its complicated molecular architecture prevented its total synthesis for several decades, with researchers only succeeding at building fragments of the molecule. Streptolydigin's structure was originally determined by the Rinehart group,[26] showing that the molecule is comprised of an epoxide-containing bicyclic ketal connected by a polyene spacer to a glycosylated, highly functionalized acyl tetramic acid.[27]

Although several total syntheses of tirandamycin A[28] (**27**) have been developed and the preparation of two advanced fragments of streptolydigin (**1**) have been described,[29] establishment of practical synthetic approaches to streptolydigin (**1**) remained challenging, in part, due to the presence of a highly labile alkenyl epoxide fragment, which is absent in tirandamycin A (**27**).

Nevertheless, our laboratory successfully overcame the challenges in STL's synthesis, building the highly decorated molecule in a longest linear sequence of 24 steps from commercially available precursors (Schemes I.1 and I.4).[5]

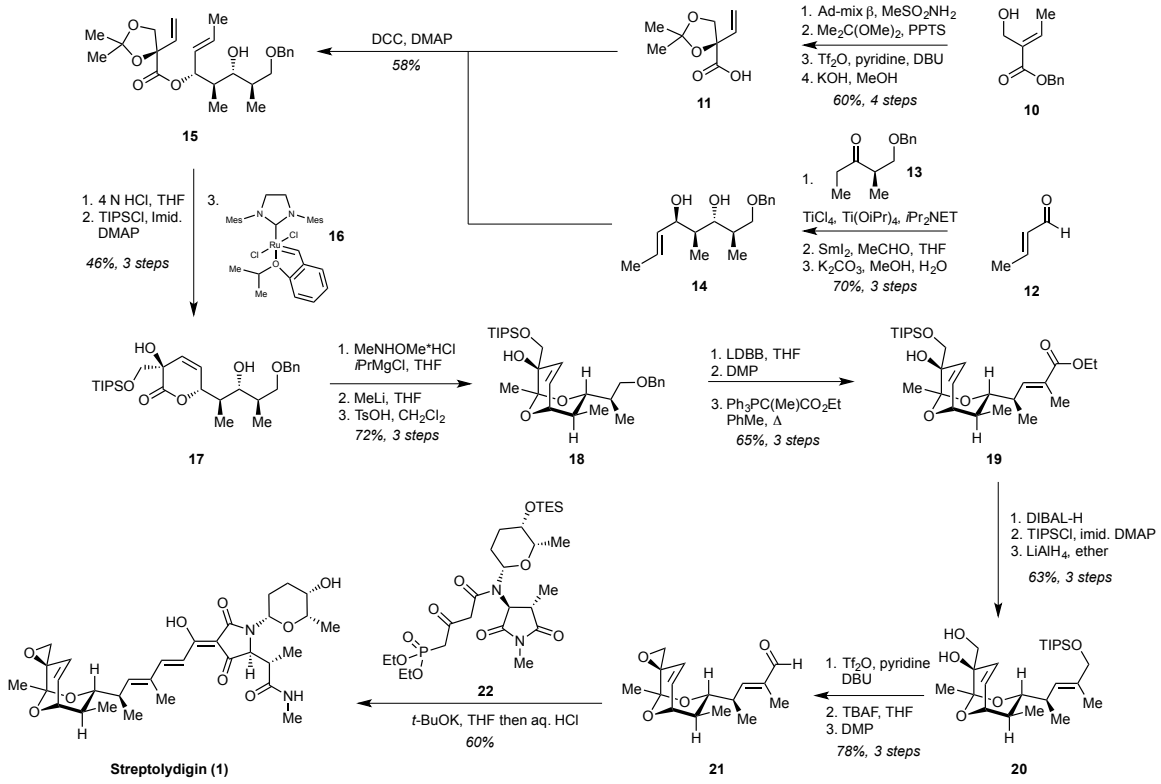


**Scheme I.1:** Synthesis of Streptolydigin (**1**) by Sergey Pronin

Full synthetic access to streptolydigin (**1**) opened the possibility of developing a better understanding of the structure-activity relationship (SAR) of the molecule, an area of its evaluation that has been previously impossible. A better understanding of streptolydigin's SAR would also enable the rational design, and development, of other potential RNAP inhibitors that do not show cross-resistance with currently used

therapeutics, as well as enabling the use of its favorable physicochemical properties for the development of novel antibiotics.

### *I.2.1. Structural Considerations for Streptolydigin's Activity*

In an effort to develop analogs of streptolydigin (**1**), we first considered structural and biochemical data regarding its mechanism of binding to bacterial RNAP. The streptolydigin (**1**) binding site is formed on the downstream DNA side of the bridge-helix, and comprises residues from both the **β** and **β'** subunits.[30] The binding site can be split into two separate sub-sites, which include strong hydrophobic interactions with streptolydigin's streptolol moiety, and accommodations for the bulky tetramic. Interestingly, only a few contacts between RNAP and the tetramic acid occur, and the rhodinose makes no contacts with the protein, at all. Additionally, the hydrogen bond formed between **β'-**Asn792 and the N2' atom of the acetamide moiety appears critical for binding of the tetramic acid fragment, and in fact, RNAP is less sensitive to tirandamycin A (**27**), which lacks the acetamide moiety. Moreover, the N792G substitution conveyed strong resistance to streptolydigin (**1**). Overall, the structure suggested that the streptolol group largely determined STL's affinity for bacterial RNAP, with little contribution from the tetramic acid due to the lack of highly specific binding sites on the protein's surface.[30]

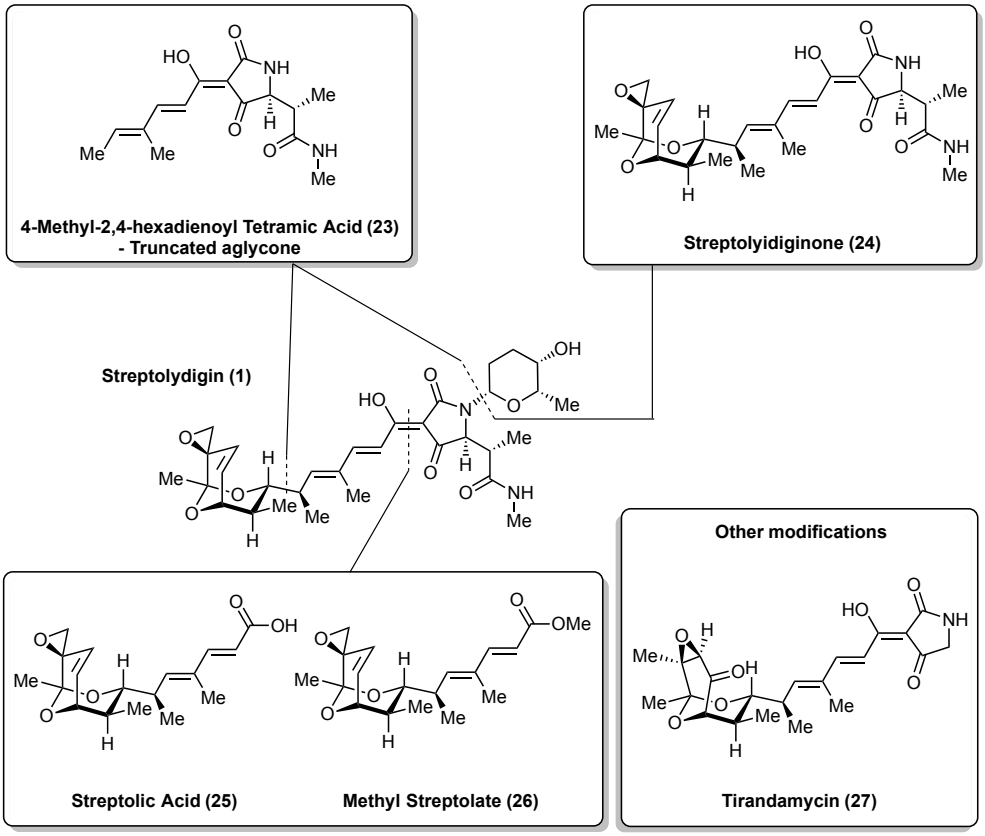


**Figure I.3:** Streptolydigin fragments for evaluation of SAR

### *I.2.2. Structure Activity Relationships (SAR) for Streptolydigin*

To evaluate the SAR of streptolydigin (**1**), we aimed to investigate the effects of removing large fragments (Figure I.3). These major fragments included the bicyclic ketal fragment (truncated aglycone, **23**), the rhodinose fragment (streptolydiginone, **24**), and the entire tetramic acid fragment (streptolic acid, **25** and methyl streptolate, **26**). Biochemical evaluation of streptolydigin (**1**), and its related analogs, was performed in collaboration with the Severinov group at Rutgers University. To evaluate the effects of the removal of major structural features mentioned above, we examined each analogs' ability to inhibit *Thermus aquaticus* RNAP[31] *in vitro* transcription in the presence of 50

μM of nucleotide triphosphates (NTPs) and two concentrations of analog (25 μM and 250 μM in Figure I.4-A and Figure I.4-B, respectively).

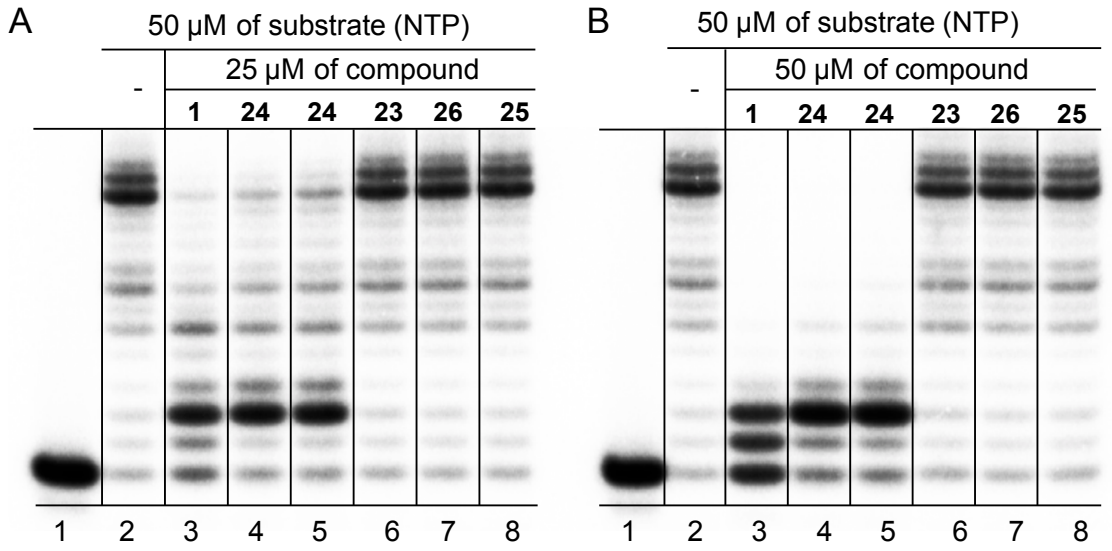


**Figure I.4:** *T. acquaticus* RNAP inhibition by streptolydigin and truncated analogs. A. RNAP inhibition in the presence of 25 μM of each compound. B. RNAP inhibition in the presence of 50 μM of each compound.

Our initial biochemical evaluation showed that truncating the entire streptolol moiety (**23**), or the tetramic acid moiety (**25** and **26**), resulted in complete loss of RNAP inhibitory activity (Figure I.4). Loss of the rhodinose fragment in streptolydiginone (**24**) slightly decreased the RNAP inhibition observed, for both the free acid (lane 4) and the corresponding sodium salt (lane 5), but the vast majority of transcription was still halted after incorporation of the third nucleotide, similar to streptolydigin (**1**). Nevertheless, we believed that modifications of the streptolol subunit could be tolerated, given the tetramic acid fragment remain unchanged.

## I.3. Rational Design of Streptolydigin Analogs

Removal of the C(10)-C(11) alkene in streptolydigin (**1**) was envisioned to significantly increase the synthetic efficiency of the molecule's assembly (Scheme I.2-A). Additionally, we believed replacement of the entire bicyclic ketal moiety by an adamantyl group would preserve the overall shape and physicochemical properties of the original subunit. As mentioned previously, strong hydrophobic interactions between the streptolol moiety and the **β** subunit are believed to dictate binding for that piece of the molecule. Therefore, the adamantyl group was an ideal replacement. Each new molecule would be derived from condensation of four building blocks, following our previously established synthetic methods.

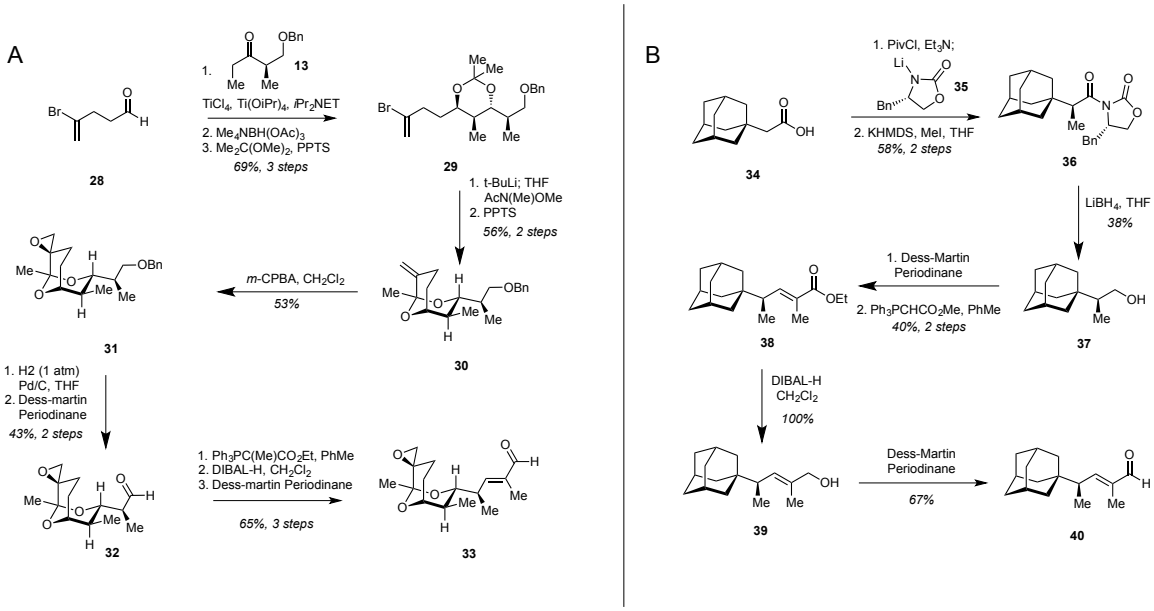


**Scheme I.2 –** Principle fragment synthesis of A. 10,11-Dihydrostreptolydigin (**48**) and B. the adamantyl-containing analog (**47**)

### *I.3.1. Synthesis of 10,11-dihydrostreptolydigin – Fragment A*

Synthesis of 10,11-dihydrostreptolydigin (**48**) began with a Ti-mediated aldol reaction between ketone **13** and aldehyde **28**, followed by an anti-reduction of the corresponding hydroxyketone. The reaction produced a diol, which was protected as acetonide **29** (Scheme I.3-A). Bromine-lithium exchange, followed by acylation gave the expected enone, which was treated with PPTS in methanol to produce bicyclic ketal **29**. Concave-face epoxidation of alkene **30** gave access to epoxide **31**. Hydrogenolysis of **31**, followed by Dess-Martin oxidation of the resulting alcohol, afforded aldehyde **32**. Subjection of **32** to a Wittig olefination furnished an unsaturated ester, which was reduced with DIBAL-H, and oxidized with Dess-Martin periodinane to deliver aldehyde **33**.

### *I.3.2. Synthesis of the Adamantyl-containing Analog – Fragment A*

The synthesis of the adamantyl-containing analog (**47**) began with the asymmetric Evans alkylation[32] of the chiral imide derived from the commercially available carboxylic acid **34** (Scheme I.3-B). Additional elaboration included reduction of imide **36** with $LiBH_4$, followed by Dess-Martin oxidation of alcohol **37**, and Wittig olefination of the resulting aldehyde to give unsaturated ester **38**. Reduction of **38** with DIBAL-H, followed by Dess-Martin oxidation of the allylic alcohol afforded aldehyde **40**.

### *I.3.3. Synthesis of Other Principle Fragments and Final Coupling*

Conversion of acid **41** to the corresponding N-acyl oxazolidinone, followed by diastereoselective azide transfer, produced imide **42**, which was treated with methylamine

and hydrogenated in the presence of $Boc_2O$ to produce alcohol **43** (Scheme I.3). TEMPO-mediated cyclization and Boc-deprotection afforded amine **44**.

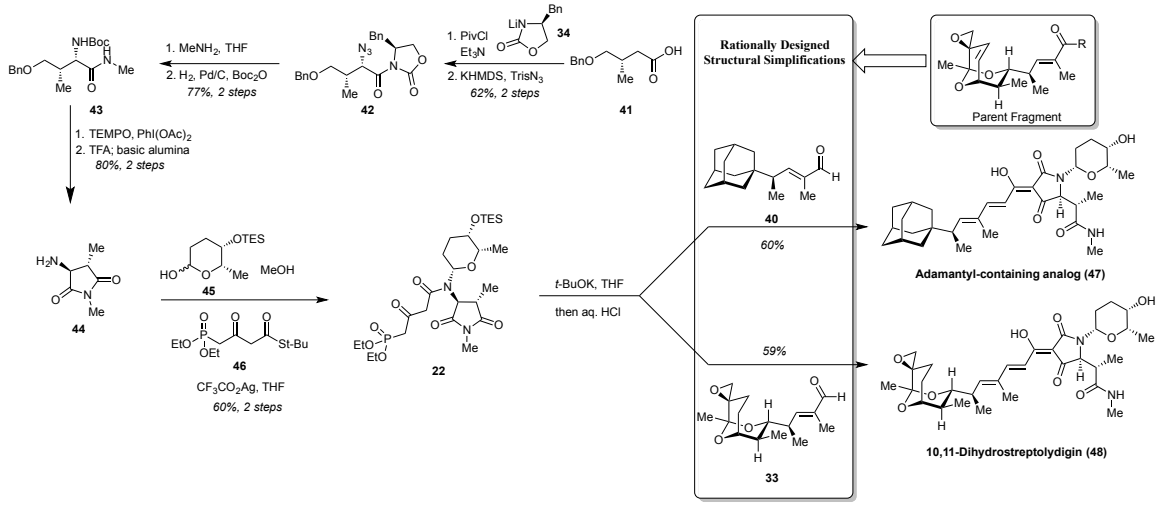


**Scheme I.3**: Synthesis of other principle fragments and final coupling of rationally designed analogs

Diastereoselective N-glycosylation of imide **44** with rhodinose **45**, followed by Ag-promoted acylation of thioate **46** resulted in phosphonate **22**. Following our previously established protocol, **22** was treated with t-BuOK, followed by addition of aldehyde **40** or **33.** Mild acidic workup directly produced the adamantyl-containing streptolydigin analog (**47**) and 10,11-dihydrostreptolydigin (**48**). Removal of the C(10)-C(11) alkene moiety greatly improved the synthetic efficiency of 10,11-dihydrostreptolydigin (15-step longest linear sequence) compared to the original approach to streptolydigin (**1**), as did replacement of the bicyclic ketal with an adamantyl core (8-step longest linear sequence).

## I.4. Biochemical and Antibacterial Evaluation of Streptolydigin Analogs

### *I.4.1. Effects of Rationally Designed Streptolydigin Analogs on Bacterial Transcription*

With each new molecule in hand, we turned to evaluate the relative efficacy of *T. aquaticus* RNAP inhibition (Figure I.5). 10,11-dihydrostreptolydigin (**48**) displayed potent inhibition of RNAP elongation, blocking incorporation of additional nucleotides past the third NTP at both 0.1 mM and 1.0 mM. The adamantyl-containing analog (**47**), however, displayed no inhibition of *T. aquaticus* RNAP, *in vitro*.

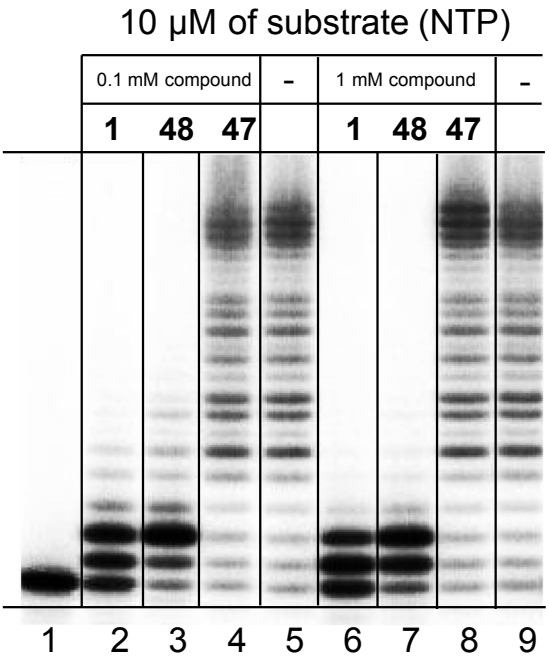


**Figure I.5 -** *T. aquaticus in vitro* RNAP inhibition by rationally designed streptolydigin analogs

Next, we proceeded to broadly evaluate our rationally designed analogs alongside streptolydigin (**1**) in order to elucidate a connection between the observed RNAP inhibitory behavior and the antimicrobial action of each molecule.

### *I.4.2. Effects of Streptolydigin and Associated Analogs on Bacterial Cell Growth*

#### *I.4.2.1. Effect of Analogs on S. salivarius*

Originally, streptolydigin (**1**) was found to be effective in inhibiting several Streptococcus species, including *S. agalactae*, *S. faecalis, S. hemolyticus, S. lactis, S. mitis, and S. viridans* with MICs in the range of 0.19-3.12 μg/mL.[11,12] Therefore, we selected *S. salivarius*, a representative Streptococcus strain, which colonizes human oral and nasopharyngeal epithelia and only becomes harmful to the host if the immune status is altered or there is a loss of control of epithelial cell sensing and discriminatory systems.[33] The results of this study, which employed a standard disk-diffusion protocol, are shown in Figure I.6. Streptolydigin (**1**) inhibited growth of *S. salivarius* in dose-dependent manner at concentrations of 5 μg, 10 μg and 20 μg per disk (Figure I.6-A). Streptolydiginone (**24**) was also found to induce potent growth inhibition, but the observed zones of inhibition were highly dose dependent, and visibly less extreme than streptolydigin (**1**). Despite substantial growth inhibition observed at 40 μg of streptolydiginone (**24**) per disk, no effect on bacterial growth occurred at the lower dose of 10 μg per disk (Figure I.6-B). 10,11-dihydrostreptolydigin (**48**) elicited dose-dependent growth inhibition at concentrations of 20 μg and 40 μg per disk (Figure I.6-B), but no antibacterial activity was observed with **7** at 10 μg per disk (Figure I.6-B). As was the case with streptolydiginone (**24**), zones of inhibition were visibly smaller than streptolydigin's. The adamantyl-containing analog (**47**) and the truncated aglycone (**23**) elicited only weak effects on bacterial growth at 100 μg/disk (Figure I.6-A and I.6-C). Additionally, streptolic acid (**25**) and methyl streptolate (**26**) were found to be completely inactive at 100 μg/disk (Figure I.6-B and I.6-C).

The antibacterial activity of all of the streptolydigin analogs analyzed was in excellent agreement with each compound's ability to inhibit *T. aquaticus* RNAP. This study demonstrated again that the presence of both streptolic and tetramic subunits of streptolydigin are required for its antibiotic activity and established that RNAP inhibition of streptolydigin-based compounds was well correlated with their antibacterial profile in *S. salivarius*.

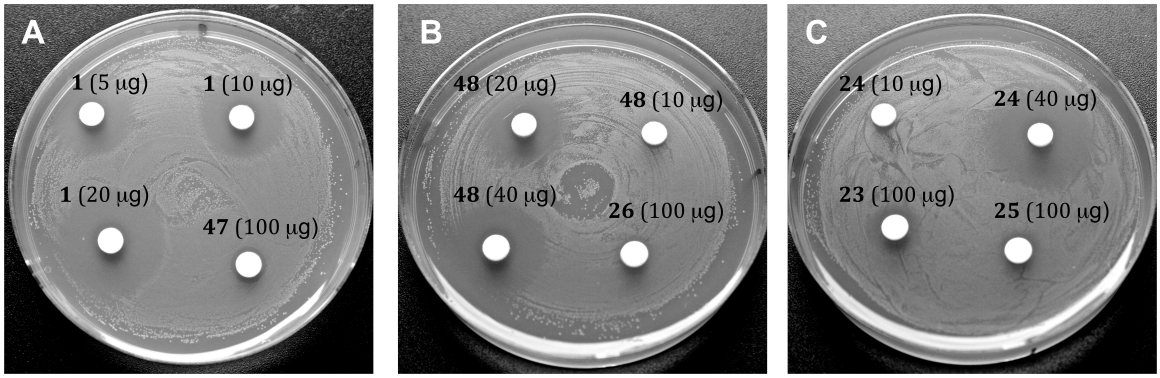


**Figure I.6 -** Disk diffusion assays to evaluate growth inhibition in *S. salivarius*

### *I.4.2.2. Evaluation of Antibacterial Activity Against C. Difficile*

While disk diffusion assays can provide a great deal of qualitative information regarding the antibacterial action of small molecules, we also aimed to quantify the biological activity of streptolydigin (**1**), and it's associated analogs. We believed this was especially relevant for the analogs, which displayed little activity in S. *salivarius*, since streptolydigin (**1**) has been demonstrated to exhibit wide ranging biological activity. In collaboration with Dr. Julian Hurdle at The University of Texas, we evaluated streptolydigin (**1**), dihydrostreptolydigin (**48**), and the adamantyl-containing analog (**47**), as well as our previously made analogs, in a variety of clinically relevant *C. difficile* strains. The results of these analyses are shown in Table I.1.

| | MICs (μg/mL) | |
|---|---|---|
| Compound | CD 1875 (RifS) | CD 1803 (RifR) |
| **1** | 4-8 | 4-8 |
| **48** | 32-64 | >64 |
| **47** | 0.06-0.25 | 1-2 |
| **25** | >64 | - |
| **26** | >64 | - |
| **23** | >64 | - |
| Rifaximin (**2B**) | 0.125 | >64 |
| Vancomycin (**7**) | 0.25-0.5 | 0.25-0.5 |
| Metronidazole (**8**) | 0.06-0.12 | 0.25 |

**Table I.1:** Evaluation of streptolydigin analogs' inhibitory activity against C. *difficile* 1875 (rifamycin-sensitive) and 1803 (Rifamycin-resistant)

When compared in rifaximin-sensitive (CD 1875) and rifaximin-resistant (CD 1803) *C. difficile* strains, 10,11-dihydrostreptolydigin (**48**) displayed significantly less activity than streptolydigin (**1**) (MICs 32-64 and 4-8 μg/mL, respectively). These results reiterate that slight modification of the streptolol moiety may only slightly alter the RNAP inhibitory profile, but can have pronounced effects on an analogs' antimicrobial activity. This observation is compounded by the alarming activity of the adamantyl-containing analog (**47**). Despite lacking activity in *in vitro* transcription experiments using *T. aquaticus* RNAP, **47** displayed potent growth inhibition of both rifamycin-sensitive and rifamycin-resistant *C. difficile* strains, with MICs of 0.06-0.25 and 1-2 μg/mL, respectively. Additionally, we compared the activity of the adamantyl-containing analog (**48**) to metronidazole (**8**) in several clinical isolates from patients suffering from CDI (Table I.2).

| | MICs (μg/mL) | | | |
|---|---|---|---|---|
| | **47** | | Metronidazole (**7**) | |
| *C. Diff.* strain | 24 H | 48 H | 24 H | 48 H |
| **CD 1803 (RifR)** | 1 | 2 | 0.5 | 0.25 |
| **CD 25** | 2 | 4 | - | - |
| **CD 9689** | 2 | 4 | 0.25 | 0.25 |
| **CD 1769** | 1 | 4 | 0.13 | 0.5 |
| **CD 1651 (RifR)** | 0.5 | 2 | 0.25 | 0.5 |
| **CD 1704 (RifR)** | 1 | 2 | 0.25 | 0.5 |

**Table I.2**: Comparison of the adamantyl-containing analog (**47**) and metronidazole (**8**) in clinical isolates from patients suffering from CDI

Although metronidazole (**8**) displayed greater efficacy at both 24 hours and 48 hours, the adamantyl-containing analog (**47**) displayed similar activity to previous experiments with rifamycin-resistant strains. Therefore, we elected to compare the adamantyl-containing analog (**47**) to streptolydigin (**1**) in a variety of rifamycin-resistant spontaneous mutants of the clinically relevant *C. difficile* strain CD0043, a variant of the NAP1 strain (Table I.3).

| | MICs (μg/mL) | | |
|---|---|---|---|
| Strain | **47** | **1** | Mutation in *rpoB* |
| **CD 43** | 0.5 | 4 | None |
| **CD 43-M9** | 0.25 | 8 | R505N |
| **CD 43-X5** | 0.5 | 4 | G510R |
| **CD 43-X2** | 0.5 | 4 | D492Y |

**Table I.3**: Comparison of **47** and **1** for activity against spontaneous rifamycin-resistant mutants derived from the CD 43 strain

The adamantyl-containing analog (**47**) exhibited a near ten-fold increase in activity over the parent streptolydigin (**1**), and displayed a four-fold increase in activity over clinical isolates (MICs of 0.25-0.5 μg/mL versus 1-2 μg/mL). Coupled with the lack of *T. aquaticus* RNAP inhibition, these results indicate that **47** should exhibit limited to no cross resistance with rifamycins, but may have an alternative mechanism of action. This may be, in part, due to the presence of the adamantyl moiety, a common motif in many biologically active small molecules.[35,36] Nevertheless, we endeavored to evaluate **47**, alongside streptolydigin (**1)** and 10,11-dihydrostreptolydigin (**48**), for their activity in mammalian cells, as well as an *in vivo* model of *C. difficile*.

## I.5. Evaluation of Streptolydigin and Associated Analogs in Eukaryotes

### *I.5.1. Effects of Analogs on Mammalian Cell Viability*

Due to STL's low toxicity in animal models, we hypothesized that if 10,11-dihydrostreptolydigin (**48**) and the adamantyl-containing analog (**47**) exhibited similar cytotoxicity profiles in mammalian cancer cells, that they would then exhibit similar toxicity profiles in animals. To that end, we evaluated **47** and **48** for their effects on cell growth in Molt-4 cells (as measured by ATP content following lysis), a human acute lymphoblastic leukemia cell line. The results of this study are shown in Figure I.7. Streptolydigin (**1**) and the dihydro-analog **48** exhibited near identical effects on cell growth, having a pronounced effect above 10 μM ($GI_{50}$: 29.6 μM and 40.5 μM, respectively). Additionally, the adamantyl-containing analog **47** displayed slightly more toxicity ($GI_{50}$: 14.4 μM). To validate the adamantyl-containing analog's activity, we

performed additional experiments to evaluate cell viability by dye exclusion (Figure I.8). While other methods for evaluating cell viability are available, they are often tied to cellular energy homeostasis (i.e. ATP content, NADH content, etc.).

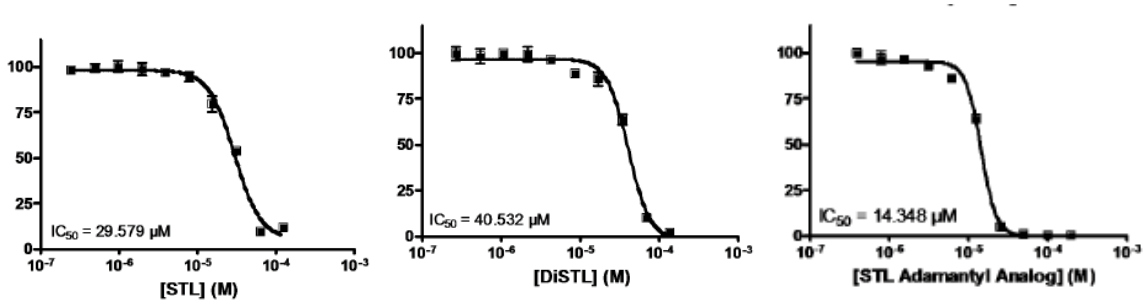


**Figure I.7:** Analysis of *in vitro* mammalian cytotoxicity for streptolydigin (**1**), and associated analogs, by analysis of ATP concentration following cell lysis.

dye exclusion allows measurement of cell viability based on the integrity of the cell membrane, and is well suited for evaluating hydrophobic molecules, which may compromise the lipid bilayer (e.g. adamantyl-containing molecules). Differences between methods of assessment can provide insight into the mechanism of small molecules.

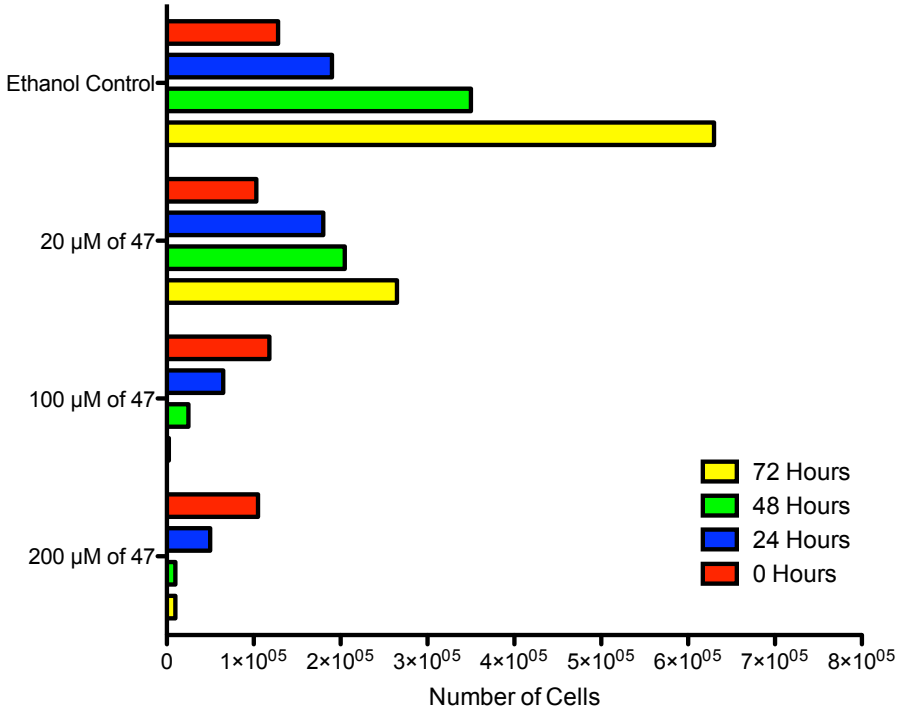


**Figure I.8**: Assessment of the effects of **47** on cell viability by dye exclusion

At the high concentration of 100 and 200 µM, the adamantyl-containing analog (**47**) showed strong cytotoxicity, killing nearly 100% of cells within 48 hours. However, at 20 µM of **47**, only moderate cell death was observed with significant cytostatic effects, corroborating the results shown in Figure I.7.

## I.6. Conclusion

Our work has demonstrated the strength of chemical synthesis by providing access to a complex natural product. With the synthetic methodologies in hand, access to a variety of rationally designed streptolydigin analogs became possible, enabling the correlation of biochemical, antimicrobial, and mammalian activities with structural considerations. Our work has demonstrated that streptolydigin's (**1**) activity is dependent

on the presence of both the streptolol and tetramic acid moieties, and removal of the rhodinose fragment (streptolydiginone, **24**) significantly alters the activity of the molecule. Additionally, we have shown that modifications to the streptolol moiety can be tolerated by the RNAP inhibitory profile, as is the case with 10,11-dihydrostreptolydigin (**48**), but can have a pronounced effect on the analogs' antimicrobial activity. Nevertheless, our discovery of the adamantyl-containing analog's activity in *in vitro* models of *C. difficile* have provided us a great launching point for the design and development of novel probes aimed at providing additional insights into the clinically relevant bacteria.

## I.7. References


1) Lewis, K. Platforms for Antibiotic Discovery. *Nat. Rev. Drug. Discov.* **2013**, 12 (5), 371-387.

2) Theuretzbacher, U.; Van Bambeke, F.; Canton, R.; Giske, C.; Mouton, J.; Nation, R.; Paul, M.; Turnidge, J.; Kahlmeter, G. Reviving old antibiotics. *J. Antimicrob. Chemother.* **2015**, 70 (8), 2177-2181.

3) Royles, B.J.L. Naturally-occurring tetramic acids: Structure, Isolation, and Synthesis. *Chem. Rev.*, **1995**, *95* (6), 1981–2001.

4) Holloway, C.; Matthews, C.; Jeong, Y.C.; Moloney, M. Roberts, C. Yaqoob, M. Novel chiral skeletons for drug discovery: Antibacterial Tetramic acids. *Chem. Biol. Drug. Des.* **2011**, 78, 229–235.

5) Pronin, S. V.; Kozmin, S. A. Synthesis of Streptolydigin, a Potent Bacterial RNA Polymerase Inhibitor. *J. Am. Chem. Soc.*, **2010**, *132* (41), 14394–14396.

6) Villain-Guillot, P.; Bastide, L.; Gaultieri, M.; Leonetti, J.P. Progress in Targeting Bacterial Transcription. *Drug Discov, Today.* **2007,** 12 (5-6), 200-208.

7) Clancy, S. RNA transcription by RNA polymerase: prokaryotes vs. eukaryotes. *Nature Education.* **2008***,* 1 (1), 125

8) Zhang, J.; Landick, R. A Two-Way Street: Regulatory Interplay between RNA Polymerase and Nascent RNA Structure. *Trends Biochem. Sci.* **2015**, 0 (0), 1-18.

9) Mariani, R.; Maffioli, S. Bacterial RNA polymerase inhibitors: an organized overview of their structure, derivatives, biological activity and current clinical development status. *Curr. Med Chem.* **2009**, 16 (4), 430-54.

10) Elbe, T. E.; Large, C. M.; DeVries, W. H.; Crum, G. F.; and Shell, J. W. *Antibiot. Ann.* **1955- 1956**, 893-896.

11) DeBoer, C.; Dietz, A.; Silver, W. S.; and Savage, G. M. Streptolydigin, a new antimicrobial antibiotic. *Antibiot. Ann.* **1955-1956**, 886- 892.

12) Lewis, C.; Wilkins, J. R.; Schwartz, D. F.; and Nikitas, C. T. Streptolydigin, a new antimicrobial antibiotic. *Antibiot. Ann.* **1955-1956**, 897-902.

13) Siddhikol, C.; Erbstoeszer, J.; Weisblum, B.; Mode of action of streptolydigin. *J. Bacteriol.* **1969**, 99, 151–155.

14) Tuske, S.; Sarafianos, S.G.; Wang, X.; Hudson, B.; Sineva, E.; Mukhopadhyay, J.; Birktoft, J.J.; Leroy, O.; Ismail, S.; Clark, A.D. Jr.; Dharia, C.; Napoli A.; Laptenko, O.; Lee, J.; Borukhov, S.; Ebright, R.H.; Arnold, E. Inhibition of

bacterial RNA polymerase by streptolydigin: stabilization of a straight-bridge-helix active-center conformation. *Cell*. **2005**, 122 (4), 541-552.

15) Rupnik, M.; Wilcox, M.H.; Gerding, D.N. Clostridium difficile infection: new developments in epidemiology and pathogenesis. *Nat. Rev. Microbiol.* **2009**, 7 (7), 526-536.

16) Lofgren, E.T.; Cole, S.R.; Weber, D.J.; Anderson, D.J.; Moehring, R.W. Hospital-acquired Clostridium difficile infections: estimating all-cause mortality and length of stay. *Epidemiology* **2014**, 25, 570-575.

17) Leffler, D.; Lamont, J.T. Clostridium difficile infection. *N. Engl. J. Med*. **2015**, 372, 1539-1548.

18) Zimlichman, E.; Henderson, D.; Tamir, O. Health care-associated infections: a meta-analysis of costs and financial impact on the US health care system. *JAMA Intern. Med.* **2013**,173, 2039-2046.

19) See, I.; Mu, Y.; Cohen, J.; Beldavs, Z.G.; Winston, L.G.; Dumyati, G.; Holzbauer, S.; Dunn, J.; Farley, M.M.; Lyons, C.; Johnston, H.; Phipps, E.; Perlmutter, R.; Anderson, L.; Gerding, D.N.; Lessa, F.C. NAP1 strain type predicts outcomes of Clostridium Difficile infection. *Clin Infect Dis.* **2014**, 58 (10), 1394-1400.

20) Shen, E.P.; Surawicz, C.M. Current Treatment Options for Severe Clostridium difficile–associated Disease. *Gastroenterol Hepatol.* **2008**, 4 (2), 134-139

21) Wilcox, M.H.; Howe, R. Diarrhoea caused by Clostridium difficile: response time for treatment with metronidazole and vancomycin. *J. Antimicrob. Chemother.* **1995**, 36 (4), 673-679.

22) Leffler, D.A.; Lamont, J.T. Treatment of Clostridium difficile-associated disease. *Gastroenterology.* **2009**, 136, 1899-1912.

23) Eiseman, B.; Silen, W.; Bascom, G.S.; Kauvar, A.J. Fecal enema as an adjunct in the treatment of pseudomembranous enterocolitis. *Surgery.* **1958**, 44, 854-859.

24) Pépin, J.; Valiquette, L.; Gagnon, S.; Routhier, S.; Brazeau, I. Outcomes of Clostridium difficile-associated disease treated with metronidazole or vancomycin before and after the emergence of NAP1/027. *Am. J. Gastroenterol.* **2007**, 102, 2781-2788.

25) Louie, T.J.; Miller, M.A.; Mullane, K.M. Fidaxomicin versus vancomycin for Clostridium difficile infection. *N. Engl. J. Med.* **2011**, 364, 422-431.

26) Rinehart, K. L. Jr.; Beck, J. R.; Borders, D. B.; Kinstle, T. H.; Krauss, D. Structure of streptolydigin. *J. Am. Chem. Soc.*, **1963**, 85, 4038-4039.

27) Pronin, S.V.; Martinez, A.M.; Kuznedelov, K.; Severinov, K.; Shuman, H.; Kozmin, S.A. Chemical Synthesis Enables Biochemical and Antibacterial Evaluation of Streptolydigin Antibiotics. *J. Am. Chem. Soc.* **2011**, 133, 12172-12184

28) (a) Schlessinger, R. H.; Bebernitz, G. R.; Lin, P.; Poss, A. *J. Am. Chem. Soc.* **1985**, 107, 1777–1778. (b) DeShong, P.; Ramesh, S.; Elango, V.; Perez, J. *J. Am. Chem. Soc.* **1985**, 107, 5219–5224. (c) Boeckman, R. K.; Starrett, J. E.; Nickell, D. G.; Sum, P. E. *J. Am. Chem. Soc.* **1986**, 108, 5549–5559. (d) Neukom, C.; Richardson, D. P.; Myerson, J. H.; Bartlett, P. A. *J. Am. Chem. Soc.* **1986**, 108, 5559–5568. (e) Shimshock, S. J.; Waltermire, R. E.; DeShong, P. *J. Am. Chem. Soc.* **1991**, 113, 8791–8796.

29) (a) Boeckman, R. K., Jr.; Potenza, J. C.; Enholm, E. J. *J. Org. Chem.* **1987**, 52, 469–472. (b) Schlessinger, R. H.; Graves, D. D. *Tetrahedron Lett.* **1987**, 28, 4385–4388. (c) Ireland, R. E.; Smith, M. G. *J. Am. Chem. Soc.* **1988**, 110, 854–860.

30) Temiakov, D.; Zenkin, N.; Vassylyeva, M.N.; Perederina, A.; Tahirov, T.H.; Kashkina, E.; Savkina, M.; Zorov, S.; Nikiforov, V.; Igarashi, N.; Matsugaki, N.; Wakatsuki, S.; Severinov, K.; Vassylyev, D.G.; Structural basis of transcription inhibition by antibiotic streptolydigin. *Mol Cell.* **2005**, 19 (5), 655-66.

31) Kuznedelov, K.; Minakhin, L.; Severinov, K. Preparation and characterization of recombinant Thermus aquaticus RNA polymerase. *Methods Enzymol.* **2003**, 370, 94–108.

32) Evans, D.A.; Ennis, M.D.; Mathre, D.J. Asymmetric alkylation reactions of chiral imide enolates. *J. Am. Chem. Soc.* **1982**, 104, 1737-1739

33) Sherman, J. M.; Niven, C. F.; Smiley, K. L. Streptococcus salivarius and Other Non-hemolytic Streptococci of the Human Throat. *J. Bacteriol.* **1943**, 45, 249–263.

34) Cho, S.H.; Warit, S.; Wan, B.; Hwang, C.H.; Pauli, G.F.; Franzblau, S.G. Low-oxygen-recovery assay for high-throughput screening of compounds against nonreplicating Mycobacterium tuberculosis. *Antimicrob Agents Chemother.* **2007**, 51 (4), 1380-1385.

35) Davies, W.L.; Grunert, R.R.; Haff, R.F.; McGahen, J.W.; Neumayer, E.M.; Paulshock, M.; Watts, J.C.; Wood, T.R.; Hermann, E.C.; Hoffmann, C.E. Antiviral activity of 1-adamantanamine (Amantadine). *Science* **1964**, 144, 862–863.

36) Maassab, H.F.; Cochran, K.W. Rubella virus: inhibition *in vitro* by amantadine hydrochloride. *Science*, **1964**, 145, 1443–1444.

# CHAPTER II

# THE HUNT FOR MODULATORS OF MITOCHONDRIAL PERMEABILITY TRANSITION

*This chapter describes the identification of a new class of small-molecule activators of mitochondrial permeability transition (mPT). The discussion begins with a review of permeability transition and its physiological role, as well as known mechanisms of its induction. The chapter then describes the characterization of a number of known mPT inducers. The subsequent sections discuss the discovery of a class of novel activators of mPT, called indoloquinolizidines, which were determined to induce permeability transition by mobilizing calcium, resulting in collapse of energy metabolism in human cancer cells.*

## II.1. Introduction

### *II.1.1. Permeability Transition*

Mitochondria are double-membrane enclosed organelles that play a central role in energy metabolism, calcium homeostasis, signaling, differentiation, and cell death. Mitochondrial function (and dysfunction) has been connected to a wide variety of severe human pathologies including cardiovascular disease, cancer, neurodegeneration, metabolic disorders like diabetes, and ageing.[1,2] Mitochondrial permeability transition (mPT) is a sudden permeabilization of the inner lipid bilayer of this organelle to solutes less than 1.5 kDa, which occurs in response to cellular stress.[3] This transition represents a critical aspect of mitochondrial physiology and is believed to entail the formation of a poorly understood multiprotein complex, which is known as the mPT pore (mPTP), that presumably spans the outer and inner mitochondrial membranes.[4,5] mPT is characterized by a rapid loss of mitochondrial membrane potential, organelle swelling, and outer membrane rupture that typically leads to cell death.[6] The composition of mPT pore and the mechanism of its operation are largely unknown.[3-7] In classical models, the pore is proposed to consist of the adenine nucleotide translocator (ANT) in the inner membrane,[8] the voltage-dependent anion channel (VDAC) in the outer membrane,[9] and cyclophilin D (CypD), which can translocate from the matrix to the inner membrane.[10] Furthermore, hexokinase II has been proposed to localize with the outer mitochondrial membrane by association with VDAC, bringing a connection between aerobic glycolysis and mitochondrial activity.[11,12] Other proteins that have been implicated in the formation of mPT pore are pro-apoptotic Bcl-2 family members, i.e. BAX and BAK,[13] as well as a

peripheral benzodiazepine receptor.[14] Additionally, p53 has been also shown to induce mPT pore opening by binding cyclophilin D.[15]

More recently, the initially proposed components of the mPTP have come under increasing scrutiny, as genetic evidence has questioned the role of some of the classical members and has pointed researchers toward alternative components.[16] For example, VDAC1$^{-/-}$ mice still exhibit normal pharmcalogical modulation of mPT.[17] Physiological induction of mPT still occurs in VDAC1$^{-/-}$ or VDAC3$^{-/-}$ mitochondria,[18] and VDAC1/3 double-null mice with subsequent siRNA knockdown of VDAC2 are still sensitive to mPT-induced cell death.[18] Additionally, genetic studies using ANT1/2 double-null mice have shown that mPT still occurs, but is significantly less sensitive to pharmacological or physiological induction of mPT, indicating that ANT may serve as a peripheral regulatory component of the pore, rather than an essential component.[19] Genetic analysis of cyclophillin D, has however, confirmed it as an essential regulatory member of the mPTP.[16] These data taken together indicate that there is still a great need for identifying primary components of the mPTP, as well as for the development of pharmacological probes that can help elucidate members of the pore and help better understand the mechanism of mPT.

While there is no consensus for the role that mPT plays in normal cell physiology, there are several feasible suggestions, including mPT leading to activation of apoptosis in specific types of cell damage,[20] mPT being a method for clearing the mitochondria of damaged or unnecessary molecules,[21] as well as mPT providing a way of removing dysfunctional mitochondria.[22] The rapid loss of mitochondrial membrane potential not

only leads to a complete shutdown of oxidative phosphorylation (OXPHOS), but also leads to a reversal of the FoF1 ATP synthase. ATP synthase quickly hydrolyzes ATP as it tries to restore normal membrane potential.[23] The coupling of OXPHOS shutdown with ATP hydrolysis leads to an enormous bioenergetic crisis, as remaining healthy mitochondria and glycolysis cannot provide sufficient ATP to power the cell. Therefore, cells experiencing prolonged mPT cannot even provide enough energy to power apoptosis, and undergo necrotic cell death. Due to its extreme effects, mPT has been found to be a potent pharmacological target for diseases involving dysfunctional mitochondria or excessive cell death, including ischemia/reperfusion, heart failure, cardiotoxicity, cancer, and neurodegeneration.[2]

Opening of the mPT pore can be induced by mitochondrial matrix sequestration of $Ca^{2+}$, production of reactive oxygen species generated during oxidative damage, and direct pharmacological action on the pore.[1-10] In addition, activation of cyclophilin D can trigger mPT by translocation of this protein from the matrix to the inner mitochondrial membrane and association with ANT.[24] This process appears to be dependent on the peptidylprolyl isomerase activity of cyclophilin D.[25] Indeed, sub-micromolar concentrations of cyclosporine A (CsA) can prevent mPT pore opening by binding to cyclophilin D and inhibiting its peptidylprolyl isomerase activity.[26]

### *II.1.2. Calcium Homeostasis and its Relevance*

In addition to its ability to activate mPT, $Ca^{2+}$ plays a central role in normal cell physiology as a versatile secondary messenger that is essential for the survival of all higher organisms.[27] In fact, it is the most abundant secondary messenger in the cell, and

very tight control is required to produce specific calcium mediated responses.[28] Aberrant calcium signaling can lead to the disruption of processes connected to growth factors, neurotransmitters, hormones, cell proliferation and excitation, motility, transcription, and cell death (apoptosis, autophagy, necrosis, etc.), underlying a variety of human pathological outcomes including cancer[29] and hearth failure.[30]

$Ca^{2+}$ signals can arise from direct transport of the ion across the plasma membrane, or can be derived from release or uptake of calcium from internal stores.[31] Calcium influx channels can be broadly grouped into four main categories, which include voltage-operated $Ca^{2+}$ channels (VOCs), receptor-operated $Ca^{2+}$ channels (ROCs), mechanically-activated $Ca^{2+}$ channels, and store-operated $Ca^{2+}$ channels (SOCs).[31] VOCs are largely utilized by excitable cells and are activated following depolarization of the plasma membrane.[32] ROCs are a structurally diverse family of $Ca^{2+}$ channels, and are activated following binding of small molecules to their extracellular domains.[33] ROCs are prevalent in secretory cells and at nerve terminals, and can be activated by a wide variety of agonists including ATP, serotonin, glutamate, and acetylcholine.[31] Mechanically-activated $Ca^{2+}$ channels, or mechanosensitive ion channels, are found in a wide variety of cell types, and are activated following physical stress (stretching or forced contraction) on the cell.[34] Finally, SOCs are one of the most widely expressed calcium channels on the plasma membrane, and are activated following depletion of intracellular stores, either by physiological $Ca^{2+}$-mobilizing messengers or action by pharmacological agents.[31] While the mechanism of $Ca^{2+}$ "sensing" by the SOC machinery is poorly understood, high-throughput RNAi-based screening has consistently identified STIM1, a type-one single transmembrane protein that resides mainly at the ER membrane, as a primary component

of store-operated calcium entry (SOCE), which appears to function as the sensor of ER luminal $Ca^{2+}$.[35] These screens also refuted the connection between SOCE and transient receptor potential (TRP) channels, which were originally believed to be the primary candidates for SOCs.[31] TRP channels may still play a role in SOCE, as recent evidence has indicated their necessity in the formation of a ternary complex which influences the magnitude of SOCE.[36] Additionally, the combination of RNAi screening and modified linkage analysis showed the protein Orai1, a four-transmembrane protein localized to the plasma membrane, to be essential for the formation of calcium release-activated channels (CRAC) and therefore SOCE.[37,38]

Maintenance of intracellular calcium is typically controlled by the endoplasmic reticulum (ER), which uses the combination of the sarcoplasmic/endosplasmic reticulum calcium ATPase (SERCA) and receptor-operated channels on the ER surface to buffer cytosolic calcium.[39] The ER primarily utilizes inositol 1,4,5-triphosphate receptors (IP3Rs) and ryanodine receptors (RyRs) to control $Ca^{2+}$ release from the ER luminal domain.[39] Although IP3Rs and RyRs are structurally and functionally analogous, RyRs have been shown to exhibit twice the conductance and have twice the molecular weight (they are also named for their high affinity for the plant alkaloid, ryanodine).[31] Nevertheless, both are sensitive to secondary messenger binding and to cytosolic calcium concentrations,[40] and are modulated by a variety of factors including phosphorylation, adenine nucleotides, thiol-reactive compounds, pH, and the $Ca^{2+}$ load within the ER/SR.[41] Mitochondria also play a critical role in buffering cytosolic calcium, and the link between the ER and the mitochondria will be reviewed in the following section.

### *II.1.3. Connecting the Mitochondria and Endoplasmic Reticulum*

The regulation of cytoplasmic and mitochondrial $Ca^{2+}$ levels are tightly connected.[42] The influx of $Ca^{2+}$ into the mitochondria is driven by the presence of a negative electrical potential across the inner mitochondrial membrane. Mitochondria can rapidly accumulate and buffer cytoplasmic $Ca^{2+}$ or release this ion if the external $Ca^{2+}$ levels are low. The control of $Ca^{2+}$ homeostasis relies on an intimate functional and structural connection between the mitochondria and the ER, which is the main intracellular $Ca^{2+}$ reservoir.[42] Indeed, mitochondria and ER can physically interact through the formation of mitochondria-associated ER membranes, allowing mitochondria to directly uptake $Ca^{2+}$ ions released from the ER.[43] Chemical agents that induce ER stress, which result in a rapid increase of cytoplasmic $Ca^{2+}$ levels, can efficiently promote mPT.[44] Such compounds include tunicamycin (TN) and thapsigargin (TG) that trigger release of $Ca^{2+}$ from ER stores by inducing ER stress. This release is followed by rapid mitochondrial accumulation of $Ca^{2+}$ and subsequent cell death in human cervix and colon carcinoma cell lines.[44] Additionally, mPT can be induced by ionophores that facilitate direct $Ca^{2+}$ transport across the plasma membrane or across the ER membrane. Ionophores also facilitate direct transfer of $Ca^{2+}$ into the mitochondrial matrix.[45]

While the prolonged elevation of $Ca^{2+}$ levels in mitochondrial matrix beyond a critical threshold is a strong trigger of mPT, the molecular details of this fundamentally important process are currently unknown. Small-molecule probes that modulate and induce mPT, by various mechanisms, are useful for gaining further understanding of this event.[46] Additionally, understanding the complex system of calcium signaling and its connection to mPT, is essential to both provide insights into normal cell physiology and

to facilitate the development of novel therapeutics aimed at a wide collection of human diseases.

### II.2. Small-molecule Perturbation of mPT

Our laboratory has previously demonstrated that combining small-molecule inhibitors of oxidative phosphorylation and glycolysis resulted in rapid depletion of cellular ATP concentrations, while the action of individual mitochondrial or glycolytic inhibitors did not substantially impact the ATP level under the same conditions.[47-49] Next, we decided to examine how ATP production in human cancer cell lines is affected by small molecules that induce mPT, since effects of such compounds on energy metabolism have not been well characterized. While we expected to observe massive ATP depletion following mPT, we hoped to gain additional insights into the kinetics and pharmacological modulation of such events. In addition to gaining further insight into the mechanism of mPT, characterization of small molecule effectors of permeability transition would establish methods for identifying novel small molecules, which may activate or inhibit mPT. Modulators of mPT can be grouped broadly into two categories, including those that act directly on individual components of the mPT pore and those that affect mitochondrial permeabilization by external mechanisms. The latter include small molecules that release secondary messengers, such as $Ca^{2+}$ ions or reactive oxygen species.

### *II.2.1. Activators of mPT*

Methyl jasmonate (**49**) is a plant hormone that mediates ubiquitination and regulates various aspects of plant physiology, including regulation of defense responses against herbivores and necrotrophic pathogens.[50] Additionally, this plant hormone was shown to have effects on cultured animal cells, displaying a range of growth-inhibiting properties, *in vitro* and *in vivo*.[51] Jasmonates and their synthetic derivatives were also shown to inhibit proliferation and induce cell death in various human and murine cancer cell lines, including breast, prostrate, melanoma, and leukemia.[52] The cytotoxic activity of **49** has been attributed to induction of mPT by binding to hexokinase, disrupting its interaction with VDAC, consequently detaching mitochondria-bound hexokinase II.[53] We first examined the effect of this plant metabolite on ATP production. We found that treatment of the human acute lymphoblastic leukemia cell line, Molt-4, with **49** resulted in rapid depletion of cellular ATP within 30 min of incubation (Figure II.1 C-E). We also established that this effect was not influenced by the presence of either antimycin A (**50**) or 2-deoxy-D-glucose (**51**), inhibitors of OXPHOS and glycolysis, respectively. Interestingly, this result was in contrast with a previously reported ability of 2-deoxy-D-glucose to potentiate jasmonate-induced ATP depletion. We also examined the ability of **49** to induce mPT using fluorescent microscopy (Figure II.1-F,G).[54] The method is based on treating human osteosarcoma cell line, 143B.TK-, with the fluorescent probe, calcein. The dye is introduced as an acetoxymethyl ester, which is rapidly cleaved inside the cell, trapping calcein in various sub-cellular compartments. In addition, the cells are treated with $Co^{2+}$, which quenches the fluorescence of calcein. Since this ion cannot cross the inner mitochondrial membrane, it is excluded from the matrix while quenching calcein

fluorescence in the cytosol and other compartments of the cell.[54] Upon mitochondrial permeabilization, $Co^{2+}$ enters the matrix and quenches the calcein fluorescence. Retention of MitoTracker Red CMXRos confirms that loss of calcein fluorescence is due to mPT induction, and not caused by non-specific action on the mitochondrial membrane. We found that treatment of 143B.TK- cells with **49** resulted in rapid decrease of calcein fluorescence due to opening of mPT pore (Figure II.1-F). In addition, we found that pretreatment of cells with 5 μM cyclosporine A blocked this effect, providing a indication that jasmonate-induced mPT is cyclophilin D dependent (Figure II.1-G). The latter observation was fully consistent with previously reported ability of cyclosporine A to prevent the cytotoxic effects of **49**. To test if the observed effect on ATP depletion was general for other inducers of mitochondrial permeabilization, we next examined a series of compounds that promote mPT indirectly by increasing cytosolic $Ca^{2+}$ concentration.

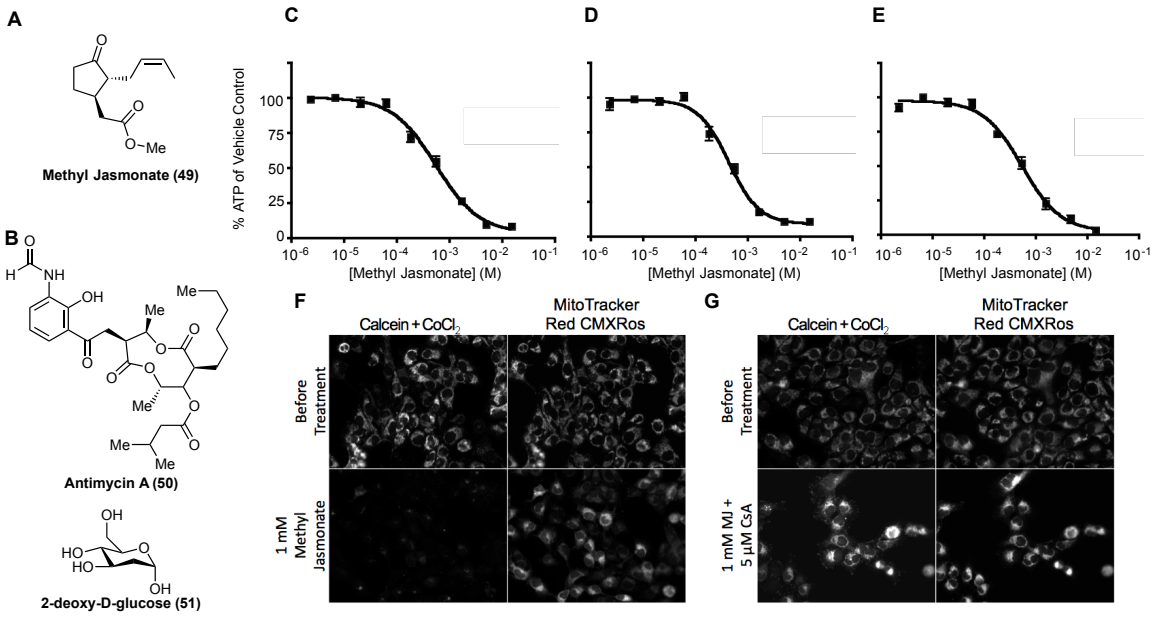


**Figure II.1**: A. Structure of plant hormone, methyl jasmonate (**49**). B. Structures of antimycin A (**50**), inhibitor of OXPHOS and 2-deoxy-D-glucose (**51**), inhibitor of glycolsis. C. ATP depletion profile of **49** without additives. ($IC_{50}$: 0.5514 mM) D. ATP depletion profile of **49** following 10 nM antimycin A (**50**) pretreatment ($IC_{50}$: 0.4308 mM). E. ATP depletion profile of **49** following 5 mM 2-deoxy-D-glucose (**51**) pretreatment ($IC_{50}$: 0.5421 mM). F. mPTP induction without additives. G. mPTP induction following 5 μM cyclosporine A pretreatment.

Tunicamycin (**52**) is an antibiotic, produced by several *Streptomyces* species, that inhibits UDP-N-acetylglucosamine: dolichol phosphate GlcNAc-1-P transferase (GPT), blocking catalysis in the first step of protein glycosylation.[55] Tunicamycin's inhibitory activity causes extensive protein misfolding, and activation of the unfolded protein response (UPR).[56] Due to the stress caused in the ER, $Ca^{2+}$ is released from the ER luminal domain into the cytoplasm, and is subsequently taken up by the mitochondria,

inducing mPT. Following the reported ability of tunicamycin (**52**) to promote mPT pore formation,[44] we measured the effect of this compound on cellular ATP levels. Treatment of Molt-4 cells with **52** for 30 min resulted in dose-dependent suppression of ATP production (Figure II.2). Similarly to methyl jasmonate (**49**), this effect was independent of the presence of either OXPHOS or glysolysis inhibitors **50** and **51**. As expected, tunicamycin promoted mPT pore opening as observed by fluorescent microscopy using calcein/$Co^{2+}$ indicator (Figure II.2-E).

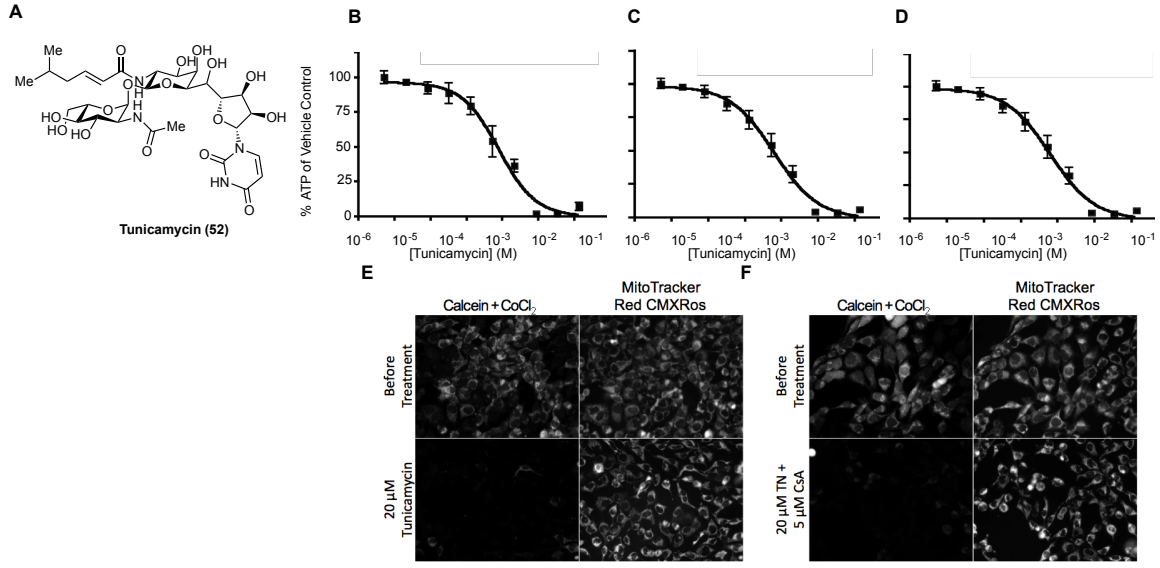


**Figure II.2**: A. Structure of tunicamycin (**52**). B. ATP depletion profile of **52** without additives. ($IC_{50}$: 8.992 µM) C. ATP depletion profile of **52** following 10 nM antimycin A (**50**) pretreatment ($IC_{50}$: 5.9629 mM). D. ATP depletion profile of **52** following 5 mM 2-deoxy-D-glucose (**51**) pretreatment ($IC_{50}$: 7.9204 µM). E. mPTP induction without additives. F. mPTP induction following 5 µM cyclosporine A pretreatment.

Thapsigargin (**53**) is a plant-derived sesquiterpene lactone, that triggers rapid calcium release from the ER by inhibiting the activity of the sarcoplasmic/endoplasmic reticulum $Ca^{2+}$ ATPase (SERCA) ion channels, which help reaccumulate calcium into the SR and ER.[57] Although thapsigargin has been shown to promote accumulation of mitochondrial $Ca^{2+}$ levels and induce permeability transition,[44] the effect of this agent on cellular ATP concentrations has not been reported. We reproduce the ability of **53** to promote mPT pore formation in 143B.TK- cells using fluoresecent microscopy (Figure II.3). We also found that **53** rapidly depleted ATP within 30 min of incubation of Molt-4 cells with this compound. Inhibition of ATP production by **53** was not affected by adding either OXPHOS or glysolysis inhibitors **50** and **51**.

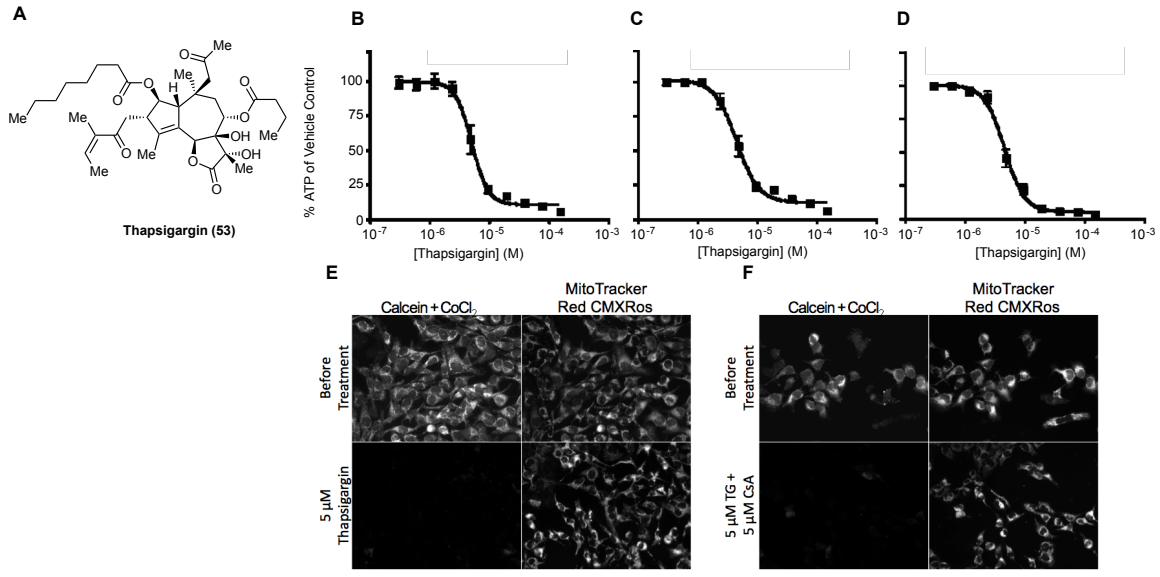


**Figure II.3**: A. Structure of thapsigargin (**53**). B. ATP depletion profile of **53** without additives. ($IC_{50}$: 5.041 μM) C. ATP depletion profile of **53** following 10 nM antimycin A (**50**) pretreatment ($IC_{50}$: 4.473 μM). D. ATP depletion profile of **53** following 5 mM 2-

deoxy-D-glucose (**51**) pretreatment ($IC_{50}$: 4.541 μM). E. mPTP induction without additives. F. mPTP induction following 5 μM cyclosporine A pretreatment.

Additionally, we examined the ability of calcium ionophores to induce mPT. Calcimycin (**54**) is an antibiotic produced by *Streptomyces Chartreusensis* and *Conglobatus*, respectively.[57] It displays a high affinity for several divalent cations, including $Ca^{2+}$.[57] As expected, **54** triggered mPT pore formation in 143B.TK- cells within 30 min of incubation (Figure II.4). Treatment of Molt-4 cells with **54** induced dose-dependent suppression of ATP production (Figure II.4). Pretreatment with 5 μM cyclosporine A was unable to rescue induction of mPT pore opening by tunicamycin (**52**), thapsigargin (**53**) and calcimycin (**54**). This result is consistent with previously published data indicating that cyclosporine A fails to block mPT at highly elevated $Ca^{2+}$ concentrations.

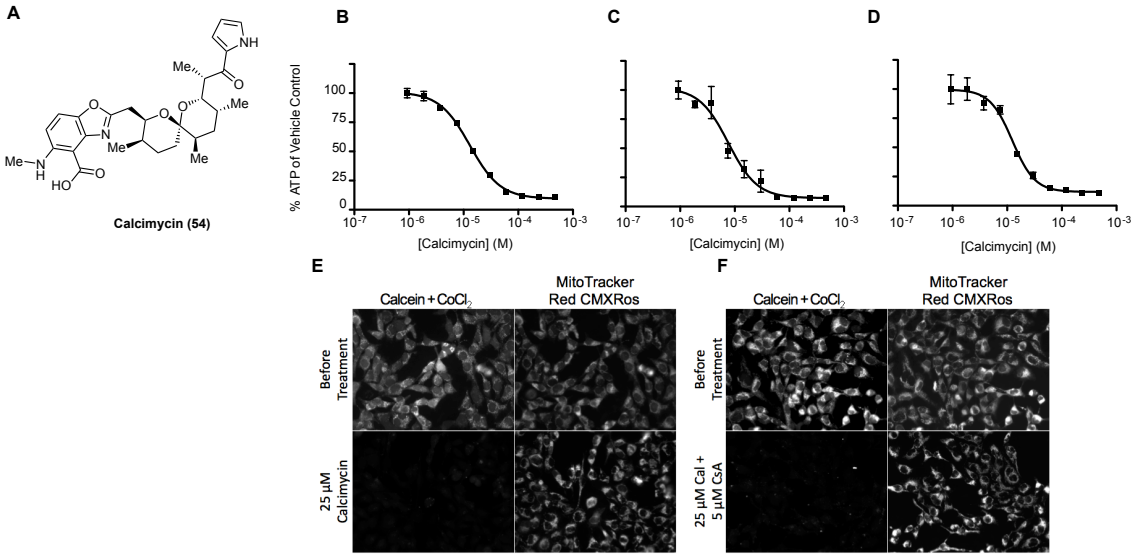


**Figure II.4**: A. Structure of calcimycin (**54**). B. ATP depletion profile of **54** without additives. ($IC_{50}$: 13.00 μM) C. ATP depletion profile of **54** following 10 nM Antimycin A (**50**) pretreatment ($IC_{50}$: 7.618 μM). D. ATP depletion profile of **54** following 5 mM 2-deoxy-D-glucose (**51**) pretreatment ($IC_{50}$: 12.44 μM). E. mPTP induction without additives. F. mPTP induction following 5 μM cyclosporine A pretreatment.

These studies established a common profile of rapid suppression of cellular ATP production by a series of mechanistically distinct small-molecule inducers of mPT. Rapid depletion of ATP occurs independently of OXPHOS or glycolysis, which indicates that mPT pore opening inactivates all energy-producing pathways. As mentioned previously, OXPHOS is blocked during mPT, presumably due to the dissipation of the mitochondrial transmemberane potential. Inactivation of glycolysis may arise due to the loss of hexokinase II activity upon mPT pore formation as this enzyme has been proposed to physically associate with VDAC, and may contribute to pore opening as a regulatory component. This highly conserved and distinct ATP suppression profile could be utilized

as a biochemical readout, that would enable discovery of new small-molecule inducers of mPT pore.

### II.3. Synthesis of Indoloquinolizidine Library

In our search for activators of permeability transition, we aimed to gain access to synthetic methodologies that would quickly provide a collection of small molecules that mimic the physicochemical properties of natural products. The corynanthe family of alkaloids displays a wide variety of bioactivities, and finds use as anticancer, anti-malarial, and anti-arrhythmic agents.[58] We designed a 480-member library of indoloquinolizidines, which was based on the molecular architecture of this family of indole alkaloids (Figure II.5).

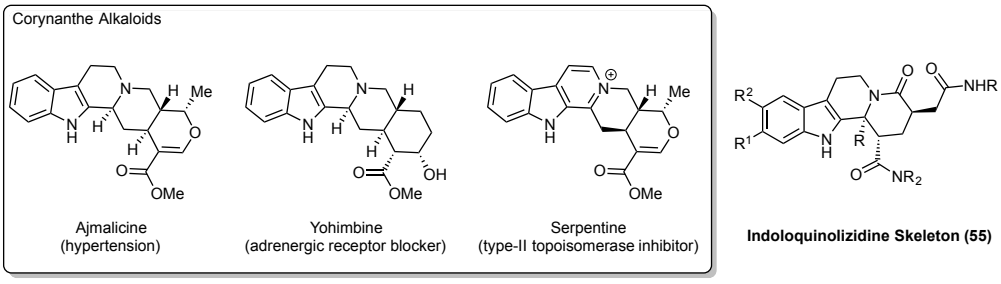


**Figure II.5**: Several members of the cornynanthe family of polycyclic indole alkaloids

We began our studies by examining construction of the indoloquinolizidine skeleton (**55**). To rapidly assemble the tetracyclic molecular framework, we took advantage of the known propensity of vinylogous carbamates to undergo *N*-acyliminium ion cyclizations when subjected to either unsaturated acid chlorides or acid anhydrides.[59] Condensation of tryptamine **56** with ketoamide **57** gave access to the corresponding

vinylogous urea **58**, which was next treated with itaconic anhydride (**59**) to give indoloquinolizidine **60** in 90% yield (Scheme II.1). The relative stereochemistry of **60** was established by X-ray crystallography. This process entailed a 1,4-addition of the vinylogous urea derived from **56** and **57** to a Michael acceptor **59**, followed by anhydride opening and *N*-acyliminium ion cyclization. Solvent and temperature optimization studies revealed that this transformation proceeded with excellent diastereoseletivity when the reaction was conducted in dioxane at 40 °C.

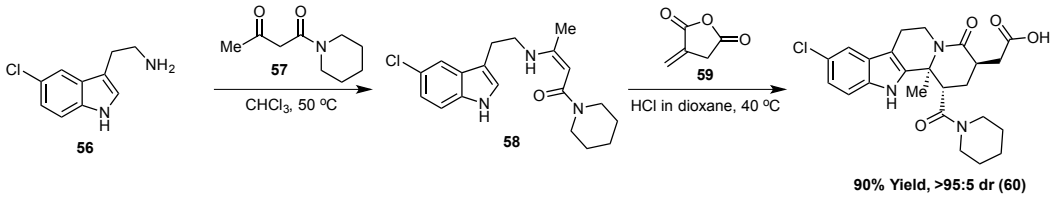


**Scheme II.1:** One-Flask Synthesis of Indoloqunolizidine **60**

We next examined the generality of this transformation and found that a range of substituted tryptamines and 1,3-ketoamides can be successfully employed to produce the corresponding indoloquinolizidines in high yields and excellent diastereoselectivity. A representative example of these studies is shown in Scheme II.2. Treatment of 5-chloro-tryptamine **56** with ketoamide **61** cleanly produced vinylogous urea **62**, which was efficiently cyclized to afford indoloqunolizidine **63** in a one-flask operation upon treatment with **59** and HCl in dioxane at 40 °C. The structure of **63** was also confirmed by X-ray crystallography.

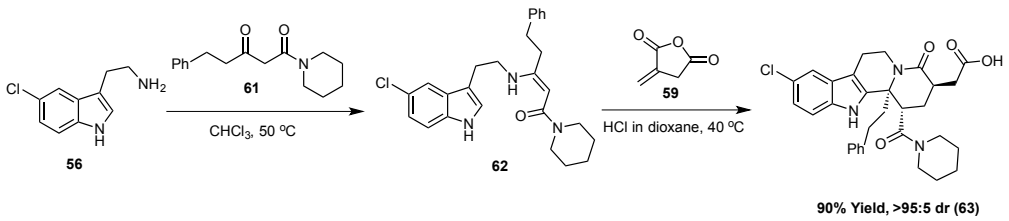


**Scheme II.2:** One-Flask Synthesis of Indoloqunolizidine **63.**

Having established the high efficiency and generality of indoloquinolizidine synthesis, we next examined its first application to a larger set of compounds based on this tetracyclic platform (Figure II.6). We planned to prepare a 480-member library **69** starting with five tryptamines **64** and eight ketoamides **65** to deliver 40 indoloquinolizidine-containg carboxylic acids **67**. Each of the initially produced acids **67**

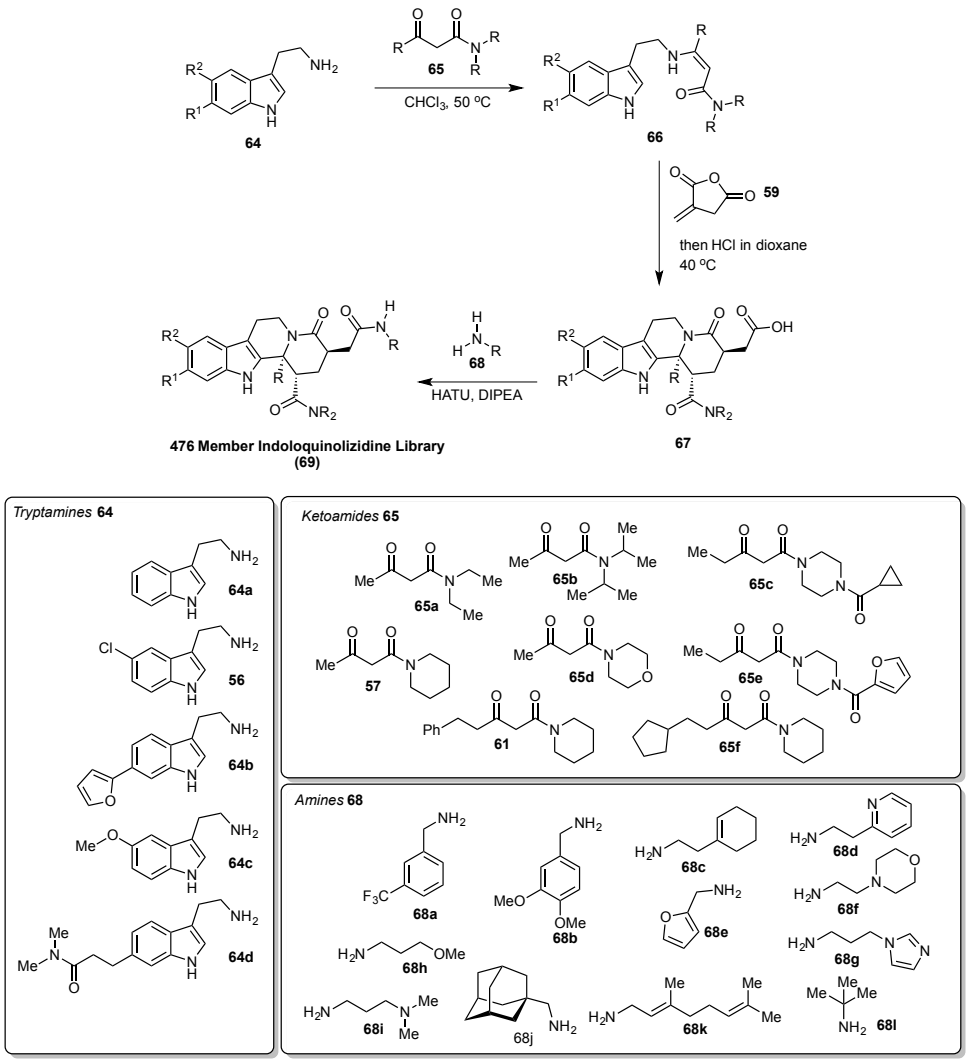


**Figure II.6:** Synthesis of 476-Member Library of indoloquinolizidines. The assembly process entailed two chromatographic steps, which included initial purification of each of the 40 acids **67** and subsequent LCMS purification of all final library members.

would be next diversfified with twelve amines **68** to deliver the final library **69**. Selection the building blocks shown in Figure II.6 was guided by Accelrys Pipeline Pilot, which enabled virtual enumeration of the target library and estimation of various molecular properties *in silico*. Specifically, during the design process, we applied

appropriate filters in order to select building blocks that would produce the target library with molecular weight below 600 g/mol and calculated logarithmic value of n-octanol/water partition coefficient (cLogP) within a range of 1−5. The synthesis began with condensations of five tryptamines **64** with eight ketoamides **68**, followed by reactions of the resulting vinylogous ureas **66** with anhydride **59** to afford forty indoloquinolizidine-containing carboxylic acids **67**. Each of the acids **67** was obtained as a single diastereomer approximately on a 500 mg scale in a single-flask operation starting with the corresponding tryptamines **64** and ketoamides **65**. In order to ensure their high chemical purity, all pyrrolidinone-containing carboxylic acids **67** were purified by conventional chromatography. The second stage of the synthesis entailed coupling of each of the acids **67** with twelve amines **68**. Following examination of several amide-coupling protocols, we established that this transformation can be efficiently accomplished using 2-(1H-7-Azabenzotriazol-1-yl)-1,1,3,3-tetramethyl uronium hexafluorophosphate (HATU) in the presence of N,N-diisopropylethylamine (DIPEA) in DMF. EDCI coupling of acids **67** with amines **68** was also determined to be quite general in the preparation of final indoloquinolizidines. Preparative LCMS purification of each final library member **69** established that 476 compounds were successfully produced on 20 mg scale in 65% average yield and >90% chemical purity.

### II.4. Identification and Initial Biological Evaluation of Indoloquinolizidines

In the effort to identify new inducers of mPT, the aforementioned library was screened in CHO-K1 cells, and cellular ATP levels were measured following 30 minutes of drug incubation. We hypothesized that we could take advantage of this simple readout

to find inducers of mPT, which acted directly on the mPTP itself, or generated secondary messages, which led to induction of permeability transition. Subsequent biological and biochemical evaluation would shed light on the mode of action of the small molecule hits. Additionally, our initial work in this area indicated that if the mechanism of mPT was connected to the perturbation of calcium homeostasis, the specific mode of action could be tracked by common phenotypic similarities within each molecular class.

### *II.4.1. Effects of Indoloquinolizidines on ATP Synthesis*

Compounds that exhibited potent ATP depletion were characterized in dose-dependent secondary assays, in the presence and absence of inhibitors of both glycolysis (2-deoxy-D-glucose, **51**) and OXPHOS (antimycin-A, **50**). Indoloquinolizidine **74** (Scheme II.3) was identified as the most active library member, and it was re-synthesized on a preparative scale, purified by conventional flash chromatography over silica gel, and subjected to a series of cell-based assays. Indoloquinolizidine **74** exhibited potent suppression of ATP synthesis, without synergy in the presence of inhibitors of primary

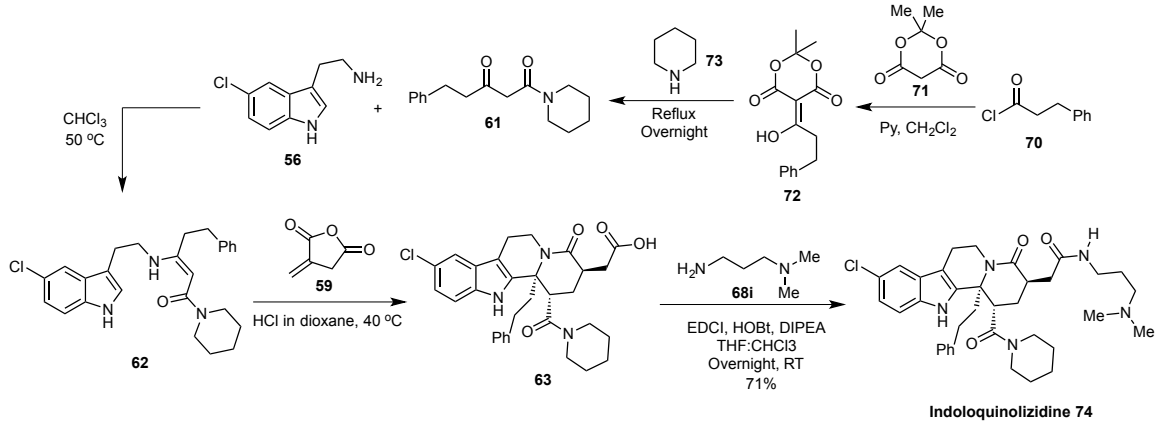


**Scheme II.3:** Synthesis of most active indoloquinolizinde analog (**74**).

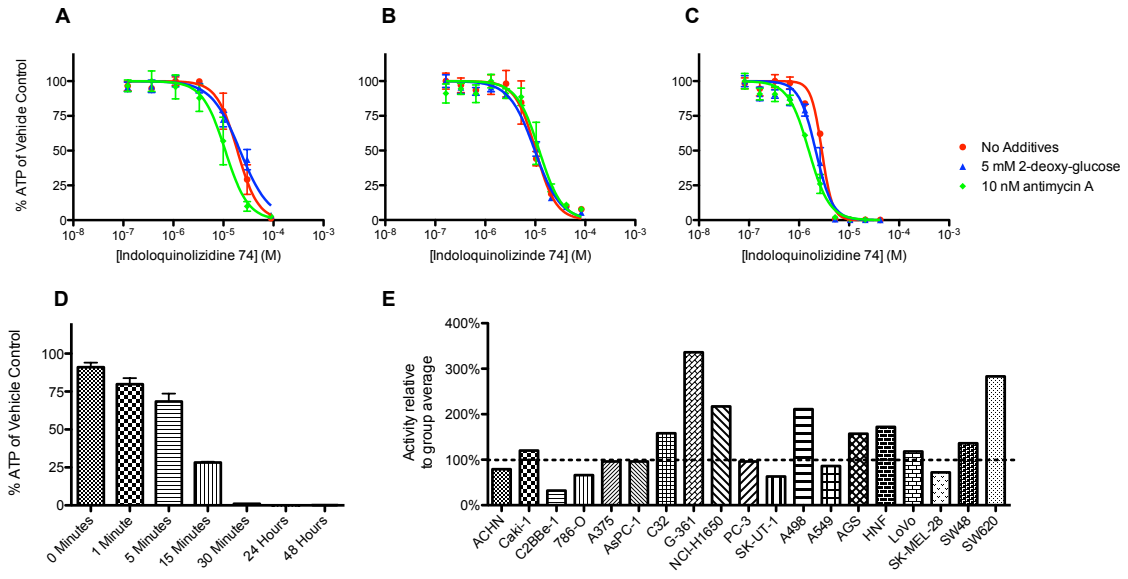


**Figure II.7.** ATP depletion profiles of **74** in A. CHO-K1 cells, B. 143B.TK- cells, C. Molt-4 cells, D. Kinetics of ATP depletion following treatment with **74**, E. Conservation of **74** activity across multiple human cancer cell lines.

carbon metabolism (Figure II.7), implicating it as a possible inducer of mPT. This response was conserved in 143B.TK- cells, as well as Molt-4 cells (Figures II.9-B and II.9-C). Additionally, treatment with indoloquinolizidine **74** against a panel of human tumor cell lines (Figure II.7-E) indicated that the effects of indoloquinolizidine **74** are highly conserved across a variety of human cancers. Kinetic analysis of ATP depletion showed that 30 minutes of drug incubation was the ideal incubation time for the maximum effect of indoloquinolizidine **74** (Figure II.7-D).

### *II.4.2. Effects of Indoloquinolizidines on Cellular Calcium*

Once identified as a potential inducer of mPT, we evaluated the ability of **74** to disrupt calcium homeostasis. Fluo-4 is a cell permeable, calcium-sensing, fluorescent dye, which is loaded in live cells as an acetoxymethyl ester. Non-specific esterases cleave the dye into its active form, labeling the entire cell. Upon calcium binding (Kd in buffer: 335 nM), fluo-4 undergoes a near 100-fold increase in fluorescence intensity and is well suited for tracking large, cell-wide changes in free $Ca^{2+}$ levels. Molt-4 cells were loaded with fluo-4 and live changes in free $Ca^{2+}$ levels were tracked by flow cytometry, in real time. The results of this analysis are shown in Figure II.8. Addition of 30 μM of indoloquinolizidine **74** led to a dramatic 10-fold increase in free calcium, which peaked after 15 minutes. Comparison of these data with our kinetic analysis of ATP depletion indicates that calcium mobilization precedes loss of ATP synthesis, and provides indirect evidence that the bioenergetic instability induced by indoloquinolizidine **74** is caused by $Ca^{2+}$-mediated opening of the permeability transition pore. Indoloquinolizidine **74**'s ability to mobilize calcium was also quite distinct from other mPT-inducers. Treatment of Molt-4 cells with calcimycin (**54**) and tunicamycin (**52**) under the same conditions resulted in elevation of cytosolic $Ca^{2+}$, but the magnitude and kinetics of the $Ca^{2+}$-mobilization event reveal that indoloquinolizidine **74** is relatively slow acting on cellular populations.

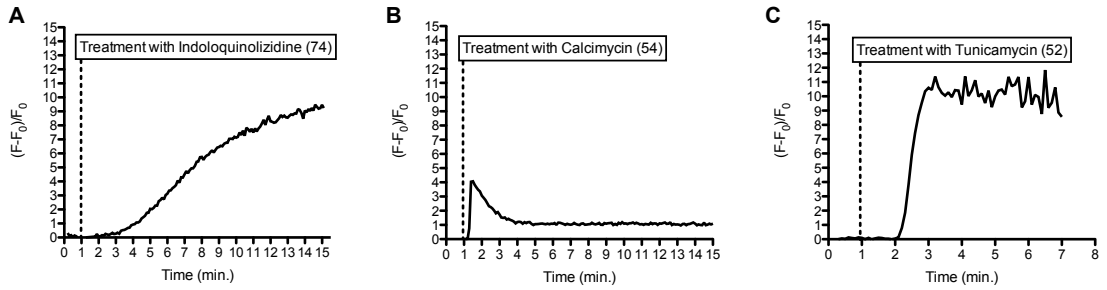


**Figure II.8.** Kinetics of calcium mobilization following treatment with A. 30 μM indoloquinolizidine **74**, B. 25 μM calcimycin (**54**), and C. 20 μM tunicamycin (**52**).

## II.5. Effects of indoloquinolizidines on mitochondria

While the primary location of intracellular $Ca^{2+}$ stores are in the endoplasmic reticulum, the mitochondria shape and decode cellular calcium signals by taking up and releasing cytosolic $Ca^{2+}$.[62] As mentioned previously, this uptake is driven forward by the negative electrical potential across the mitochondrial inner membrane, and has a variety of consequences depending on the organization of mitochondria within the cell.[62] For example, in excitable cells, mitochondria localized around voltage-dependent $Ca^{2+}$ channels on the plasma membrane, buffer the $Ca^{2+}$ microdomain, reducing the magnitude of exocytosis.[63] Direct action of indoloquinolizidine **74** on mitochondria, either through induction of permeability transition or by nonspecific action on the mitochondrial membrane, could cause loss of mitochondrial calcium and subsequent uptake by adjacent mitochondria, leading to further induction of mPTP opening. This domino-like collapse of mitochondrial integrity could lead to the collapse of energy homeostasis that we observed in our initial evaluation of **74,** as well as the sustained increase in cytosolic $Ca^{2+}$ that we observed in follow up experiments. To better understand the effect of

indoloquinolizidine **74** on these organelles, we performed experiments with both whole cells and isolated mitochondria.

### *II.5.1. Effect of Indoloquinolizidines on Mitochondrial Permeability Transition*

Initially, we aimed to test the effects of indoloquinolizidine **74** on the mPT pore in whole cells. Therefore, treated cells were analyzed by fluorescent microscopy using the calcein/$Co^{2+}$ indicator system. (Figure II.9). Cells were additionally treated with 5 μM cyclosporine A in a parallel experiment to determine whether indoloquinolizidine **74**

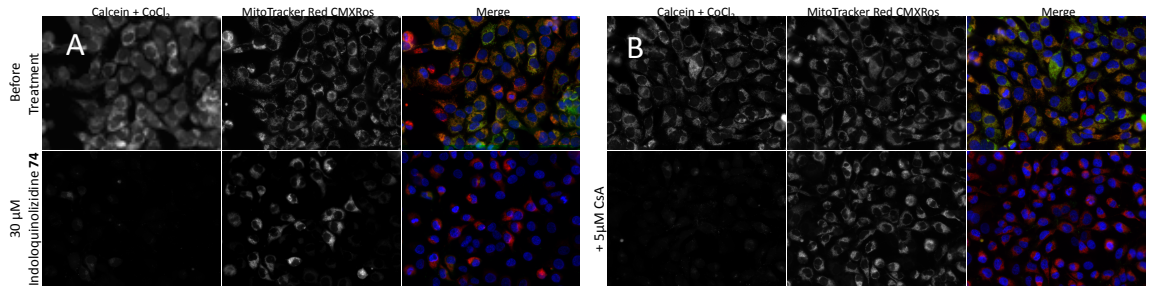


**Figure II.9:** Permeability transition, induced by indoloquinolizidine **74**. A. mPT without additives. B. mPT following pretreatment with 5 μM cyclosporine A. Merge channels: mitochondria loaded with calcein (green), mitochondria loaded with MitoTracker Red (red), nuclei loaded with Hoechst 33342.

was inducing pore opening via a similar mechanism to methyl jasmonate (**49**). Following 30 minutes of incubation at room temperature, 30 μM indoloquinolizidine **74** induced mPT (Figure II.9). However, pretreatment with 5 μM cyclosporine A had no protective effects, indicating that indoloquinolizidine **74** was inducing mPT via a mechanism distinct from methyl jasmonate (**49**, Figure II.1). This evidence corroborates our

hypothesis that indoloquinolizidine **74** induces mPT via a mechanism involving secondary messengers (instead of acting directly on the pore itself), however, understanding the kinetics of calcium mobilization with respect to loss of mitochondrial integrity was essential to understanding mechanism of **74**.

### *II.5.2. Kinetic Analysis of Calcium Mobilization and Mitochondrial Membrane Potential Loss*

To evaluate the kinetics of calcium mobilization and mitochondrial membrane potential simultaneously, we performed dual-dye experiments, which tracked cell-wide calcium mobilization and mitochondrial membrane potential ($\Psi_m$) in real time (Figure II.10). 143B.TK- cells were loaded with fluo-4 AM, as well as tetramethylrhodamine ethyl ester (TMRE) and individual cells were tracked following treatment with **74** using confocal microscopy. TMRE is a cell-permeant, red-orange dye, that when cleaved to its active form by nonspecific esterases is cationic, and is therefore readily taken up mitochondria due to the large negative potential across the mitochondrial membrane.[61] TMRE is ideally suited for tracking changes in $\Psi_m$, as the dye is quickly dissipated following loss of mitochondrial integrity, and massive loss of TMRE fluorescence is indicative of permeability transition.[62] While treatment with 30 μM of indoloquinolizidine **74** led to a gradual increase of free $Ca^{2+}$ across an entire population of cells (Figure II.8), individual cells experienced an extreme, very fast mobilization of calcium following a lag phase of approximately 4 minutes. The dramatic increase in free $Ca^{2+}$ immediately precedes loss of mitochondrial integrity (Figure II.10), however we

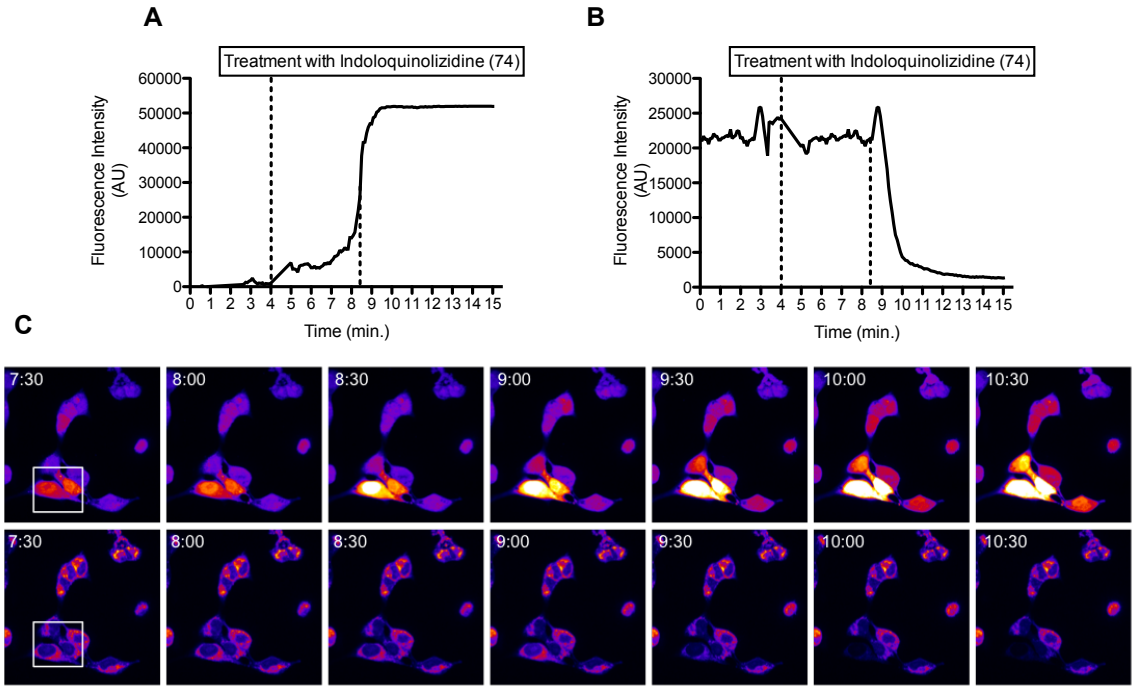


**Figure II.10:** A. Fluo-4 intensity of the indicated region of C. B. TMRE intensity of the indicated region of C. C. Calcium response imaged by spinning disk confocal microscopy. 143B.TK- were loaded with Fluo-4 AM (top row) and TMRE (bottom row).

observed an increase in $\Psi_m$ prior to this collapse. The increase in $\Psi_m$ was presumed to be caused by $Ca^{2+}$-activation of the TCA cycle, causing hyperpolarization of the mitochondrial membrane. While this observation continues to support this compound's action being dependent on a secondary messenger, it does not eliminate the possibility of direct action on the mitochondria, as the sharp increase in free $Ca^{2+}$ is quite close, temporarily, to the loss of $\Psi_m$. Therefore, we elected to evaluate indoloquinolizidine **74** for its ability to sensitize, or protect, isolated rat liver mitochondria from induction of permeability transition.

### *II.5.3. Effect of Indoloquinolizidines on Isolated Rat Liver Mitochondria*

In isolated mitochondria, induction of permeability transition leads to similar consequences as in whole cells. Initially, opening of the pore leads to matrix swelling with consequent distention and disruption of the mitochondrial outer membrane, loss of soluble products from the intermembrane space, dissipation of $\Psi_m$, and loss of small molecules up to 1500 Daltons from the mitochondrial matrix.[61] Driven by the strong negative potential across the mitochondrial membrane, isolated mitochondria also retain their ability to take up calcium, which can induce permeability transition.[64] Isolated mitochondria are loaded in a swelling buffer, which maintains appropriate osmotic pressure, and ATP is added to provide enough chemical energy for the mitochondria to drive transfer of $Ca^{2+}$.[64] Subsequent pulses of calcium are then taken up by the mitochondria, leading to initial spike in absorbance that settles immediately. Once sufficient calcium has been taken up by the mitochondria, permeability transition is induced, resulting in a loss of mitochondrial membrane integrity. As the membrane opens, isolated mitochondria begin to swell, and absorbance at 540 nm collapses. This method proves a convenient way to track direct action on the mPT pore or nonspecific action on the mitochondrial membrane.

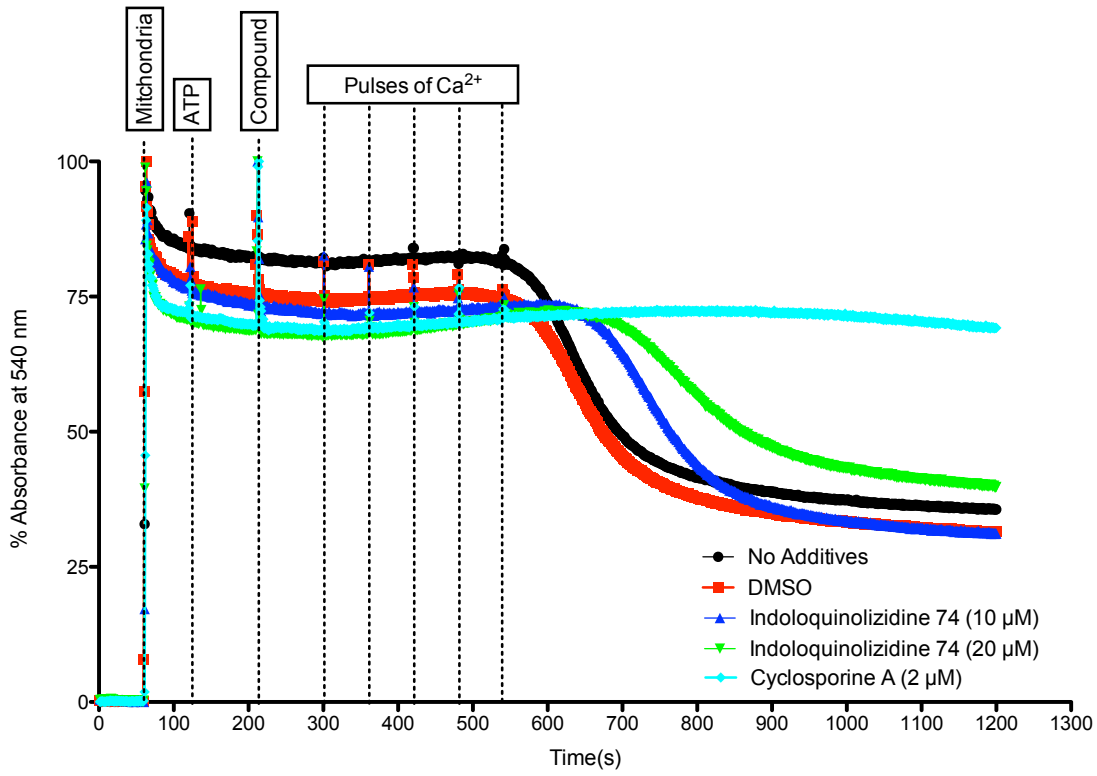


**Figure II.11**: mPTP induction in isolated rat liver mitochondria. Duplicate experiments were performed for each compound, and average absorbance at 540 nm was normalized to vehicle controls.

Our evaluation of indoloquinolizidine **74** in isolated mitochondria is shown in Figure II.11. Treatment of isolated mitochondria with 2 µM of cyclosporine A produced a significant protective effect, completely blocking loss of absorbance following five consecutive pulses of 5 µM of calcium. This corroborates previous reports that cyclosporine A's inhibitory effect on cyclophilin D can decrease mitochondrial sensitivity to calcium. Interestingly, indoloquinolizidine **74** also displayed protective activity, delaying the kinetics of pore opening in a concentration dependent manner. These results confirm our previous observations regarding indoloquinolizidine **74**'s

mechanism of mPT induction being connected to elevation of cytosolic $Ca^{2+}$, and not being the result of direct induction of pore opening. Therefore, we elected to comprehensively evaluate the dynamics of calcium mobilization and its effect on cell physiology.

## II.6. Effects of calcium on indoloquinolizidine activity

### *II.6.1. Extracellular calcium and its role in indoloquinolizidine mediated mPT*

Due to the magnitude of calcium mobilized in our initial evaluation of indoloquinolizidine **74**, we hypothesized that calcium from the extracellular environment must be essential to the mechanism of mPT induced by that class of small molecules. We evaluated the extent that extracellular calcium plays a role in mPT by measuring the $Ca^{2+}$-mobilization in live cells using $Ca^{2+}$-free buffer, as well as using $Ca^{2+}$-chelating agents. First, we loaded Molt-4 cells with Fluo-4 AM, and measured intracellular $Ca^{2+}$ concentrations by flow cytometry, in the presence and absence of

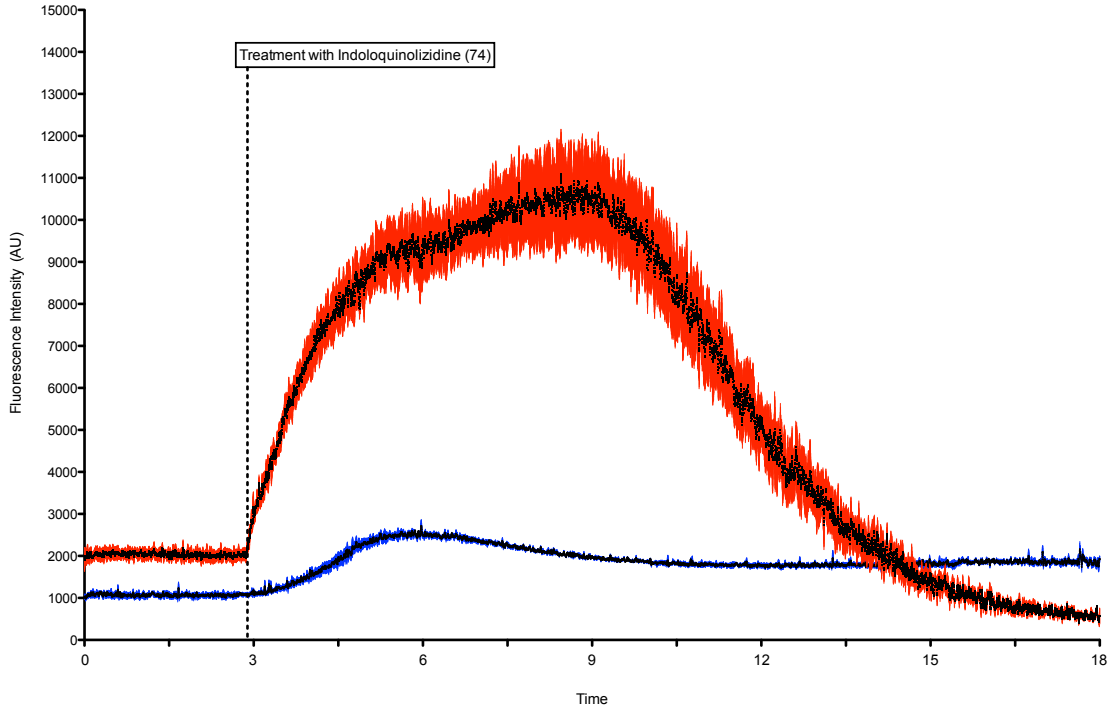


**Figure II.12**: Calcium mobilization following 50 µM treatment with indoloquinolizidine **74**, in the presence or absence of extracellular calcium. Red curve: 2 mM $CaCl_2$ containing buffer, Blue curve: 0 mM $CaCl_2$ containing buffer. Color denotes error between triplicate experiments.

extracellular calcium, following treatment with 50 µM of indoloquinolizidine **74** (Figure II.12). When extracellular $Ca^{2+}$ is absent (blue curve), the magnitude of calcium mobilized is significantly less. However, treatment with indoloquinolizidine **74** still led to an increase in intracellular calcium concentrations, indicating the possibility of mobilization of $Ca^{2+}$ from intracellular storage. To evaluate the effects of extracellular calcium chelation, dose-dependent analyses of intracellular calcium concentrations were performed for both indoloquinolizidine (**74**) and tunicamycin (**52**) (Figure II.13). These analyses show that treatment of Molt-4 cells with **74** (Figure II.13-A) and tunicamycin

(**52**) (Figure II.13-C) both rapidly and potently increase cytosolic $Ca^{2+}$ concentrations, and these effects can be partially rescued by sequestration of extracellular $Ca^{2+}$ by pretreatment with 5 mM EGTA. Additionally, the effects of both compounds on cellular ATP levels can be partially rescued by pretreatment with EGTA (Figures 15-B and 15-D). The partial rescue of ATP synthesis further implicates intracellular $Ca^{2+}$ in the induction of permeability transition.

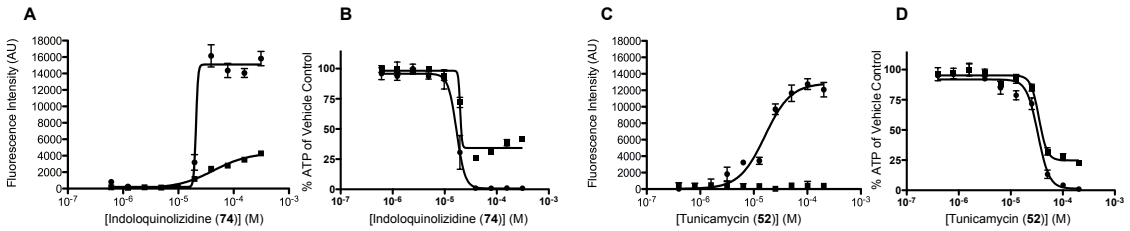


**Figure II.13:** Dose-dependent measurement of intracellular calcium and ATP levels, with and without 5 mM EGTA pretreatment. ● - No additives, ■ - Pretreatment with 5 mM EGTA

### *II.6.2. Intracellular Calcium and its Role in Indoloquinolizidine Mediated mPT*

To test the effects of indoloquinolizidine **74** on intracellular calcium stores, Molt-4 cells were loaded with Fluo-4 and $Ca^{2+}$ concentrations were analyzed by flow cytometry, in the absence of extracellular calcium. Average fluorescence intensities were calculated and are shown in Figure II.14. Thapsigargin (**53**), a potent inducer of ER stress, was used as a positive control for mobilization of intracellular calcium stores and activation of SOCE. When cells were treated in buffer lacking $Ca^{2+}$ (Figure II.14), mobilization of intracellular calcium can be resolved. Following the depletion of intracellular stores, addition of 2 mM $CaCl_2$ to the assay buffer resulted in a sharp

increase in cytosolic $Ca^{2+}$, in both TG (**53**) and cells treated with **74**, implicating SOCE as a major contributor to the calcium influx from the extracellular environment. SOCE is typically activated when intracellular stores are depleted, which strongly implicates endoplasmic reticulum stress as the initial event that leads to heightened cytosolic $Ca^{2+}$ concentrations. Therefore, we aimed to evaluate the effects of **74** on the ER.

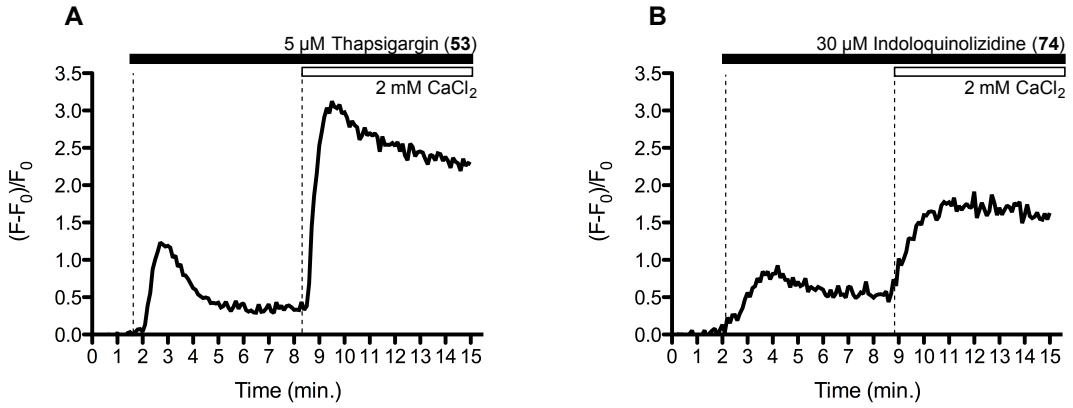


**Figure II.14:** Average Fluo-4 fluorescence intensity in Molt-4 cells determined by flow cytometry following treatment with A. Thapsigargin (**53**) or indoloquinolizidine **74** in $Ca^{2+}$-free buffer.

### II.7. Endoplasmic reticulum stress

As mentioned previously, the endoplasmic reticulum is the primary storage location for intracellular $Ca^{2+}$. In addition to its function as a $Ca^{2+}$ reservoir, the ER is the cellular site for synthesis, folding, and maturation of most secreted and transmembrane proteins.[65] Physiological, pathological, or pharmacological processes that disturb protein folding in the ER lead to the activation of a set of stress response pathways called the Unfolded Protein Response (UPR).[66] The pathways initiated by UPR lead to reductions in

translation of misfolded proteins, upregulation in translation of ER chaperones, and degradation of misfolded proteins through ER-assisted degradation.[67] Activation of UPR can be efficiently tracked by monitoring UPR-associated proteins following the ER stress event, including phosphorylation of PK-like ER kinase (PERK), phosphorylation of eukaryotic initiation factor 2-alpha, upregulation of the molecular chaperone GRP78/BiP, and upregulation of C/EBP homologous protein (CHOP).[68] To evaluate the ability of **74** to induce ER stress and activate UPR, we monitored cellular concentrations of the aforementioned proteins by western blotting following treatment with both **74**, and classical ER stress inducers. Despite enormous effort in the evaluation of UPR stress markers, indoloquinolizidine **74** was never observed to increase the cellular concentration of phospho-PERK, phospho-eIF2-alpha, GRP78/BiP, or CHOP, despite observing increases following treatment with classical ER stress inducers thapsigargin (**53**) and tunicamycin (**52**). These results indicate that the mechanism of **74** may not be connected to ER stress and activation of UPR, since the massive bioenergetic crisis experienced by the cell following treatment with **52** or **53** still allows for UPR activation. Therefore, our attention turned toward the evaluation of other sources of intra- and extracellular calcium that connect to SOCE.

### II.8. Transient receptor potential (TRP) channels

Transient receptor potential channels (TRPs) are a cation-channel superfamily with diverse physiological functions.[69] When activated, TRP channels conduct $Ca^{2+}$, as well as $Na^{+}$ and $K^{+}$, but the activation/gating mechanisms have not been described for most members of the super family.[70] Initial reports indicated that TRP channels were

solely plasma membrane channels mediating $Ca^{2+}$ entry, but the majority of TRPs studied have been shown to localize to intracellular membranes.[71] Therefore, activation of intracellular TRPs results in mobilization of calcium from intracellular stores, but there have been no reports to date linking TRP activation with permeability transition. However, we have demonstrated that known activators of TRP channels lead to a similar bioenergetic crisis in the cell, and result in dose-dependent depletion of cellular ATP concentrations (Figure II.15), similar to other known inducers of mPT. This bioenergetic crisis is coupled to massive $Ca^{2+}$ mobilization, which can be attenuated by known TRP-channel inhibitor, ruthenium red.

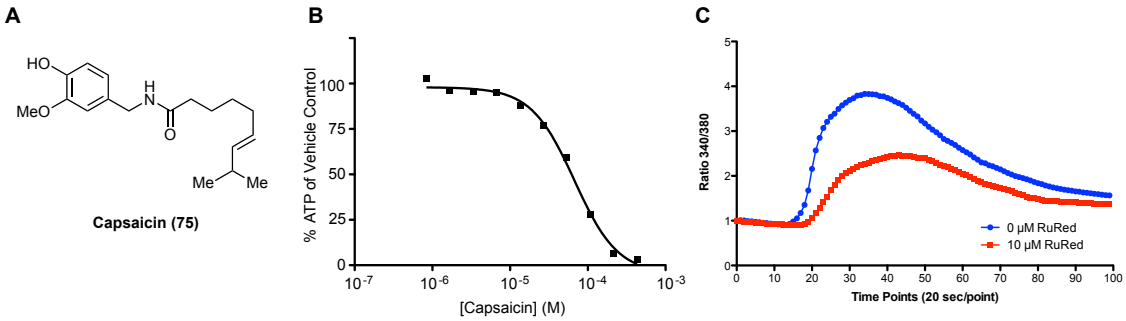


**Figure II.15**: Biological profile of TRPV1 antagonist capsaicin, A. Structure of capsaicin (**75**). B. ATP depletion profile of **75** ($IC_{50}$: 60.88 µM) C. Calcium mobilization of **75** in the presence and absence of ruthenium red (RuRed).

### *II.8.1. Modulation of Indoloquinolizidine Activity with TRP Channel Inhibitors*

To evaluate the effects of **74** on $Ca^{2+}$ mobilized through TRP channels, we examined cells loaded with Fura-2 by confocal microscopy. Fura-2 is a ratiometric calcium indicator that is added to live cells as an acetoxymethyl ester. Following

cleavage to the active dye, Fura-2's binding to calcium changes its fluorescence excitation spectrum, allowing for measurements to be performed ratio-wise, eliminating the effect of dye concentration on $Ca^{2+}$ measurement.[72] Ratiometric measurement of $Ca^{2+}$ concentrations also provides greater detail than other methods, allowing for measurement of very small $Ca^{2+}$ changes. 143B.TK- cells were pretreated with a vehicle control, or known inhibitors of TRP channels: 2-aminoethoxydiphenylborate (2-APB) or ruthenium red (RuRed).

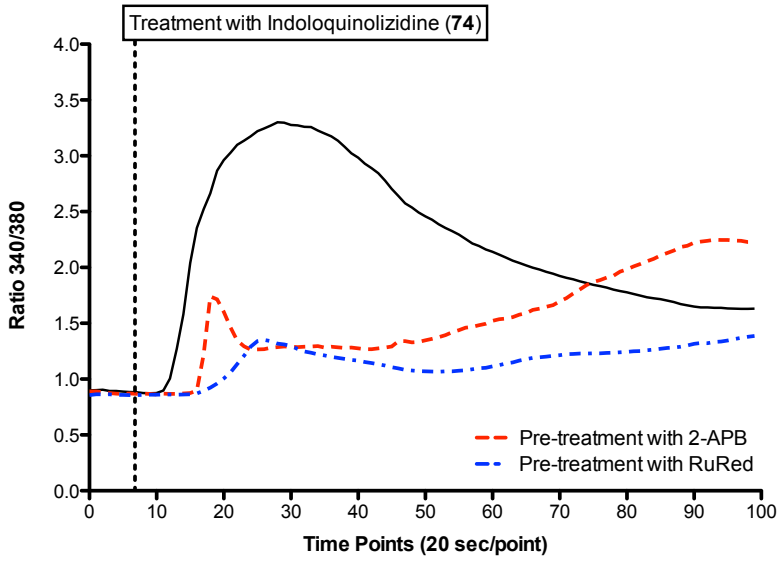


**Figure II.16**: Calcium mobilization following treatment with 30 μM of indoloquinolizidine **74**, in the presence or absence of TRP channel inhibitors 2-aminoethoxydiphenyl borate (2-APB) or Ruthenium Red (RuRed).

After allowing for equilibration, indoloquinolizidine **74** was added, and changes in fluorescence were measured in real time. The results of these analyses are shown in Figure II.16. As observed previously, treatment with indoloquinolizidine **74** resulted in a

dramatic increase in cytosolic $Ca^{2+}$, which reached a maximum after approximately 5 minutes. Interestingly, pretreatment with 2-APB dramatically altered the kinetic profile of $Ca^{2+}$ mobilization, and pretreatment with RuRed led to a near complete shutdown. The difference between 2-APB and RuRed pretreatment is presumably attributed to the breadth of their activities; RuRed affects a much wider group of the TRP super family. These results indicate that the $Ca^{2+}$ mobilization induced by indoloquinolizidine (**74**) is likely connected to the activities of several members of the TRP channel family, providing a connection between mobilization of intra- and extracellular $Ca^{2+}$, as well as activation of SOCE.

## II.9. Development of affinity based methods for determining indoloquinolizidine mechanism of action

Due to the phenotypic similarity between **74** and TRP channel modulators, as well as its ability to mobilize internal calcium stores, initiating cell death in the absence of external calcium, we elected to develop affinity-based approaches to determine the small molecule's mechanism of action. While electrophysiology may have shed light on some of the action of **74,** only several isoforms of TRP channels have been studied at significant length. To this date, little evaluation of organellar TRP channels has been reported.[70] Therefore, determination of the molecular target for **74** was prioritized over additional cell-based experiments. To that end, we developed a comprehensive approach, which began with evaluation of the structure-activity relationship (SAR) of **74**, and continued with the development of a photo-activated probe, designed to covalently label the molecular target.

### *II.9.1. Determining indoloquinolizidine structure activity relationships*

To evaluate the structure-activity relationships (SAR) of indoloquinolizidine **74**, we began by evaluating the activities recorded in our initial screen (data not included). Modification of fragment A was highly tolerable, however, modification of fragment B or C led to a moderate decrease in activity, and to fragment D led to a complete loss of activity (Figure II.17-A). Therefore, we synthesized a focused library of indoloquinolizidine analogs that contained moieties relevant for the development of affinity-based approaches. The design of this focused library is shown in Figure II.17-B and -C, and we used our previously established methods for the construction of each analog (Figure II.17-B). Following synthesis and isolation of each member, the focused library was screened for ATP depletion (Figure II.17-D).

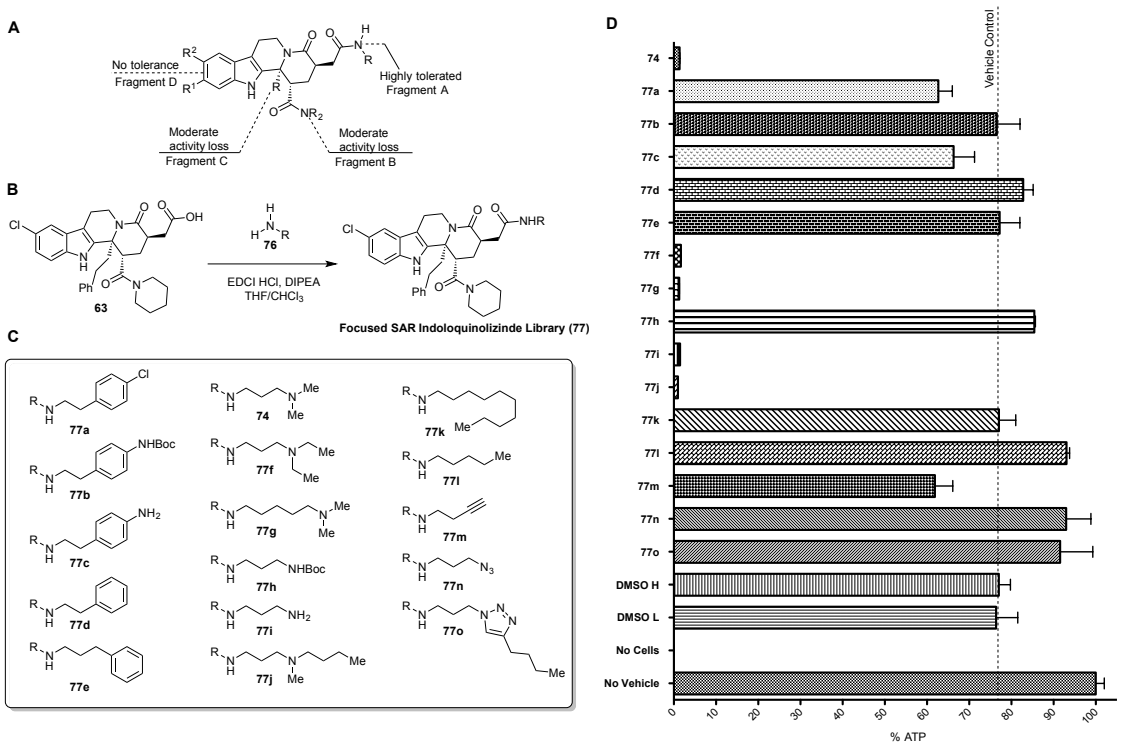


**Figure II.17:** Focused SAR indoloquinolizidine library (**77**) A. Logic gathered from high-throughput screening of indoloquinolizidine library (**69**) B. General synthesis of SAR library (**77**) C. Indoloquinolizidine analogs evaluated for SAR D. ATP depletion profile of library **77**. Compounds were evaluated at 25 μM in Molt-4 cells, and subsequently confirmed by dose-dependent analysis of ATP depletion.

Analysis of the bioactivities of our focused library revealed that the activity of indoloquinolizidines is intimately connected to an *intra cellulas* cation at fragment A. Replacement of the tertiary amine in the parent compound with a methyl ether resulted in a slight loss of activity (initial screen), and protection of the free amine **77i** as Boc-carbamate **77h** resulted in complete loss of bioactivity. This observation was reiterated by the lack of activity in any analog containing a hydrophobic tail as part of fragment A. Drawing on data we gathered from our initial screen and evaluation of our focused

library, we envisioned the design of a photo-activated probe, which will be discussed in the following sections.

### *II.9.2. Synthesis of Photoaffinity indoloquinolizidine*

Photoaffinity labeling (PAL) is a powerful technique, which allows the covalent capture of the protein targets of small molecules.[73] By including a photophore in the design of a small molecule analog, cells can be treated for a given amount of time, and subsequently irradiated to produce a highly reactive intermediate. The reactive intermediate then covalently attaches the analog to its protein target.[74] Incorporation of a bio-orthogonal ligation handle, such as an azide or alkyne, allows for successive pull-down or connection to a reporter group following capture of the protein target.[75] Drawing on methods established during the synthesis of the initial library, we constructed the analog shown in Scheme II.4.

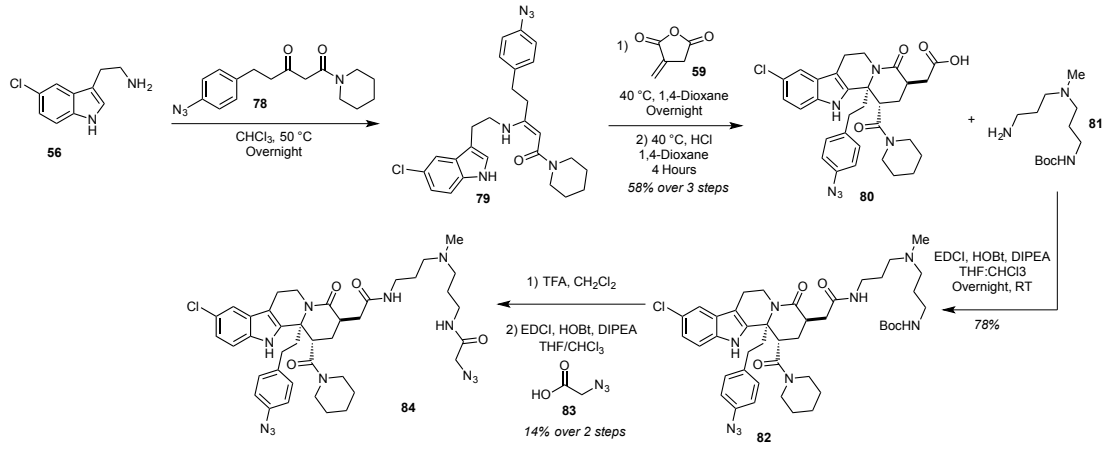


**Scheme II.4:** Synthesis of photo-affinity indoloquinolizidine probe **84**

Indoloquinolizidine **84** was evaluated for its ability to deplete cellular ATP concentrations prior to use in affinity based profiling. Indoloquinolizidine **84** showed a

significant increase in activity over **74** ($IC_{50}$: 0.181 μM), but failed to elucidate specific indoloquinolizidine-binding proteins in labeling studies.

## II.10. Conclusion

We have developed robust and simple methods for screening and characterizing small molecules, which induce permeability transition. We currently hypothesize that indoloquinolizidine **74** can possibly activate members of the TRP super family of $Ca^{2+}$ channels, leading to mobilization of intracellular stores. Subsequent activation of store operated calcium entry (SOCE), leads to a rapid, dramatic increase in cytosolic $Ca^{2+}$, which is taken up by active mitochondria. Once the mitochondrial matrix $Ca^{2+}$ concentration reaches a critical threshold, permeability transition is activated, resulting in a complete collapse of mitochondrial integrity, resulting in rapid depletion of cellular ATP concentrations. Treated cells then rapidly undergo necrotic cell death, as the bioenergetic crisis leaves little room for activation of cellular stress responses. Our work has yielded a new class of pharmacological probes, which may find future use in studying the $Ca^{2+}$-mediated induction of mPT.

## II.11. References


1) Lin, M.; Beal, F. Mitochondrial dysfunction and oxidative stress in neurodegenerative diseases**.** *Nature.* **443**, 787-795.

2) Brenner, C.; Moulin, M. Physiological Roles of the Permeability Transition Pore. *Circ. Res*. **2012**, 111 (9), 1237-1247.

3) Haworth, R. A.; Hunter, D. R. The $Ca^{2+}$-induced membrane transition in mitochondria. *Arch. Biochem. Biophys.* **1979**, 195, 460–467.

4) Kromer, G.; Galluzzi, L.; Brenner, C. Mitochondrial membrane permeabilization in cell death *Physiol. Rev.* **2007**, *87*, 99–163.

5) Zorov, D. B.; Juhaszova, M.; Yaniv, Y.; Nuss, H. B.; Wang, S.; Sollott, S. J. Regulation and pharmacology of the mitochondrial permeability transition pore. *Cardiovasc. Res.* **2009**, 83, 213–225.

6) Baines, C. P. The cardiac mitochondrion: nexus of stress. *Annu. Rev. Physiol.* **2010**, 72, 61–80.

7) Forte, M.; Bernardi, P. Genetic dissection of the permeability transition pore. *J. Bioenerg. Biomemb.* **2005**, *37*, 121–128.

8) Halestrap, A. P.; Brenner, *C*. The adenine nucleotide translocase: a central component of the mitochondrial permeability trasntion pore. *Curr. Med. Chem.* **2003**, 10, 1507–1525.

9) Granville, D. J.; Gottlieb, R. A. The mitochondrial voltage-dependent anion channel as a therapeutic target for initiating cell death. *Curr. Med. Chem.* **2003**, *10*, 1527–1533.

10) Waldmeier, P. C.; Zimmermann, K.; Qian, T.; Tintelnot-Blomey, M.; Lemasters, J. J. Cyclophilin D as a drug target. *Curr. Med. Chem.* **2003**, 10, 1485–1506.

11) Pastorino, J. G.; Hoek, J. B. Hexokinase II: the integration of energy metabolism and control of apoptosis. *Curr. Med. Chem.* **2003**, *10*, 1535–151.

12) Mathupala, S. P.; Ko, Y. H.; Pedersen, P. L. Hexokinase II. *Oncogene* **2006**, *25*, 4777–4786.

13) (a) Pastorino, J. G.; Chen, S. T.; Tafani, M.; Snyder, J. W.; Farber, J. L. Functional consequences of the sustained or transient activation by Bax of the mitochondrial transition pore. *J. Biol. Chem.* **1998**, 273, 7770–7775.

14) Galiegue, S.; Tinel, N.; Casellas, P. The peripheral benzodiazepine receptor. *Curr. Med. Chem.* **2003**, *10*, 1563–1572.

15) Vaseva, A. V.; Marchenko, N. D.; Ji, K.; Tsirka, S. E.; Holzmann, S.; Moll, U. M. p53 opens the mitochondrial permeability transition pore to trigger necrosis. *Cell.* **2012**, 149, 1536–1548.

16) Baines, C. The Molecular Composition of the Mitochondrial Permeability Transition Pore. *J. Mol. Cell Cardiol.* **2009**, 46 (6), 850–857.

17) Krauskopf, A.; Eriksson, O.; Craigen, W.J.; Forte, M.A.; Bernardi, P. Properties of the permeability transition in VDAC1$^{-/-}$ mitochondria. *Biochim. Biophys. Acta* **2006**,1757, 590–595.

18) Baines, C.P.; Kaiser, R.A.; Sheiko, T.; Craigen, W.J.; Molkentin, J.D. Voltage-dependent anion channels are dispensable for mitochondrial-dependent cell death. *Nat. Cell. Biol.* **2007**, 9, 550–555.

19) Kokoszka, J.; Waymire, K.G.; Levy, S.E.; Sligh, J.E.; Cai, J.; Jones, D.P.; MacGregor, G.R.; Wallace, D.C. The ADP/ATP translocator is not essential for the mitochondrial permeability transition pore. *Nature,* **2004**, 427, 461–465.

20) Kroemer, G.; Zamzami, N.; Susin, S.A. Mitochondrial Control of Apoptosis. *Immunol*. *Today*, **1997**, 18, 44–51.

21) Gunter, T.E.; Pfeiffer, D.R. Mechanisms by which mitochondria transport calcium. *Am. J. Physiol.* **1990**, 258, C755–C786.

22) Broekemeier, K.M.; Iben, J.R.; le Van, E.G.; Crouser, E.D.; Pfeiffer, D.R. Pore formation and uncoupling initiate a $Ca^{2+}$-independent degradation of mitochondrial phospholipids. *Biochemistry*, **2002,** 41, 7771–7780.

23) Long, Q.; Yang, K.; Yang, Q. Regulation of mitochondrial ATP synthase in cardiac pathophysiology. *Am. J. Cardiovasc. Dis.* **2015**, 5 (1), 19–32.

24) Woodfield, K.; Ruck, A.; Brdiczka, D.; Halestrap, A. P. Direct demonstration of a specific interaction between Cyp-D and the adenine nucleotide translocase confirms their role in the mitochondrial permeability transition. *Biochem. J*. **1998,** *336*, 287–290.

25) Baines, C. P. et al. Loss of cyclophillin D reveals a critical role for mitochondrial permeability transition in cell death. *Nature* **2005**, *434*, 658–662.

26) Crompton, M.; Ellinger, H.; Costi, A. Inhibition by cyclosporine A of a $Ca^{2+}$-dependent pore in heart mitochondria activated by inorganic phosphate and oxidative stress. *Biochem. J.* **1988**, *255*, 357–360.

27) Harr, M.W.; Disterlhorst, C.W. Apoptosis and Autophagy: Decoding Calcium Signals that Mediate Life or Death. *Cold Spring Harb. Perspect. Biol.* **2010**, 2 (10).

28) Park, C.; Sadaghiani, A.; Dolmetsch, R. C, A. B. Compounds That Modulate Store Operated Calcium Channels. The Board Of Trustees Of The Leland Stanford Junior University, assignee. **2012**. Patent WO 2012079020 A2.

29) Roderick, H.L.; Cook, S.J. $Ca^{2+}$ signaling checkpoints in cancer: Remodeling $Ca^{2+}$ for cancer cell proliferation and survival. *Nature Reviews Cancer.* **2008**, 8, 361–375.

30) Goonasekera, S.A.; Molkentin, J.D. Unraveling the secrets of a double life: contractile versus signaling $Ca^{2+}$ in a cardiac myocytes. *Journal of Molecular and Cellular Cardiology*. **2012**, 52, 317–322.

31) Bootman, M.D.; Lipp, P. Calcium Signaling and Regulation of Cell Function. *Encyclopedia of Life Sciences*. **2001**, 3, a003947.

32) Catterall, W. Voltage-gated Calcium Channels. *Cold Spring Harb. Persp. Biol.* **2011**, 3 (8).

33) Antkiewicz-Michaluk, L. Receptor and voltage-operated ion channels in the central nervous system. *Pol. J. Pharmacol.* **1995**, 47 (3), 253-264.

34) Sachs, F. Stretch-Activated Ion Channels: What are they? **2010**, 25 (1), 50-56.

35) Roos, J.; DiGregorio, P.J.; Yeromin, A.V.; Ohlsen, K.; Lioudyno, M.; Zhang, S.; Safrina, O.; Kozak, J.A.; Wagner, S.L.; Cahalan, M.D.; Velicelebi, G.; Stauderman, K.A. STIM1, an essential and conserved component of store-operated $Ca^{2+}$ channel function. *J. Cell Biol.* **2005**, 169, 435–445.

36) Ong, H.L.; Cheng, K.T.; Liu, X.; Bandyopadhyay, B.C.; Paria, B.C.; Soboloff, J.; Pani, B.; Gwack, Y.; Srikanth, S.; Singh, B.B.; Gill, D.L.; Ambudkar, I.S. Dynamic assembly of TRPC1–STIM1–Orai1 ternary complex is involved in store-operated calcium influx: evidence for similarities in store-operated and calcium release-activated calcium channel components. *J. Biol. Chem.* **2007**, 282, 9105–9116.

37) Vig, M.; Peinelt, C.; Beck, A.; Koomoa, D.L.; Rabah, D.; KoblanHuberson, M.; Kraft, S.; Turner, H.; Fleig, A.; Penner, R.; Kinet, J.P. CRACM1 is a plasma membrane protein essential for store-operated $Ca^{2+}$ entry. *Science*. **2006**, 312, 1220–1223.

38) Zhang, S.L.; Yeromin, A.V.; Zhang, X.H.; Yu, Y.; Safrina, O.; Penna, A.; Roos, J.; Stauderman, K.A.; Cahalan, M.D. Genome-wide RNAi screen of $Ca^{2+}$ influx identifies genes that regulate $Ca^{2+}$ release-activated $Ca^{2+}$ channel activity, *Proc. Natl. Acad. Sci. U. S. A.* **2006**, 103, 9357– 9362.

39) He, H.; Lam, M.; McCormick, T.S.; Distelhorst, C.W. Maintenance of Calcium Homeostasis in the Endoplasmic Reticulum by Bcl-2. *J. Cell Biol.* **1997**, 138 (6), 1219-1228.

40) Luciani, D.S.; Gwiazda, K.S.; Yang, T.L.; Kalynyak, T.B.; Bychkivska, Y.; Frey, M.H.; Jeffrey, K.D.; Sampaio, A.V.; Underhill, T.M.; Johnson, J.D. Roles of IP3R and RyR Ca2+ channels in endoplasmic reticulum stress and beta-cell death. *Diabetes.* **2009**, 58 (2), 422-432.

41) Hajnoczky, G.; Csordas, G.; Madesh, M.; Pacher, P. Control of apoptosis by IP(3) and ryanodine receptor driven calcium signals. *Cell Calcium.* **2000,** 28, 349–363.

42) Walter, L.; Hajnóczky, G. Mitochondria and endoplasmic reticulum. *J. Bioenerg. Biomebr.* **2005**, *37*, 191–206.

43) Vance, J. E. Phospholipid synthesis in a membrane fraction associated with mitochondira. *J. Biol. Chem.* **1990**, *265*, 7248–7256.

44) Deniaud, A.; Sharaf el dein, O.; Maillier, E.; Poncet, D.; Kroemer, G.; Lemaire, C.; Brenner, C. Endoplasmic reticulum stress induces calcium-dependent permeability transition, mitochondrial outer membrane permeabilization and apoptosis. *Oncogene* **2008**, *27*, 285-299.

45) Petersén, A.; Castilho, R.F.; Hansson, O.; Wieloch, T.; Brundin, P. Oxidative stress, mitochondrial permeability transition and activation of caspases in calcium ionophore A23187-induced death of cultured striatal neurons. *Brain Res*. **2000**, 857 (1-2), 20-29.

46) Costantini, P.; Jacotot, E.; Decaudin, D.; Kroemer, G. Mitochondrion as a novel target of anticancer therapy. *J. Natl. Cancer Inst.* **2000**, *92*, 1042–1053.

47) Ulanovskaya, O.A.; Janjic, J.; Suzuki, M.; Sabharwal, S.S.; Schumacker, P.T.; Kron, S.J.; Kozmin, S.A. Synthesis enables identification of the cellular target of leucascandrolide A and neopeltolide. *Nature Chem. Biol.* **2008**, *4*, 418–424.

48) Ulanovskaya, O.A.; Cui, J.; Kron, S.J.; Kozmin, S.A. A pairwise chemical genetic screen identifies new inhibitors of glucose transport. *Chem. Biol.* **2011**, *18*, 222–230.

49) Cui, J.; Hao, J.; Ulanovskaya, O.A.; Dundas, J.; Liang, J.; Kozmin, S.A. Creation and manipulation of common functional groups en route to a skeletally diverse chemical library. *Proc. Natl. Acad. Sci. USA* **2011**, *17*, 6763–6768.

50) Browse, J. Jasmonate Passes Muster: A Receptor and Targets for the Defense Hormone. *Annu. Rev. Plant Biol.* **2009**, *60*, 183–205

51) Flescher, E. Jasmonates in cancer therapy. *Cancer Lett.* **2007**, 245, 1–10.

52) Fingrut, O.; Flescher, E.; Plant stress hormones suppress the proliferation and induce apoptosis in human cancer cells. *Leukemia.* **2002**, 16, 608–616.

53) Goldin, N.; Arzoine, L.; Heyfets, A.; Israelson, A.; Zaslavsky, Z.; Bravman, T.; Bronner, V.; Notcovich, A.; Shoshan-Barmatz, V.; Flescher, E. Methyl jasmonate

binds to and detaches mitochondria bound hexokinase. *Oncogene* **2008**, *27*, 4636–4643.

54) Petronilli, V. et al. Transient and long-lasting openings of the mitochondrial transition pore can be monitored directly in intact cells by changes in mitochondrial calcein fluorescence. *Biophys. J.* **1999**, *76*, 725–734.

55) Heifetz, A.; Keenan, R.W.; Elbein, A.D. Mechanism of action of tunicamycin on the UDP-GlcNAc:dolichyl-phosphate GlcNAc-1-phosphate transferase. *Biochemistry*. **1979**, 18 (11), 2186–2192

56) Price, N.P.; Tsvetanova, B. Biosynthesis of the tunicamycins: a review. *J. Antibiot.* **2007**, 60 (8), 485-491.

57) (a) Qian, T.; Herman, B.; Lemasters, J.J. The mitochondrial permeability transition mediates both necrotic and apoptotic death of hepatocytes exposed to Br-A23187. *Toxicol. Appl. Pharmacol.* **1999**, 154 (2), 117-125. (b) Morgan, A.J.; Jacob, R. Ionomycin enhances Ca2+ influx by stimulating store-regulated cation entry and not by a direct action at the plasma membrane. *Biochem J.* **1994**, 300 (Pt. 3), 665–672.

58) O'Connor, S.E.; Maresh, J.J. Chemistry and biology of monoterpene indole alkaloid biosynthesis. *Nat. Prod. Rep.* **2006**, 23 (4), 532-547.

59) Abelman, M.; Curtis, J.; James, D. Formal [3+3] cycloaddition reactions. *Tetrahedron Lett.* **2003**, *44*, 6527–6531.

60) Scaduto, R.C.; Grotyohann, L.W. Measurement of mitochondrial membrane potential using fluorescent rhodamine derivatives. *Biophys. J.* **1999**, 76 (1), 469-477.

61) Zamzami, N.; Kroemer, G. Methods to Measure Membrane Potential and Permeability Transtion in the Mitochondria During Apoptosis. *Methods in Molecular Biology*. **2004,** 282, 103-115

62) Santo-Domingo, J.; Demaurex, N. Calcium uptake mechanisms of mitochondria. *Biochimica et Biophysica Acta*. **2010**, 1797 (6), 907-912.

63) Montero, M.; Alfonso, M.T.; Carnicero, E.; Cuchillo-Ibanez, I.; Albillos, A.; Garcia, A.G.; Garcia-Sancho, J.; Alvarez, J. Chromaffin-cell stimulation triggers fast millimolar mitochondrial $Ca^{2+}$ transients that modulate secretion. *Nat. Cell Biol.* **2000**, 2, 57-61.

64) Pan, X.; Nguyen, T. et al. The physiological role of mitochondrial calcium revealed by mice lacking the mitochondrial calcium uniporter. *Nat. Cell Biol.,* **2013,** 15, 1464–1472.

65) Samali, A.; FitzGerald, U.; Deegan, S.; Gupta, S. Methods for Monitoring Endoplasmic Reticulum Stress and the Unfolded Protein Response. *Int. J. Cell. Biol.* **2010.**

66) Ron, D.; Walter, P. Signal integration in the endoplasmic reticulum unfolded protein response," *Nat. Rev. Mol. Cell Biol.* **2007**, 8 (7), 519–529.

67) Schroder, M.; Kaufman, R.J. The mammalian unfolded protein response. *Annu. Rev. Biochem.* **2005,** 74, 739-789.

68) Mekahli, D.; Bultynck, G.; Parys, J.B.; De Smedt, H.; Missiaen, L. Endoplasmic-Reticulum Calcium Depletion and Disease. *Cold Spring Harb. Perspect. Biol.* **2011,** 3 (6), pii.

69) Clapham, D.E. TRP channels as cellular sensors. *Nature*. **2003**, 426, 517–524.

70) Dong, X.; Wang, X.; Xu, H. TRP Channels of Intracellular Membranes. *J. Neurochem.* **2010**, 113 (2), 313–328.

71) Bezzerides, V.J.; Ramsey, I.S.; Kotecha, S.; Greka, A.; Clapham, D.E.; Rapid vesicular translocation and insertion of TRP channels. *Nature Cell Biology*. **2004**, 6, 709–720.

72) Malgaroli, A.; Milani, D.; Meldoslesi, J.; Pozzan, T. Fura-2 Measurement of Cytosolic Free $Ca^{2+}$ in Monolayers and Suspensions of Various Types of Animal Cells. *J. Cell. Biol.* **1987,** 105, 2145-2155.

73) Geurink P.P.; Prely, L.M.; van der Marel, G.A.; Bischoff, R.; Overkleeft, H.S. Photoaffinity labeling in activity-based protein profiling. *Top. Curr. Chem.* **2012**, 324, 85-113.

74) Vodovozova, E.L. Photoaffinity labeling and its application in structural biology. *Biochemistry.* **2007**, 72 (1), 1-20

75) van Swieten, P.F.; Leeuwenburgh, M.A.; Kessler, B.M.; Overkleeft, H.S. Bioorthogonal organic chemistry in living cells: novel strategies for labeling biomolecules. *Org. Biomol. Chem*. **2005**, 3 (1), 20-27.

76) Rostovtsev, V.V.; Green, L.G.; Fokin, V.V.; Sharpless, K.B. A stepwise huisgen cycloaddition process. *Angew. Chem., Int. Ed.* **2002**, 41, 2596−2599

# CHAPTER III

## ANALYSIS OF EDOGENOUS OXIDATION LEVELS OF VARIOUS CANCER CELLS

*This chapter describes our efforts toward evaluating endogenous levels of oxidative stress, in both the mitochondria and cytosol of a wide variety of cancel cell lines, derived from various tissues. Using a novel, ratiometric, protein-based redox sensor, we evaluated cells from melanoma, colon, breast, lung, renal, central nervous system, and ovarian cancers. The discussion begins with a review of oxidative stress, as well as cellular mechanisms that contribute to the production and elimination of reactive oxygen species (ROS) and other highly reactive metabolites. A brief discussion of ROS and their role in cancer follows. Finally, the chapter concludes with a discussion of our results and their therapeutic implications. Tumor cell lines display wide variability in the level of oxidation of subcellular compartments, ranging from 15% to 99% in the mitochondria and from 7% to 86% in the cytosol. This necessitates enormous care when administering ROS-modulating therapies, as large differences between oxidative stresses can manifest themselves even within the same tissue type.*

## III.1. Introduction

### III.1.1. Oxidative Stress

Oxidative stress is defined as an imbalance in the dynamic equilibrium formed between the generation of free radicals or reactive metabolites, termed oxidants or reactive oxygen species (ROS), and removal of these highly reactive intermediates by antioxidant mechanisms.[1] Although generation of reactive intermediates is a natural consequence of a variety of cellular processes including mitochondrial oxidative phosphorylation (OXPHOS) and protein folding, imbalances can arise from overproduction of reactive molecules, incorporation of reactive species from the exogenous environment (as well as exogenous agents which produce ROS, e.g. ionizing radiation), or a decrease in the capability of cellular antioxidant machinery to clear reactive molecules.[2] Oxidative stress has been implicated in a wide variety of disease states, including atherosclerosis, diabetes, cancer, neurodegeneration, and aging.[3] However, the verdict on oxidative stress and ROS is not so clear. At low levels, ROS can act as signaling molecules, reversibly oxidizing thiol groups to effectively modify protein structure and function.[4] However, at higher concentrations, ROS can non-specifically oxidize proteins, lipids, and DNA,[5] both contributing to genetic instability and leading to global disruption of cellular homeostasis. Additionally, increasing evidence suggests a more prominent role for ROS as direct or indirect mediators of programmed cell death in mammalian and plant cells,[6] and it is now known that mitochondrial ROS are biologically relevant in a variety of other cellular functions, including adaptation to hypoxia, regulation of autophagy, of immunity, of differentiation, and of longevity.[7] The paradoxical relationship that ROS has with cellular function, acting as both a mediator of

cell death and as a driver of proliferation and cell survival, may limit the therapeutic potential of targeting redox homeostasis. However, developing a more complete understanding of ROS, and their roles in both normal and diseased cells, may unlock a therapeutic window for a variety of pathologies and increase our understanding of the action of redox-modulating agents.

### III.1.2. Generation of Reactive Oxygen Species

Most cellular ROS are generated by the mitochondrial respiratory chain, and production is modulated largely by the rate of electron flow through chain complexes.[8] Additionally, it is possible under hypoxic conditions for the respiratory chain to produce nitric oxide, a precursor for other reactive nitrogen species (RNS).[8] Although complex IV (cytochrome oxidase) retains all partially reduced intermediates until full reduction is achieved, other redox centers along the respiratory chain may leak electrons to molecular oxygen, partially reducing it to the superoxide anion. In fact, there are more than eight sites along the mitochondrial respiratory chain that are known to leak electrons to produce reactive intermediates, but their complete roles, especially *in vivo*, are still poorly understood.[9] Superoxide may not be a particularly strong oxidant alone, but it is the precursor to most other ROS, and contributes to the propagation of oxidative chain reactions.[10] For example, dismutation of superoxide by superoxide dismutases (SODs) results in the production of hydrogen peroxide, which can then collaborate with superoxide to generate the vastly reactive hydroxyl radical.[11] Hydrogen peroxide also plays an important physiological role since it is significantly more stable than other ROS, and is small enough to diffuse across long distances within or between cells.[12] Hydrogen

peroxide can also be transported out of the mitochondria via aquaporins,[13] or can passively diffuse through the inner and outer mitochondrial membranes, either to be reduced in the cytosol or to oxidize relevant biomolecules (e.g. DNA in the nucleus).[14] Therefore, at low concentrations, $H_2O_2$ can act as an important signaling molecule, but at higher concentrations can result in irreversible damage resulting in cell death, requiring the cell to tightly control $H_2O_2$ levels.[15] In addition to being the primary source of ROS, the mitochondria also serve as the principal gatekeepers with respect to ROS signaling, hence the tight regulation of ROS is critically important for physiological ROS signaling.

### III.1.3. Antioxidant Defense Mechanisms

Regulation of mitochondrial ROS is performed by several mechanisms. Broadly, antioxidant defense mechanisms include removal of $O_2$, scavenging of reactive oxygen or nitrogen species and their precursors, inhibition of ROS/RNS production, binding of metals needed in the catalysis of ROS generation, and transcriptional/translational up-regulation of endogenous reductases.[16] Superoxide concentration is controlled primarily through its enzymatic conversion to $H_2O_2$ by SODs,[17] and must be kept at very low levels due to its involvement in oxidizing Fe-S clusters or generating peroxynitrite.[10] The mitochondrial matrix contains a specific SOD isoform, which contains manganese in its active site (Mn-SOD or SOD2).[18] Additionally, a copper/zinc-containing SOD (SOD1) and an extracellular SOD (SOD3) contribute to superoxide processing, and are localized to the cytosol and extracellular space, respectively.[19,20]

Several enzymes are responsible for clearing $H_2O_2$, including peroxiredoxins,[21] glutathione peroxidase,[22] and catalase.[23] Unlike other peroxidase antioxidant enzymes,

which derive their peroxidase activity from heme functionality or a selenocysteine in the active site, peroxiredoxins use an active-center cysteine sulfur for catalytic action against the peroxyl –O–O– bond.[24] Activation of this residue imparts, at least for some peroxiredoxins, similar catalytic efficiency to other peroxidases,[24] as well as broad enough substrate specificity as to reduce hydrogen peroxide, organic hydroperoxides, and peroxynitrite.[25,26] Peroxiredoxins are restored to a reduced state by thioredoxins, which are themselves reduced by thioredoxin reductases through the consumption of NADPH as the source of electrons.[21] Gluthathione peroxidases rely on a conserved catalytic triad composed of selenocysteine, tryptophan, and glutamine to reduce hydroperoxides to corresponding alcohols at the expense of thiol functionalities, typically of glutathione (GSH).[22] Gluthathione is itself an essential component of the cell's antioxidant machinery, being the most abundant cellular antioxidant, present at millimolar levels and accounting for up to 90% of the cells' non-protein sulphur.[27] Finally, catalase converts hydrogen peroxide to oxygen and water, and is largely found in peroxisomes.[28] Together, these enzymes maintain endogenous hydrogen peroxide concentrations in the sub-micromolar range, with redox-sensitive transcription maintaining homeostasis in response to dramatic changes in the level of oxidative stress.[29] However, various pathologies can result in increased oxidative stress, either through increased production of ROS, or through decreases in antioxidant capability. Due to ROS's negative effects on cellular homeostasis, it has been suggested that administration of antioxidant therapy may provide benefits in a variety of diseases, and it has been reported in epidemiological studies that many antioxidant compounds posses anti-inflammatory, anti-atherosclerotic, anti-tumor, anti-mutagenic, anti-carcinogenic, anti-bacterial, and anti-viral

activities.[30,31,32] Additionally, it has been suggested that natural intake of antioxidant compounds can reduce the risk of the aforementioned pathologies,[33] but as with ROS, the role of antioxidants in the progression of a variety of diseases is at times paradoxical. This is supported by the observation that the glutathione and thioredoxin antioxidant pathways synergize to drive cancer initiation and progression, with reductions in antioxidant activity being chemopreventive,[34] as well as the observation that administration of antioxidant therapy can, in fact, increase mortality.[35] It appears that cells walk an incredibly fine line between life and death when it comes to the balance between ROS generation and antioxidant pathways, and this razor's edge is most visible in the role that oxidative stress plays in cancer.

### III.2. Oxidant Stress, ROS, and Cancer

Cancer is a heterogeneous collection of diseases with genomic heterogeneities between histologically similar tumors, effectively eliminating the possibility for a universal cancer metabolism model which describes the metabolic requirements to support tumor growth.[36] Nevertheless, oxidative stress and reactive oxygen species have long been associated with cancer. Historically, the increased ROS production observed in cancer cells has been viewed as a negative, toxic, consequence of oncogenic transformation,[37] However, evidence supports that the increased oxidative stress experienced by most cancer cells is caused by heightened metabolic activity and ROS production, and drives the cancer phenotype by stimulating cell growth and proliferation,[38] genetic instability,[39] and senescence evasion.[40] The beneficial effects of increased oxidative stress, are in part, due to modifications of a variety of cellular

signaling pathways including the mitogen-activated protein (MAP) kinase/Erk cascade, phosphoinositide-3-kinase (PI3K)/Akt-regulated signaling cascades, and the IκB kinase (IKK)/nuclear factor κ-B (NF-κB)-activating pathways.[41] Although these benefits can drive and support carcinogenesis, heightened ROS generation can result in detrimental effects to cellular homeostasis. Therefore transformed cells counteract the accumulation of ROS by up regulating antioxidant mechanisms, creating a paradoxical situation of high ROS production alongside high antioxidant levels, requiring very tight control over the redox status of the tumor cell.[42] Additionally, H-Ras-transformed cells, known to produce high levels of ROS, also expressed elevated levels of peroxiredoxin-1 and thioredoxin peroxidase when compared with their benign parental cells,[43] suggesting that enhanced antioxidant activity is necessary for tumor progression.[44]

It has been postulated that the intrinsic ROS stress associated with oncogenic transformation makes tumor cells especially dependent on their antioxidant machinery to counteract the damaging effects of ROS and maintain redox balance in a dynamic state, making these cells particularly sensitive to further oxidative insults, either from increases in ROS production or from deactivation of antioxidant pathways.[45] This hypothesis is supported by reports, which implicate oxidative stress (caused by a variety of chemotherapeutic agents) in the induction of cell death,[14] that promotion of mitochondrial ROS generation can selectively kill cancer cells,[46] and that disruptions in GSH concentrations alongside glutathione peroxidase inhibition can effectively induce cell death.[45] Taken together, these observations indicate that cancer cells rest on a fine edge between life and death, but how can this edge be used therapeutically? In a clinical setting, individualized choice of an optimal ROS-manipulation strategy, whether to use

ROS-elevating or ROS-depleting therapies, requires accurate and convenient measurements for endogenous ROS for prediction of efficacy and systemic toxicity.[47]

Although evaluation of the redox status of several tumor cell lines has been performed, a comprehensive evaluation of the redox status across a wide variety of cancer cells, from a variety of tissues, has not been completed. By developing methods to quickly evaluate a wide variety of cell lines in parallel, it may be possible to link the level of cellular oxidation with phenotypic behavior, resistance to therapy, originating tissue, or metastatic potential.[48] A more complete picture of the redox status of various tumor cell lines may also provide therapeutic insight in the evaluation of agents which alter the redox status of the cell. To that end, we have developed an assay which enables facile evaluation of cellular oxidation levels, in multiple subcellular compartments, providing insights into variable phenotypic behavior between tissue types and cell lines within a tissue class. The results of this study are discussed in the following section.

### III.3. Measurement of Cellular Oxidation Levels

Measurement of cellular oxidation levels, can at times, be quite challenging. This is in large part due to technical limitations of methods designed to measure oxidative stress,[49] as well as the cell's spatial and temporal control of ROS signaling events. For example, use of lucigenin luminescence to track superoxide concentration is convoluted by lucigenin's mediation of superoxide production.[50] Also, many probes, like DCF, fail to resolve oxidant stress between subcellular compartments, or are not ratiometric, resulting in artifacts from changes in intracellular dye concentration, excitation intensity, or path length caused by changes in cell shape.[49,51] To avoid the negative aspects of using the

aforementioned probes, we employed a novel, redox-sensitive protein sensor, which was separately targeted to both the cytosol and mitochondrial matrix, to measure differences in cellular oxidation levels amongst a wide variety of different cancer cell lines, originating from different tissue sources. This sensor, RoGFP, contains engineered cysteine residues, enabling dithiol formation in response to oxidant stress, strongly and reversibly tying its fluorescence emission/excitation spectra to the redox state of the contained cysteines.[52] Additionally, by exposing treated cells to strong reducing or oxidizing (DTT or $H_2O_2$, respectively) agents at the conclusion of an experiment, percent oxidation levels can be calibrated and compared between cell and tissue types.

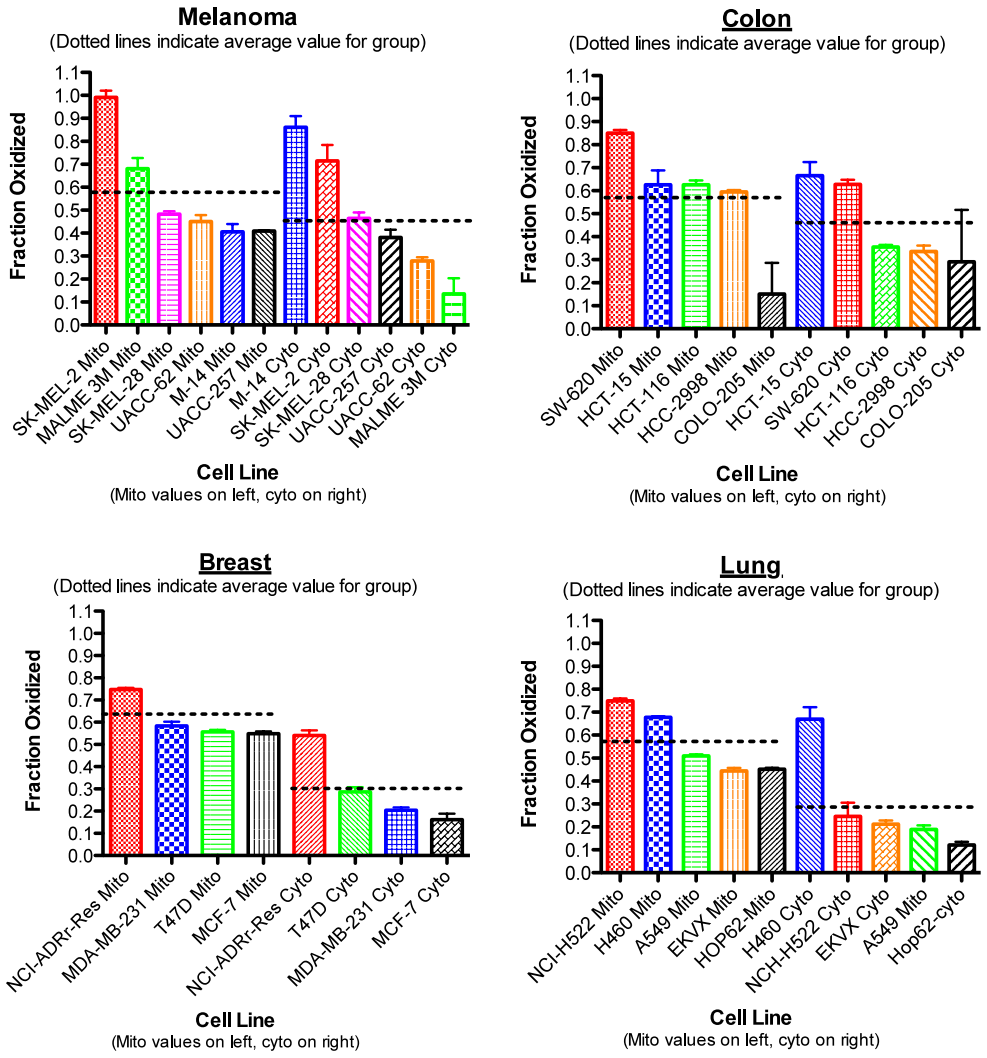


**Figure III.1:** Fractional oxidation of tumor cell lines in both the mitochondrial matrix (left panels) and cytosol (right panels). Colors are matched to connect subcellular compartments, and dotted lines indicate averages within a given group. Experiments were performed in quadruplicate, and error bars are shown. A. Melanoma cell lines, B. Colon cell lines, C. Breast cell lines, D. Lung cell lines, E. Renal cell lines, F. Central nervous system cell lines, G. Ovarian cell lines.

Remaining graphs (see below) are part of **Figure III.1**.

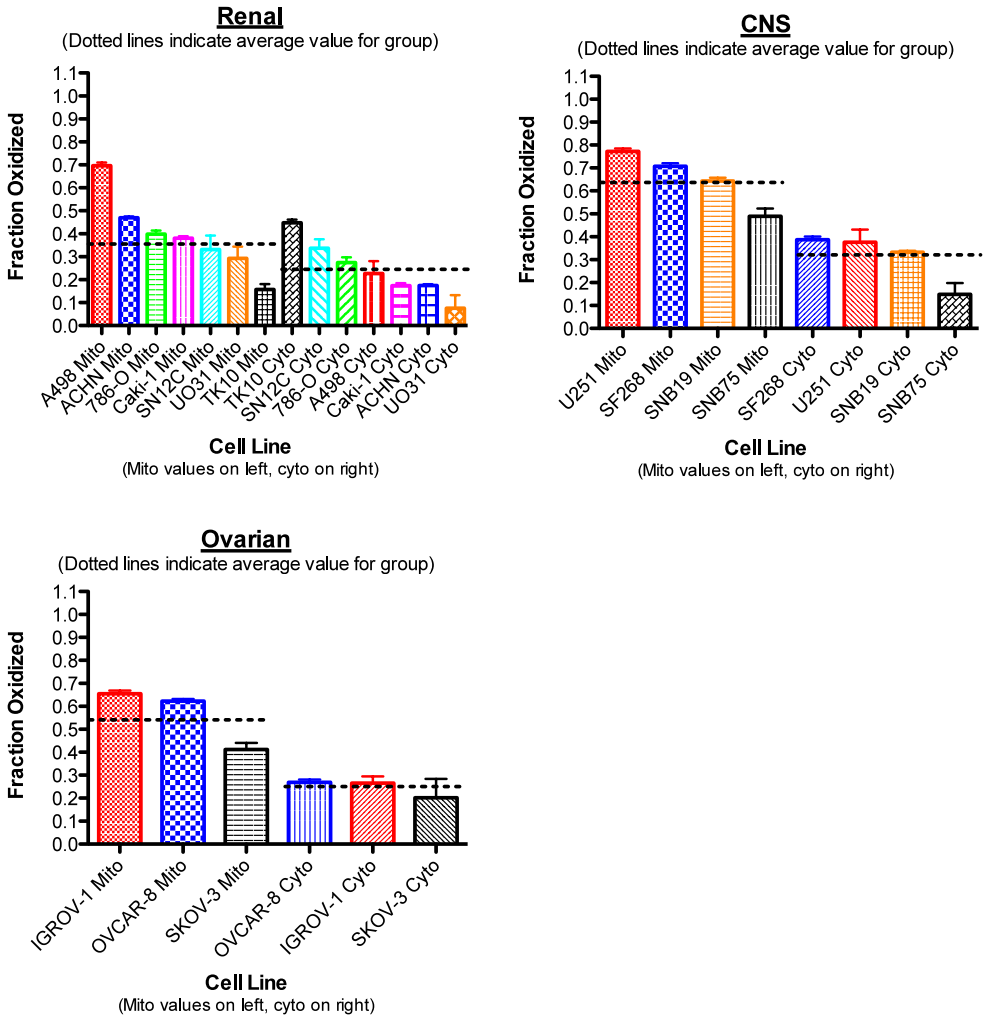


Several common trends emerged during the evaluation of the redox status of multiple cell lines. As expected, the mitochondrial matrix was generally more oxidized (Average mitochondrial oxidation level: 56%; Average cytosolic oxidation level: 33%) than the cytosol, which correlates well with mitochondria being the primary source of ROS production. However, several notable exceptions were found in several different tissue types, including melanoma, colon, and renal. M-14 cells (melanoma) displayed significantly higher oxidation levels in the cytosol (41% mitochondria, 86% cytosol), as

did TK10 cells (renal, 15% mitochondria, 44% cytosol). COLO-205 and HCT-15 cells (both colon), as well as SN12C cells (renal) displayed similar levels of oxidation in both the mitochondria and cytosol, with the cytosol being slightly more oxidized. This may suggest that mitochondrial antioxidant defense mechanisms are up-regulated in these cell lines, but it may also suggest aberrant antioxidant machinery are failing to scavenge ROS before they enter the cytosol.

Generally, all tissue types displayed similar average oxidation levels in the mitochondria, except for renal lines, which were significantly lower. Additionally, there were large discrepancies in cytosolic measurements. Melanoma and colon cell lines both showed much higher oxidation levels in the cytosol than other lines.

### III.4. Conclusion

Our results indicate several key aspects about oxidative stress. First, ROS is highly compartmentalized, with significant differences between subcellular locations. This has been highlighted by cell lines, which exhibit large differences in oxidation levels between compartments, as well as lines that go against the common trend of higher mitochondrial oxidation. This observation also correlates well with other reports regarding the spatial resolution of ROS signaling,[12,49] and indicates that ROS-modulating therapies should likely be targeted to subcellular compartments, rather than globally administered. Second, some tissue sources show significantly less oxidation than others. For example, average oxidation levels in renal lines were approximately 38% in the mitochondria, and 25% in the cytosol, significantly less than other tissues. This may, in part, explain why renal cell carcinomas are resistant to various chemotherapeutic

approaches,[53] and at face value reiterates the need for assessment of endogenous oxidative stress when choosing therapies that perturb cellular redox balance. This point is echoed by the large differences in oxidation level across all lines assessed, ranging from 15% to 99% in the mitochondria and from 7% to 86% in the cytosol. This wide variability in oxidation level may also find relevance in therapies that do not modulate ROS, as different levels of oxidation should chemically affect a wide variety of small molecule therapeutics. Finally, the variability in oxidation levels between cell lines shows clearly how heterogeneous histologically similar tumors can be, and warrants more attention to be focused on the mechanisms that tumor cells use to survive these sometimes incredibly harsh conditions, as well as the benefits they derive from existing in such states.

## III.5. References


1. Reuter, S.; Gupta, S.C.; Chaturvedi, M.M.; Aggarwal, B.B. Oxidative stress, inflammation, and cancer: How are they linked? *Free Radic. Biol. Med.* **2010**, 49 (11), 1603–1616.

2. Duracková, Z. Some current insights into oxidative stress. *Physiol. Res.* **2010**, 59 (4), 459-69.

3. Ray, P.D.; Huang, B.W.; Tsuji, Y. Reactive oxygen species (ROS) homeostasis and redox regulation in cellular signaling. *Cell Signal.* **2012**, 24 (5), 981-990.

4. Schumacker, P. Reactive Oxygen Species in Cancer: A Dance with the Devil. *Cancer Cell.* **2015**, 27 (2), 156-157.

5. Muphy, M.P.; Holmgren, A.; Larsson, N.; Halliwell, B.; Chang, C.J.; Kalyanaraman, B.; Rhee, S.G.; Thornalley, P.J.; Partridge, L.; Gems, D.; Nystrom, T.; Belousov, V.; Schumacker, P.T.; Winterbourn, C.C. Unraveling the Biological Roles of Reactive Oxygen Species. *Cell. Metab*. **2011**, 13 (4), 361-366.

6. Jabs, T. Reactive oxygen intermediates as mediators of programmed cell death in plants and animals. *Biochem. Pharma.* **1999**, 57 (3), 231-245.

7. Sena, L.A.; Chandel, N.S. Physiological Roles of Mitochondrial Reactive Oxygen Species. *Mol. Cell*, **2012**, 48 (2), 159-167.

8. Poyton, R.O.; Ball, K.A.; Castello, P.R. Mitochondrial generation of free radicals and hypoxic signalling. *Trends Endocrin. Metab.* **2009**, 20 (7), 332-340.

9. Brand, M.D. The sites and topology of mitochondrial superoxide production. *Exp. Gerontol*. **2010**, 45, 466–472.

10. Turrens, J.F. Mitochondrial formation of reactive oxygen species. *J. Physiol.* **2003**, 552 (2), 335-344.

11. Liochev, S.I.; Fridovich, I. Superoxide and iron: partners in crime. *IUBMB- Life*, **1999**, 48 (2), 157-161.

12. Mishina, N.M.; Tyurin-Kuzmin, P.A.; Markvicheva, K.N.; Vorotnikov, A.V.; Tkachuck, V.A.; Laketa, V.; Schultz, C.; Lukyanov, S.; Belousov, V.V. Does Cellular Hydrogen Peroxide Diffuse or Act Locally? *Antioxid. Redox Signal.*, **2011**, 14 (1), 1-7.

13. Bienert, G.P.; Møller, A.L.; Kristiansen, K.A.; Schulz, A.; Møller, I.M.; Schjoerring, J.K.; Jahn, T.P. Specific aquaporins facilitate the diffusion of hydrogen peroxide across membranes. *J. Biol. Chem.* **2007**, 282, 1183–1192.

14. Schumacker, P.T. Reactive oxygen species in cancer cells: live by the sword, die by the sword. *Cancer Cell*. **2006**, 10 (3), 175-176.

15. Groeger, G.; Quiney, C.; Cotter, T.G. Hydrogen Peroxide as a Cell-Survival Signaling Molecule**.** *Antioxid. Redox Signal.* **2009**, 11 (11), 2655-2671.

16. Gilgun-Sherki, Y.; Melamed, E.; Offen, D. Oxidative stress induced-neurodegenerative diseases: the need for antioxidants that penetrate the blood brain barrier. *Neuropharmacology*. **2001**, 40 (8), 959-975.

17. Fridovich, I. Superoxide radical and superoxide dismutases. *Annu. Rev. Biochem*. **1995**, 64, 97-112.

18. Borgstahl, G.E.; Parge, H.E.; Hickey, M.J.; Beyer, W.F.; Jr., Hallewell, R.A.; Tainer, J.A. The of human mitochondrial manganese superoxide dismutase reveals a novel tetrameric interface of two 4-helix bundles. *Cell*, **1992**, 71,: 107–118.

19. Okado-Matsumoto A. and Fridovich I. Subcellular distribution of superoxide dismutases (SOD) in rat liver: Cu,Zn-SOD in mitochondria. *J. Biol. Chem.* **2001**, 276, 38388–38393.

20. Folz, R.J.; Crapo, J.D. Extracellular superoxide dismutase (SOD3): tissue-specific expression, genomic characterization, and computer-assisted sequence analysis of the human EC SOD gene. *Genomics*. **1994**, 22, 162–171.

21. Hanschmann, E-M.; Godoy, J.R.; Berndt, C.; Hudemann, C.; Lillig, C.H. Thioredoxins, Glutaredoxins, and Peroxiredoxins—Molecular Mechanisms and Health Significance: from Cofactors to Antioxidants to Redox Signaling. *Antioxid. Redox Signal.* **2013**, 19 (13), 1539-1605.

22. Maiorino, M.; Scapin, M.; Ursini, F.; Biasolo, M.; Bosello, V.; Flohe L. Distinct promoters determine alternative transcription of gpx-4 into phospholipid-hydroperoxide glutathione peroxidase variants. *J. Biol. Chem.* **2003**, 278, 34286–34290.

23. Halliwell, B.; Gutteridge, J.M.C. Free Radicals in Biology and Medicine. *Oxford: Clarendon Press,* **1989**

24. Poole, L.B. Peroxiredoxin Systems: The Catalytic Mechanism of Peroxiredoxins. *Subcell. Biochem.* **2007**, 44, 61-81.

25. Hofmann, B.; Hecht, H.-J.; Flohé, L. Peroxiredoxins. *Biol. Chem.* **2002**, 383, 347–364.

26. Wood, Z.A.; Schröder, E.; Harris, J.R.; Poole, L.B.; Structure, mechanism and regulation of peroxiredoxins. *Trends Biochem. Sci.* **2003**, 28, 32–40.

27. Meister, A. Glutathione metabolism and its selective modification. *J. Biol. Chem.* **1988**, 263 (33), 17205-17208.

28. Weydert, C.J.; Cullen, J.J. Measurement of superoxide dismutase, catalase, and gluthatione peroxidase in cultured cells and tissue. *Nat. Protoc.* **2010**, 5 (1), 51-66.

29. Winterbourn, C.C.; Hampton, M.B. Thiol chemistry and specificity in redox signaling. *Free Radic. Biol. Med.* **2008**, 45 (5), 549-561.

30. Mitscher, L.A.; Telikepalli, H.; McGhee, E.; Shankel, D.M. Natural antimutagenic agents. *Mutat. Res.* **1996**, 350 (1), 142–143.

31. Owen, R.W.; Giacosa, A.; Hull, W.E.; Haubner, R.; Spiegelhalder, B.; Bartsch, H. The antioxidant/anticancer potential of phenolic compounds isolated from olive oil. *Eur. J. Cancer.* **2000**, 36 (10), 1235–1247.

32. Sala, A.; Recio, M.D.; Giner, R.M.; Manez, S.; Tournier, H.; Schinella, G.; Rios, J.L. Anti-inflammatory and antioxidant properties of *Helichrysum italicum*. *J. Pharm. Pharmacol.* **2002**, 54 (3), 365–371.

33. Uttara, B.; Singh, A.V.; Zamboni, P.; Mahajan, R.T. Oxidative Stress and Neurodegenerative Diseases: A Review of Upstream and Downstream Antioxidant Therapeutic Options. *Curr. Neuropharmacol.* **2009**, 7 (1), 65-74.

34. Harris, I.S.; Treloar, A.E.; Inoue, S.; Sasaki, M.; Gorrini, C.; Lee, K.C.; Yung, K.Y.; Brenner, D.; Knobbe-Thomsen, C.B.; Cox, M.A.; Elia, A.; Berger, T.; Cescon, D.W.; Adeoye, A.; Brüstle, A.; Molyneux, S.D.; Mason, J.M.; Li, W.Y.; Yamamoto, K.; Wakeham, A.; Berman, H.K.; Khokha, R.; Done, S.J.; Kavanagh, T.J.; Lam, C.W.; Mak, T.W. Glutathione and thioredoxin antioxidant pathways synergize to drive cancer initiation and progression. Cancer Cell. **2015**, 27 (2), 211-222.

35. Bjelakovic, G.; Nikolova, D.; Gluud, L.L.; Simonetti, R.G.; Gluud, C. Mortality in randomized trials of antioxidant supplements for primary and secondary prevention: systematic review and meta-analysis. *JAMA.* **2007**, 297 (8), 842-857.

36. Chandel, N.S. Navigating Metabolism. Cold Spring Harbor Lab. Press. **2015**.

37. Hamanaka, R.B.; Chandel, N.S. Mitochondrial reactive oxygen species regulate cellular signaling and dictate biological outcomes. *Trends Biochem. Sci.* **2010**, 35 (9), 505-513.

38. Hu, Y.; Rosen, D.G.; Zhou, Y.; Feng, L.; Yang, G.; Liu, J.; Huang, P. Mitochondrial manganese-superoxide dismutase expression in ovarian cancer: Role in cell proliferation and response to oxidative stress. *J. Biol. Chem.* **2005**, 280, 39485–39492.

39. Radisky, D.C.; Levy, D.D.; Littlepage, L.E.; Liu, H.; Nelson, C.M.; Fata, J.E.; Leake, D.; Godden, E.L.; Albertson, D.G.; Nieto, M.A.; Werb, Z.; Bissel, M.J. Rac1b and reactive oxygen species mediate MMP-3-induced EMT and genomic instability. *Nature.* **2005**, 436, 123–127.

40. Chen, Z.; Trotman, L.C.; Shaffer, D.; Lin, H.K.; Dotan, Z.A.; Niki, M.; Koutcher, J.A.; Scher, H.I.; Ludwig, T.; Gerald, W.; Cordon-Cardo, C.; Pandolfi, P.P. Crucial role of p53-dependent cellular senescence in suppression of Pten-deficient tumorigenesis. *Nature.* **2005**, 436, 725–730.

41. Klaunig, J.E.; Xu, Y.; Isenberg, J.S.; Bachowski, S.; Kolaja, K.L.; Jiang, J.; Stevenson, D.E.; Walborg, E.F. The role of oxidative stress in chemical carcinogenesis. *Environ. Health Perspect.* **1998**, 106, 289-295.

42. Cairns, R.A.; Harris, I.S.; Mak, T.W. Regulation of cancer cell metabolism. *Nat. Rev. Cancer.* **2011**, 11 (2), 85-95.

43. Young, T.W.; Mei, F.C.; Yang, G.; Thompson-Lanza, J.A.; Liu, J.; Cheng, X. Activation of antioxidant pathways in Ras-mediated oncogenic transformation of human surface ovarian epithelial cells revealed by functional proteomics and mass spectrometry. *Cancer Res.* **2004**, 64, 4577–4584.

44. Gough, D.R.; Cotter, T.G. Hydrogen peroxide: a Jekyll and Hyde signaling molecule. *Cell Death and Disease*, **2011**, 2, e213.

45. Trachootham, D.; Zhou, Y.; Zhang, H.; Demizu, Y.; Chen, Z.; Pelicano, H.; Chiao, P.J.; Achanta, G.; Arlinghaus, R.B.; Liu, J.; Huang, P. Selective killing of oncogenically transformed cells through a ROS-mediated mechanism by b-phenylethyl isothiocyanate. *Cancer Cell.* **2006**, 10 (3), 241-252.

46. Pelicano, H.; Feng, L.; Zhou, Y.; Carew, J.S.; Hileman, E.O.; Plunkett, W.; Keating, M.J.; Huang, P. Inhibition of mitochondrial respiration: A novel strategy to enhance drug-induced apoptosis in human leukemia cells by a reactive oxygen species-mediated mechanism. *J. Biol. Chem.* **2003**, 278, 37832–37839.

47. Wang, J.; Yi, J. Cancer cell killing via ROS: to increase or decrease, that is the question. *Cancer Biol. Ther.* **2008**, 7 (12), 1875-1884.

48. Sabharwal, S.S.; Schumacker, P.T. Mitochondrial ROS in cancer: initiators, amplifiers, or an Achilles' heel? *Nat. Rev. Cancer.* **2014**, 14 (11), 709-721.

49. Waypa, G.B.; Marks, J.D.; Guzy, R.; Mungpai, P.T.; Schriewer, J.; Dokic, D.; Schumacker, P.T. Hypoxia triggers subcellular compartmental redox signaling in vacular smooth muscle cells. *Circ. Res.* **2010**, 106 (3), 526-535.

50. Spasojevic, I.; Liochev, S.I.; Fridovich, I. Lucigenin: redox potential in aqueous media and redox cycling with $O_2^-$ production. *Arch. Biochem. Biophys*. **2000**, 373, 447–450.

51. Kalyanaraman, B.; Darley-Usmar, V.; Davies, K.J.A.; Dennery, P.A.; Forman, H.J.; Grisham, M.B.; Mann, G.E.; Moore, K.; Roberts, L.J.; Ischiropoulos, H. Measuring reactive oxygen and nitrogen species with fluorescent probes: challenges and limitations. *Free Radic. Biol. Med.* **2012**, 52 (1), 1-6.

52. Hanson, G.T.; Aggeler, R.; Oglesbee, D.; Cannon, M.; Capaldi, R.A.; Tsien, R.Y.; Remington, S.J. Investigating mitochondrial redox potential with redox-sensitive green fluorescent protein indicators. *J. Biol. Chem.* **2004**, 279, 13044–13053.

53. Hartmann, J.T.; Bokemeyer, C. Chemotherapy for renal cell carcinoma. *Anticancer Res.* **1999**, 19 (2C), 1541-1543.

# CHAPTER IV

# EXPERIMENTAL

*This chapter describes, in detail, the materials and experimental procedures used in the previous chapters.*

## IV.1. General

### *IV.1.1. Chemistry Notes*

All reactions were performed under positive pressure of nitrogen unless otherwise noted. Methanol (HPLC grade), ethyl acetate (ACS grade and HPLC grade), hexane (ACS grade and HPLC grade), chloroform (HPLC grade), benzene (ACS grade), toluene (ACS grade), ethanol (200 Proof ACS grade), 1,4-dioxane (ACS grade), water (HPLC grade), acetonitrile (HPLC grade) were purchased from Fisher Scientific and used without further purification. Dichloromethane was distilled from calcium hydride under positive pressure of nitrogen. Tetrahydrofuran was distilled from sodium-benzophenone under positive pressure of nitrogen. Commercially available reagents were used without further purification, unless otherwise noted. Reactions were monitored by thin layer chromatography (TLC) using Whatman pre-coated silica gel plates. Flash column chromatography was performed over ultra pure silica gel (230-400 mesh) from Silicycle. $^{1}$H NMR and $^{13}$C NMR spectra were recorded on Bruker DMX-500 and Bruker DMX-400 spectrometers using residual solvent peaks as an internal standard. Optical rotations were measured with JASCO DIP-1000 digital polarimeter, using the sodium D line. High-resolution mass spectra were recorded with Waters Q-Tof Ultima tandem quadrupole/Time-of-Flight instrument. LC/MS purification and analyses were performed using Waters LC/MS system consisting of a Waters 2545 binary gradient module, Waters 515 HPLC pump, Waters 3100 quadrupole mass spectrometer, Waters system fluidics organizer, Waters 2767 sample manager, Waters 2489 dual channel UV-Vis detector, Waters 2424 evaporative light scattering detector, and Masslynx software v4.1. An

authentic sample of streptolydigin was purchased from ChemCon GmbH (http://www.chemcon.com/).

### *IV.1.2. Biology Notes*

All cell lines were purchased from the American Type Culture Collection (ATCC) or received from Northwestern University's screening core facility, and were maintained under conditions recommended by ATCC, unless otherwise noted. All culture media were supplemented with 10% fetal bovine serum and 1% Penicillin-Streptomycin-Glutamine solution. Prior to an experiment, adherent cells were harvested by treatment with 0.25% Trypsin/EDTA solution for 2 minutes, and re-suspended in growth medium. Plated cells were incubated at 37 $^{o}$C overnight to allow adherence. All Hanks' buffered saline and phosphate buffered saline solutions contained no phenol red.

## IV.2. Experimental Procedures for Chapter I

### *IV.2.1. Synthesis of Selected Intermediates*

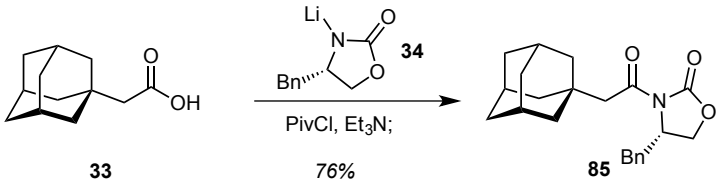


33 85

**Imide 85.** Triethyl amine (2.0 mL, 0.01435 mol) was added drop-wise to a stirred solution of 1-adamantane acetic acid (**33**) (2.2106 g, 0.01138 mol) in 80 mL of THF at -78 °C. To this solution, 1.5 mL of pivaloyl chloride was added drop-wise, and stirred at -78°C for 15 minutes. The solution was subsequently warmed to 0°C for 45 minutes and

returned to -78°C. A separate flask was charged with 3.2219 g of (4*S*)-4-benzyl-1,3-oxazolidin-2-one (**34**) (0.01818 mol) and equipped with a stir bar. Lithium Oxazolidinone **34** was dissolved in 40 mL of THF and cooled to -78°C. This solution was treated drop wise with 9.0 mL of n-butyllithium (2.59M in hexanes) and stirred for 5 minutes. This solution was added to the reaction mixture via cannula, and stirred at -78°C for 15 minutes. The solution was warmed to room temperature and stirred for 1 hour. The reaction was quenched with 82 mL of 1 M potassium bisulfate. The resulting solution was extracted three times with $Et_2O$. The combined organic extracts were washed with saturated aqueous sodium bicarbonate and brine, and dried over $Na_2SO_4$ and concentrated *in vacuo*. Purification by flash chromatography on silica gel (elution with 100% $CH_2Cl_2$) afforded 3.0354 g (76% yield) of imide **85**. $[\alpha]^{23.1}_D$ = -1.7 (c = 0.53, acetone); $^1$H NMR (500 MHz, $CDCl_3$) δ 1.70 (s, 12H), δ 1.97 (s, 3H), δ 2.69 (t, 1H, *J* = 11.65 Hz), δ 2.82 (q, 2H, *J* = 13.88 Hz), δ 3.35 (d, 1H, *J* = 13.20 Hz), δ 4.13 (s, 1H), δ 7.13 – 7.42 (m, 5H); $^{13}$C NMR (125 MHz, $CDCl_3$) δ 28.88, 34.14, 36.98, 38.34, 42.47, 47.09, 55.67, 65.96, 127.51, 129.16, 129.63, 135.71, 153.75, 171.53; HRMS (ESI) calculated for $C_{22}H_{28}NO_3$ $[M+H]^+$ 354.2069, found 354.2045.

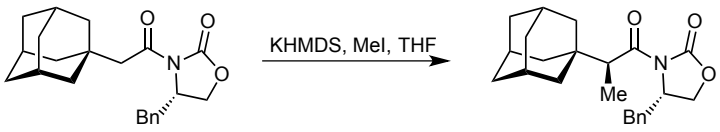


**85** *76%* **35**

**Imide 35.** A round bottom flask was charged with 17.5 mL of KHMDS solution (0.6M in toluene). The flask was equipped with a magnetic stir bar and 25.75 mL of THF was added. The resulting solution was cooled to -78°C. A separate flask was charged with

3.0354 g of imide **85** (0.00859 mol). This flask was equipped with a stir bar and 57.25 mL of THF was added. The resulting solution was cooled to -78°C and added to the KHMDS solution via cannula. After 1 hour, 1.60 mL of iodomethane (0.02576 mol) was added drop-wise to the stirred reaction mixture. The solution was warmed to room temperature, and quenched with saturated aqueous solution of $NH_4Cl$. The pH of the aqueous layer was adjusted to 2 with 1 M HCl. The resulting mixture was extracted three times with ethyl acetate. The combined organic extracts were washed with saturated aqueous $NaHCO_3$, saturated aqueous $Na_2S_2O_3$, and brine, and dried over $MgSO_4$, and concentrated *in vacuo*. Purification by flash chromatography on silica gel (elution with hexanes:ethyl acetate 9:1) afforded 2.3896 g of imide **35**. $[\alpha]^{24.9}_D$ = +40.1 (c = 5.0, acetone); $^1$H NMR (500 MHz, $CDCl_3$) δ 1.18 (d, 3H, *J* = 7.01 Hz), 1.51 – 1.85 (m, 12H), 2.01 (s, 3H), 2.79 (dd, 1H, *J* = 9.70, 13.31 Hz), 3.31 (dd, 1H, *J* = 3.12, 13.32) 3.83 (q, 1H, *J* = 6.99 Hz), 4.69 – 4.78 (m, 1H), 7.22 – 7.42 (m, 5H); $^{13}$C NMR (125 MHz, $CDCl_3$) δ 11.61, 28.93, 35.90, 37.28, 38.21, 39.67, 45.88, 55.89, 66.02, 127.63, 129.25, 129.81, 135.80, 153.81, 176.59. HRMS (ESI) calculated for $C_{23}H_{30}NO_3$ $[M+H]^+$ 368.2226, found 368.2202.

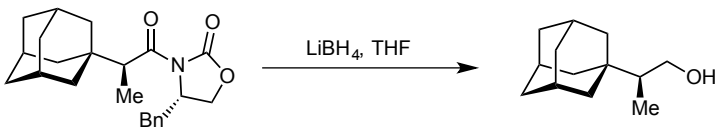


**35** *38%* **36**

**Alcohol 36.** A stirred solution of imide **35** (1.1948 g, 0.00327 mol, in 30 mL of THF) was cooled to 0°C. To this solution, 0.20 mL of MeOH was added, followed by 3.50 mL of $LiBH_4$ solution (2M in THF, 0.00700 mol). After stirring for 2 hours at 0°C, the

solution was warmed to room temperature, and stirred for an additional 4 hours. The reaction mixture was washed with 20 mL of aqueous 2M NaOH, and stirred until both phases were clear. The organic phase was separated and the aqueous layer was extracted three times with $Et_2O$. The combined organic extracts were washed with $H_2O$ and brine, dried over $Na_2SO_4$, and concentrated *in vacuo*. Purification by flash chromatography on silica gel (elution using 30% $Et_2O$ in pentanes) afforded 0.2379 g (37.5% yield) of pure alcohol **36**. $[\alpha]^{25.2}_D$ = +110.16 (c = 0.64, acetone); $^1$H NMR (500 MHz, $CDCl_3$) δ 0.91 (d, 3H, *J* = 6.9 Hz), 1.12-1.26 (m, 2H), 1.58 (ddt, 12H, *J* = 7.08, 7.08, 12.12, 32.82 Hz), 1.95 (s, 3H), 3.36 (dd, 1H, *J* = 8.46, 10.38 Hz), 3.84 (dd, 1H, *J* = 3.91, 10.42 Hz); $^{13}$C NMR (125 MHz, $CDCl_3$) δ 11.03, 28.81, 34.24, 37.43, 40.01, 46.21, 64.56; HRMS (ESI) calculated for $C_{13}H_{22}O$ $[M]^+$ 194.16707, found 194.16516.


**36** *71%* **86**

**Aldehyde 86.** A round bottom flask was charged with 0.0404 g of alcohol **36** (0.208 mmol), and equipped with a magnetic stir bar. Dichloromethane (1.0 mL) was added to the flask, and the resulting solution was cooled to 0°C. This solution was then treated with 0.1406 g of dess martin periodinane (0.3315 mmol). After 5 hours, the reaction was quenched with saturated aqueous $NaHCO_3$ solution, washed with saturated aqueous $Na_2S_2O_3$, and extracted three times with $Et_2O$. The combined organic extracts were dried over $MgSO_4$ and concentrated *in vacuo*. Purification by flash chromatography (elution with hexanes:ethyl acetate 4:1) afforded 0.0282 g (70.5% yield) of pure aldehyde **86**.

$[\alpha]^{24.7}_{D}$ = +36.86 (c = 0.64, acetone); $^{1}$H NMR (500 MHz, $CDCl_3$) δ 1.00 (d, 3H, *J* = 7.02 Hz), 1.60 – 1.78 (m, 12H), 2.01 (s, 4H), 9.82 (dd, 1H, *J* = 0.93, 3.46 Hz); $^{13}$C NMR (125 MHz, $CDCl_3$) δ 7.45, 28.40, 35.18, 36.84, 39.99, 56.21, 206.76; HRMS (ESI) calculated for $C_{13}H_{20}O$ $[M]^+$ 192.15142, found 192.15038.

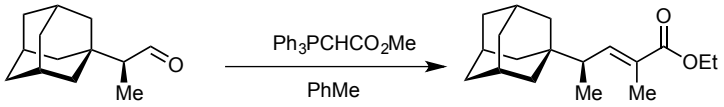


**86** *56%* **37**

**Ester 37.** (Carbethoxyethylidene)triphenylphosphorane (0.2000 g, 0.5519 mmol) was added to a stirred solution of aldehyde **86** (0.0233 g, 0.121 mmol) in toluene (1.5 mL). The flask was equipped with a water condenser, and the mixture was stirred at reflux overnight. Ice-cold $Et_2O$ was added, and the mixture was filtered. The filtrate was collected and concentrated *in vacuo*. Purification by flash chromatography (elution with 5% ethyl acetate in hexanes) afforded 0.0187 g (55.9% yield) of pure ester **37**. $[\alpha]^{24.9}_{D}$ = +23.47 (c = 0.85, acetone); $^{1}$H NMR (500 MHz, $CDCl_3$) δ 0.89 (d, 3H, *J* = 6.88 Hz), 1.30 (t, 3H, *J* = 7.12 Hz), 1.45 – 1.72 (m, 12H), 1.82 (d, 3H, *J* = 1.43 Hz), 1.95 (s, 3H), 2.13 (dd, 1H, *J* = 6.87, 10.99 Hz), 4.19 (qd, 2H, *J* = 1.04, 7.11, 7.08, 7.08 Hz), 6.73 (dd, 1H, *J* = 1.44, 10.99 Hz); $^{13}$C NMR (125 MHz, $CDCl_3$) δ 12.81, 13.13, 14.47, 28.81, 35.70, 37.36, 39.84, 43.71, 60.52, 126.95, 145.44, 168.68; HRMS (ESI) calculated for $C_{18}H_{29}O_2$ $[M+H]^+$ 277.2168, found 277.2168.

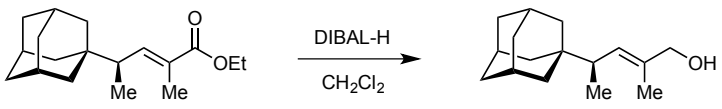


**37** *100%* **38**

**Alcohol 38.** A stirred solution of ester **37** (0.0152 g, 0.0550 mmol) in $CH_2Cl_2$ (0.55 mL) was cooled to -78°C and 0.165 mL of DIBAL solution (1 M in toluene, 0.165 mmol) was added drop wise. After stirring for 1 hour, the reaction was quenched with 0.10 mL of methanol, and stirred for 5 minutes. Then, 0.10 mL of brine solution was added, and the resulting mixture was warmed to room temperature. Sodium sulfate was added to the flask, and the solution was diluted with 3.0 mL of $Et_2O$. The resulting solution was stirred for 30 minutes, filtered, and washed with $Et_2O$. The solution was dried over $MgSO_4$ and concentrated *in vacuo* to afford 0.0128 g (quantitative yield) of alcohol **38**. $[\alpha]^{24.7}_D$ = +10.08 (c = 1.82, acetone); $^1$H NMR (500 MHz, $CDCl_3$) δ 0.84 (d, 3H, *J* = 6.78 Hz), 1.29 (s, 1H), 1.43 – 1.54 (m, 6H), 1.55 – 1.71 (m, 9H), 1.94 (s, 3H), 2.01 (dq, 1H, *J* = 10.4, 6.9 Hz), 4.02 (s, 2H), 5.33 (dd, 1H, *J* = 1.25, 10.44 Hz); $^{13}$C NMR (125 MHz, $CDCl_3$) δ 14.02, 14.19, 28.88, 35.41, 37.49, 39.78, 42.35, 69.60, 129.56, 133.84; HRMS (ESI) calculated for $C_{16}H_{26}O$ $[M]^+$ 234.19837, found 234.19706.


**38** *67%* **39**

**Aldehyde 39.** A stirred solution of alcohol **38** (0.0170 g, 0.0730 mmol) in $CH_2Cl_2$ (0.50 mL) was cooled to 0°C, and 0.0462 g of Dess-Martin periodinane (0.109 mmol) was added. After stirring for 5 hours, the reaction was quenched with the addition of saturated

aqueous $NaHCO_3$ solution and washed with saturated aqueous $Na_2S_2O3$ solution. The organic layer was separated, and the aqueous layer was extracted three times with $Et_2O$. The combined organic extracts were dried over $MgSO_4$ and concentrated *in vacuo*. Purification by flash chromatography on silica gel (elution with 10% ethyl acetate in hexanes) afforded 0.0114 g (67.2% yield) of aldehyde **39**. $[\alpha]^{25.6}_D$ = +6.17 (c = 0.34, acetone); $^1$H NMR (500 MHz, $CDCl_3$) δ 0.96 (d, 1H, *J* = 6.9 Hz), 1.45 - 1.73 (m, 1H), 1.74 (d, 3H, *J* = 1.3 Hz), 1.98 (s, 3H), 2.34 (dq, 1H, *J* = 10.9, 6.9 Hz), 6.46 (dd, 1H, *J* = 10.8, 1.3 Hz), 9.41 (s, 1H); $^{13}$C NMR (125 MHz, $CDCl_3$) δ 9.73, 13.03, 28.75, 35.84, 37.28, 39.87, 44.01, 138.56, 158.40, 195.79; HRMS (ESI) calculated for $C_{16}H_{24}ONa$ $[M+Na]^+$ 255.1725, found 255.1725

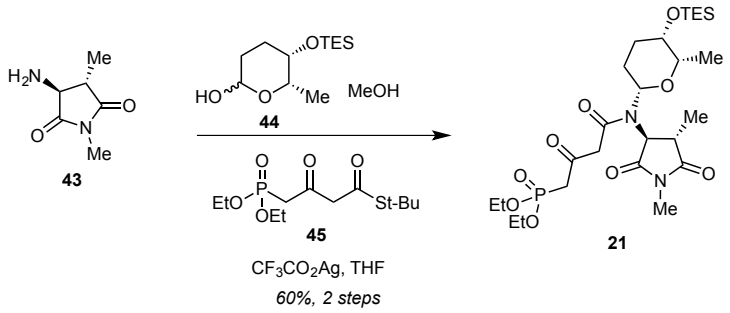


**Phosphonate 21**. Protected rhodinose **44** (0.2 g, 0.812 mmol) and amine **43** (0.115 g, 0.812 mmol) were dissolved in methanol (3 mL). The solution was left overnight and concentrated *in vacuo* to afford crude *N*-glycosyl imide. Molecular sieves (5Å, 0.8 g, activated under vacuum) were added to the solution of crude *N*-glycosyl imide and thioate **45** (0.31 g, 1 mmol) in THF (7 mL). The resulting slurry was treated with the solution of silver (I) trifluoroacetate (0.29 g, 1.3 mmol) in THF (3 mL), and the reaction was stirred for 1.5 h at room temperature. Diethyl ether was added and the resulting

suspension was washed twice with saturated aqueous solution of $NaHCO_3$. The organic layers were dried over $MgSO_4$, filtered through Celite, and concentrated *in vacuo*. Purification by flash chromatography on silica gel (elution with ethyl acetate) afforded 0.29 g (60% yield over two steps) of phosphonate **21**. $[a]^{23.0}_D$ = -36.0 (*c* = 3.0, $CHCl_3$); $^1H$ NMR (ketone and enol forms, 500 MHz, $CDCl_3$) d 0.56 (m, 6H), 0.92 (m, 9H), 1.13 (m, 3H), 1.32 (m, 9H), 1.60 (m, 1H), 1.74 (s, 1H), 1.89 (m, 1H), 2.02 (m, 1H), 2.75 (d, 1H, *J* = 22.5 Hz), 2.93 (m, 1H), 2.99 (m, 3H), 3.18 (d, 1H, *J* = 22.5 Hz), 3.52 (s, 1H), 3.60 (q, 1H, *J* = 6.0 Hz), 3.74 (dd, 2H, *J* = 20.0, 15.5 Hz), 3.85 (d, 1H, *J* = 5.5 Hz), 4.12 (m, 4H), 4.94 (dd, 0.7H, *J* = 11.0, 3.0 Hz), 5.00 (dd, 0.2H, *J* = 11.0, 3.0 Hz), 5.31 (d, 0.2H, *J* = 3.0 Hz), 13.96 (s, 0.2H); $^{13}C$ NMR (data for ketone form only, 125 MHz, $CDCl_3$) d 4.8, 6.8, 13.9, 16.19, 16.24, 17.7, 23.2, 24.9, 30.5, 40.5, 41.5, 42.5, 49.7, 59.1, 62.7, 62.8, 65.9, 75.9, 84.6, 165.8, 174.2, 178.2, 195.1; HRMS (ESI) calculated for $C_{26}H_{48}N_2O_9SiP$ $[M+H]^+$ 591.2867, found 591.2871.

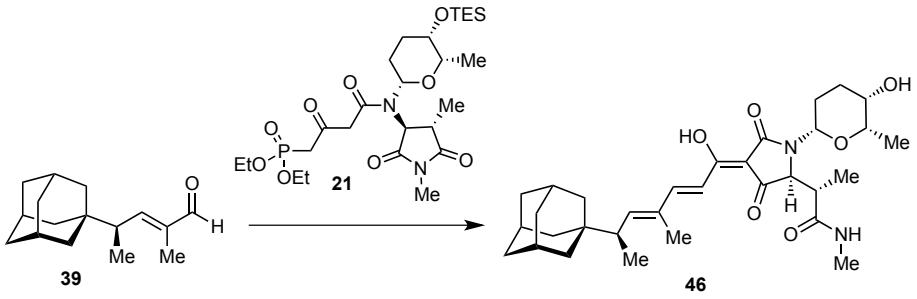


**Adamantane-Containing Tetramic Acid (46).** A stirred solution of phosphonate **21**(23.0 mg, 0.039 mmol) in THF (0.3 mL) was treated with potassium *tert*-butoxide (0.12 mL of 1 M solution in THF, 0.12 mmol) at 0 °C. The resulting solution was stirred 30 min and transferred into a solution of aldehyde **39** (6.0 mg, 0.0259 mmol)

in THF (0.1 mL) at 0 °C. The reaction was warmed to room temperature and left overnight. THF (0.4 mL) was added, and the reaction was quenched with aqueous HCl (0.15 mL of 1 M solution, 0.15 mmol, slight excess with respect to potassium *tert*-butoxide) at 0 °C. After 1 h, ethyl acetate and water were added. Phases were separated, and the organic phase was washed three times with water and once with brine, dried over $MgSO_4$, and concentrated in vacuo. Purification by flash chromatography on silica gel (chloroform, followed by the elution with chloroform:methanol 100:3) afforded 8.5 mg (59% yield) of **46**. $[\alpha]^{25}_{D} = -96.4$ ($c$ = 0.8, $CHCl_3$); $^1$H NMR (500 MHz, $CDCl_3$) δ 0.90 (d, 3H, $J$ = 7.0 Hz), 1.10 (m, 6H), 1.46 (d, 3H, $J$ = 11.5 Hz), 1.54 (d, 3H, $J$ = 11.5 Hz), 1.60 (d, 3H, $J$ = 12.0 Hz), 1.67 (d, 3H, $J$ = 12.0 Hz), 1.77 (m, 1H), 1.88 (s, 3H), 1.95 (s, 3H), 2.04 (m, 1H), 2.23 (m, 1H), 2.50 (q, 1H, $J$ = 12.0 Hz), 2.89 (d, 3H, $J$ = 4.5 Hz), 3.05 (q, 1H, $J$ = 7.0 Hz), 3.40 (s, 1H), 3.64 (m, 1H), 4.86 (s, 1H), 5.57 (d, 1H, $J$ = 11.0 Hz), 5.85 (s, 1H), 6.05 (d, 1H, $J$ = 10.5 Hz), 7.12 (d, 1H, $J$ = 15.5 Hz), 7.55 (d, 1H, $J$ = 15.5 Hz); $^{13}$C NMR (125 MHz, $CDCl_3$) δ 10.1, 12.5, 13.3, 17.2, 21.2, 26.8, 28.7, 30.2, 36.0, 37.2, 39.8, 42.1, 44.0, 62.8, 66.3, 76.5, 78.9, 99.5, 115.5, 133.6, 150.6, 151.2, 173.8, 175.1, 175.4, 193.8.

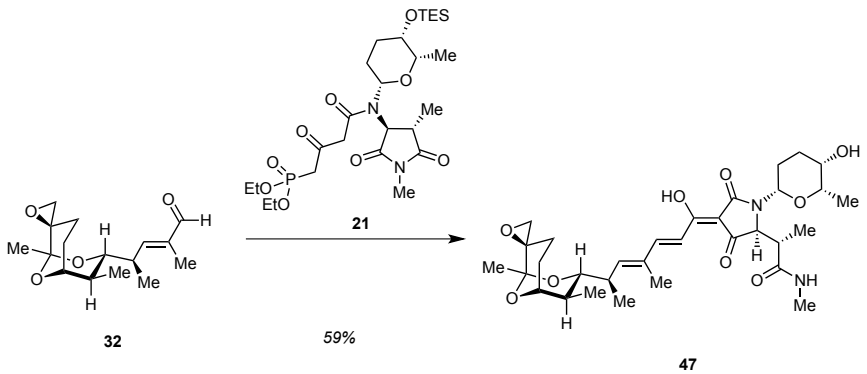

**10,11-Dihydrostreptolydigin (47).** A stirred solution of phosphonate **21**(23.6 mg, 0.04 mmol) in THF (0.3 mL) was treated with potassium *tert*-butoxide (0.12 mL of 1 M solution in THF, 0.12 mmol) at 0 °C. The resulting solution was stirred 30 min and transferred into a solution of aldehyde **32** (7.5 mg, 0.0268 mmol) in THF (0.1 mL) at 0 °C. The reaction was warmed to room temperature and left overnight. THF (0.4 mL) was added, and the reaction was quenched with aqueous HCl (0.15 mL of 1 M solution, 0.15 mmol, slight excess with respect to potassium *tert*-butoxide) at 0 °C. After 1 h, ethyl acetate and water were added. Phases were separated, and the organic phase was washed three times with water and once with brine, dried over $MgSO_4$, and concentrated in vacuo. Purification by flash chromatography on silica gel (chloroform, followed by the elution with chloroform:methanol 100:3) afforded 9.0 mg (56% yield) of 10,11-dihydrostreptolydigin (**47**). $[\alpha]^{25}_{D} = -53.3$ ($c$ = 0.9, $CHCl_3$);$^1$H NMR (500 MHz, $CDCl_3$) δ 0.76 (d, 3H, $J$ = 7.0 Hz), 1.07–1.12 (m, 9H), 1.22 (s, 3H), 1.73–1.82 (m, 4H), 1.90 (s, 3H), 1.93 (m, 1H), 2.04 (m, 1H), 2.14 (m, 1H), 2.51 (q, 1H, $J$ = 12.0 Hz), 2.64 (d, 1H, $J$ = 5.0 Hz), 2.81 (d, 1H, $J$ = 5.0 Hz), 2.84 (m, 1H), 2.89 (d, 3H, $J$ = 4.5 Hz), 3.05 (q, 1H, $J$ = 7.0 Hz), 3.40 (s, 1H), 3.65 (m, 1H), 3.82 (d, 1H, $J$ = 11.0 Hz), 3.98 (m, 1H), 4.86 (s, 1H), 5.59 (d, 1H, $J$ = 11.0 Hz), 5.85 (d, 1H, $J$ = 4.0 Hz), 6.24 (d, 1H, $J$ = 10.0 Hz), 7.15 (d, 1H, $J$ = 15.5 Hz), 7.56 (d, 1H, $J$ = 16.0 Hz); $^{13}$C NMR (125 MHz, $CDCl_3$) δ 10.1, 12.3, 12.7, 17.2, 21.0, 21.2, 22.5, 26.8, 27.2, 27.4, 30.2, 30.4, 35.1, 35.3, 42.1, 51.3, 58.5, 62.8, 66.3, 70.3, 76.5, 78.9, 98.2, 99.7, 116.1, 134.3, 146.3, 150.6, 173.7, 175.0.

### *IV.2.2. RNAP and Scaffolds*

For in vitro transcription experiments, recombinant *T. aquaticus* core RNAP was purified as described earlier.[1] To assemble a previously described[2] nucleic acid scaffold used in the Figure I.4 experiment, the following oligonucleotide strands were used: RNA (5′-GUAGCGGA-3′), template DNA (3′ CATCGCCTGTACATTTCAGACAGGACC-5′), and nontemplate DNA (5′ TGTAAAGTCTGTCCTGG-3′). To assemble a scaffold with longer transcribed part used in Figure I.5, the same RNA was combined with 3′ CATCGCCTGTACATTTCAGACAGGACCAGGTGTTGGG-5′ template DNA and 5′-TGTAAAGTCTGTCCTGGTCCACAACCC-3′ nontemplate DNA. To visualize transcription products, RNA was $^{32}$P-labeled at the 5′-end with T4 polynucleotide kinase before scaffold assembly.

### *IV.2.3. Transcription Assays*

Transcription elongation complexes were reconstituted by combining 200 nM RNAP and 50 nM nucleic acids scaffold in 10 μL of transcription buffer (25 mM Tris-HCl, 50 mM NaCl, 5 mM $MgCl_2$, 0.5 mM DTT, pH 7.9) and incubation at 37 °C for 10 min. Following the addition of streptolydigin derivatives and a 10 min incubation at 37 °C, transcription was initiated by the addition of NTPs at concentrations indicated in the figures. After a 3 min incubation at 37 °C, reactions were terminated by the addition of 1 volume of formamide loading buffer. After being heated at 100 °C for 1 min, samples were separated by 20% PAGE with 7 M Uurea, followed by PhosphorImager analysis. For single-nuceotide addition experiments, the concentration of CTP was 5 μM, and reaction incubation temperature was 25 °C.

### *IV.2.4. Bacterial Strains and Media*

*Streptococcus salivarius* Andrewes and Horder was obtained from ATCC (9758) and was grown in Bacto Tryptic Soy Broth Medium at 37 °C.

### *IV.2.5. Antibacterial Testing*

The antibiotic activity of all compounds was analyzed via disk diffusion assay. Several drops of *S. salivarius* culture were spread in a Petri dish containing Difco Tryptic Soy Agar. Paper disks of 5 mm diameter were used. Each disk was treated with a solution of each individual compound dissolved in ethanol (2–15 μL depending on the sample). Following evaporation of the ethanol, the disks were placed on top of agar. Plates were incubated at 37 °C for 24 h.

To determine MIC values for streptolydigin and related analogs, each compound was dissolved in approx. 100 mL of absolute alcohol to give a 10mg/mL solution. All microbial strains were obtained from ATCC. Compounds were added to microwell plates giving doubling final test concentrations of 64-0.125 mg/mL in 1 mL volume when culture was added. Testing was done in 24-well plates in TY broth as described by Hurdle et al.[3] Plates were incubated for 48 h before the MIC was read as the lowest concentration of antibiotic that inhibited growth.

### *IV.2.6. Quantification of Cell Viability*

To use ATP as a proxy for cell viability, cells were seeded in 96- well plates at a density of 5000 cells/well in their respective growth medium. The following day, cells

were treated with graded concentrations of small molecules and incubated for 30 minutes. The ATPlite assay kit (PerkinElmer) was used to measure ATP levels. All assays were performed in triplicate for each concentration tested.

To evaluate cell viability by dye exclusion, cells were seeded in 6 well plates and treated with small molecules. Aliquots of cell suspension were removed at various times and combined with an equal volume of Trypan Blue. Cell viability was measured using a Countess Automated Cell Counter (ThermoFischer).

## IV.3. Experimental Procedures for Chapter II

### *IV.3.1. Synthesis of Selected Intermediates*

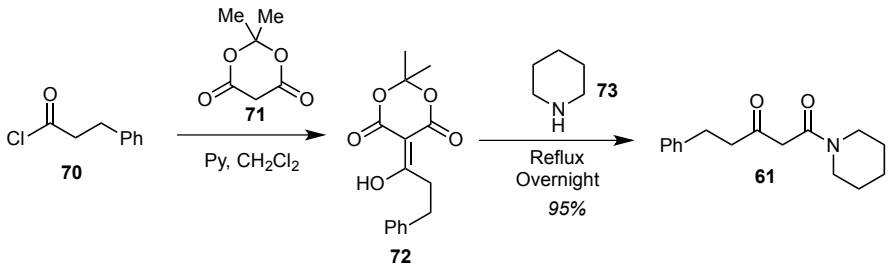


**Ketoamide 61.** A solution of Meldrum's acid **71** (1.43 g, 9.7 mmol) in $CH_2Cl_2$ (12 mL) was cooled to 0 °C, and pyridine (1.96 mL, 23.8 mmol) was added. After stirring for 15 min, 3- phenylpropanoyl chloride 283 (1.43 mL, 9.4 mmol) was added dropwise. The reaction mixture was stirred at 0 °C for 1 h followed by 2 h at room temperature. The reaction mixture was diluted with $CH_2Cl_2$ (5 mL), poured into ice-cooled aqueous HCl (2 M, 13 mL), and extracted with $CH_2Cl_2$ (2×20 mL). The combined organic layers were washed with brine, dried over MgSO4, filtered, and concentrated in vacuo to afford a

corresponding acyl Meldrum's acid **72** (2.60 g, quantitative), which was used directly in next step without further purification. To a solution of crude acyl Meldrum's acid **72** in benzene (50 mL) was added piperidine (0.79 mL, 8.0 mmol). The reaction mixture was refluxed overnight and then solvent was removed in vacuo. The crude product was purified by flash chromatography on silica gel (elution with EtOAc:hexane = 1:1) to give ketoamide **61** (1.96 g, 95%, keto:enol = 7.5:1). Major keto tautomer: $^{1}$H NMR (500 MHz, $CDCl_3$) δ 1.46-1.51 (m, 2H), 1.52-1.55 (m, 2H), 1.58-1.61 (m, 2H), 2.91 (t, 4H, J = 4.0 Hz), 3.24 (t, 2H, J = 5.5 Hz), 3.50 (s, 2H), 3.52 (t, 2H, J = 5.5 Hz), 7.16-7.22 (m, 3H), 7.25-7.29 (m, 2H); $^{13}$C NMR (125 MHz, $CDCl_3$) δ 24.3, 25.4, 26.2, 29.5, 42.9, 44.1, 47.4, 49.7, 126.1, 128.4, 128.4, 140.7, 164.6, 203.7; HRMS calculated for $C_{16}H_{22}NO_2$ 260.1651 [M+H]+ , found 260.1643.

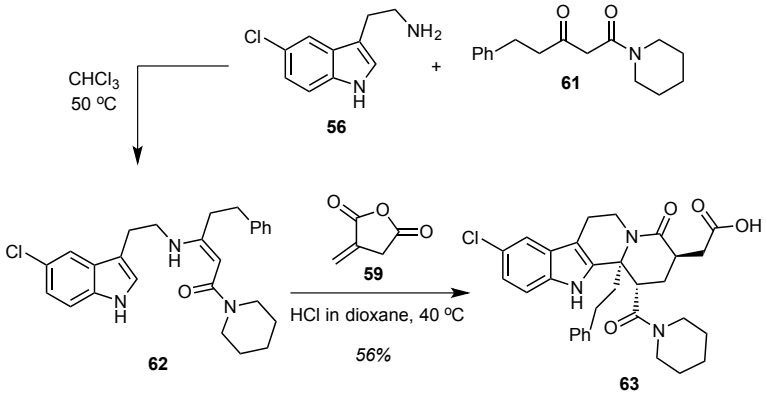


**Indoloqunolizidine 63.** To a solution of 5-chlorotryptamine (205.5 mg, 1.06 mmol) in $CHCl_3$ (4 mL) was added ketoamide **61** (273.1 mg, 1.05 mmol) and 4 Å molecular sieves (0.25 g). The reaction mixture was heated at 50 ˚C overnight, filtered and the filtrate was concentrated *in vacuo*. To a solution of crude enamide in 1,4-dioxane (4 mL) was added itaconic anhydride (114.7 mg, 1.02 mmol). The reaction mixture was heated at 40 ˚C

overnight, followed by dropwise addition of HCl (4 M in 1,4-dioxane, 0.40 mL, 1.60 mmol). Stirring was continued for 3 h at the same temperature before the solvent was removed *in vacuo*. The crude product was purified by flash chromatography on silica gel (elution with $CHCl_2$:$CHCl_3$:MeOH = 2:2:1 + 2% formic acid) to give indoloquinolizidine **63** (322.9 mg, 56%). $^1$H NMR (500 MHz, CDCl3) δ 0.28 (br s, 1H), 0.92 (br s, 1H), 1.16 (s, 1H), 1.37 (s, 1H), 1.68 (dd, 1H, J = 7.5, 5.5 Hz), 2.30 (t, 1H, J = 11.3 Hz), 2.41 (td, 1H, J = 14.0, 4.4 Hz), 2.52 (td, 1H, J = 12.6, 4.1 Hz), 2.61-2.89 (m, 7H), 2.93-3.18 (m, 6H), 3.40 (dd, 1H, J = 11.2, 7.9 Hz), 3.51-3.60 (m, 1H), 5.26 (d, 1H, J = 8.6), 7.06 (dd, 3H, J = 11.5, 4.5 Hz), 7.10 (t, 1H, J = 7.3 Hz), 7.18 (t, 2H, J = 7.5 Hz), 7.30 (d, 1H, J = 8.6 Hz), 7.45 (s, 1H), 9.67 (s, 1H), 11.45 (br s, 1H); $^{13}$C NMR (125 MHz, CDCl3) δ 20.94, 23.92, 25.38, 25.86, 27.52, 31.33, 34.58, 36.95, 37.50, 40.89, 43.86, 47.36, 48.15, 62.67, 110.80, 112.39, 117.88, 122.66, 125.31, 126.14, 127.12, 128.27, 128.50, 134.73, 134.93, 141.20, 171.31, 171.56, 176.75; HRMS calculated for $C_{31}H_{35}N_3O_4Cl$ 548.2316 $[M+H]^+$, found 548.2264.

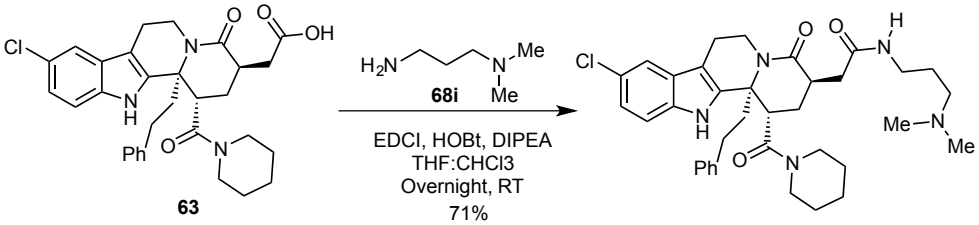


**Indoloqunolizidine 74.** To a solution of indoloquinolizidine **63** (136.5 mg, 0.249 mmol) in 1:1 THF-$CHCl_3$ (6.0 mL) was added EDCI (74.7 mg, 0.390 mmol), HOBt (60.5 mg, 0.395 mmol) and DIPEA (152 μL, 0.873 mmol). The reaction mixture was stirred

overnight at room temperature, and then solvent was removed *in vacuo*. The crude product was purified by flash chromatography on silica gel (elution with $CHCl_3$:MeOH = 9:1 + 2% $NH_4OH$) to give indoloquinolizidine **74** (115.5 mg, 71%). $^1H$ NMR (500 MHz, CDCl3) δ 0.78-0.88 (m, 1H), 1.34 (ddd, 3H *J* = 15.8, 11.8, 11.3 Hz), 1.44-1.54 (m, 2H), 1.71-1.82 (m, 2H), 1.89-1.97 (m, 1H), 2.40 (s, 7H), 2.44-2.67 (m, 6H), 2.78 (dd, 1H, J = 11.6, 4.8 Hz), 2.85-2.96 (m, 2H), 3.02-3.13 (m, 2H), 3.25 (t, 2H, J = 5.4 Hz), 3.32-3.47 (m, 5H), 3.63 (s, 1H), 5.30 (dd, 1H, J = 13.1, 3.9 Hz), 7.13-7.21 (m, 5H), 7.28 (s, 1H), 7.29 (d, 1H, J = 2.9 Hz), 7.32 (d, 1H, J = 2.3 Hz), 7.54 (d, 1H, J = 1.8 Hz), 8.92 (s, 1H); $^{13}C$ NMR (125 MHz, CDCl3) δ 20.81, 24.27, 25.65, 25.96, 26.56, 27.30, 31.54, 35.42, 37.61, 38.32, 39.35, 40.33, 43.34, 44.99, 47.37, 48.25, 57.73, 62.42, 110.66, 112.17, 117.92, 122.44, 125.20, 126.02, 127.30, 128.29, 128.44, 134.36, 135.74, 141.45, 171.45, 171.59, 171.89; HRMS calculated for $C_{36}H_{47}N_5O_3Cl$ 632.3367 $[M+H]^+$, found 632.3364.

### *IV.3.2. Quantification of Cellular ATP Levels*

Cells were seeded in 96- well plates at a density of 5000 cells/well in their respective growth medium. The following day, cells were treated with graded concentrations of small molecules and incubated for 30 minutes. The ATPlite assay kit (PerkinElmer) was used to measure ATP levels. For 2-deoxy-D-glucose pretreatment, cells were incubated in growth media containing 5 mM 2-deoxy-D-glucose for one hour prior to small molecule addition. For antimycin A pretreatment, antimycin A was added immediately before addition of small molecules. For EGTA pretreatment, cells were incubated in growth medium containing 5 mM EGTA for one hour prior to small molecule addition. All assays were performed in triplicate for each concentration tested.

### *IV.3.3. Analysis of mPT Induction*

143B.TK- cells were harvested in the same manner as indicated above. Cells were plated on 35 mm glass-bottomed dishes in growth medium at a density of 250,000 cells/dish. The next day, the growth medium was aspirated and cells were covered in Hank's buffered saline solution (HBSS) supplemented with 10 mM HEPES, containing 1.0 μM Calcein AM, 200 nM MitoTracker Red CMXRos, 2 μM Hoechst 33342, and 2 mM $CoCl_2$. Cells were incubated at 37 $^{o}$C for 15 minutes to allow for dye loading. The cells were checked by fluorescence microscopy to ensure proper dye loading and were subsequently imaged. Cells were then covered in assay buffer containing small molecules, incubated for 30 minutes at room temperature, and imaged. Cyclosporine A pretreatment was performed for one hour prior to addition of small molecules. In these experiments, cells were covered in growth medium containing 5 mM cyclosporine A, and 5 mM cyclosporine A was added to each solution for the remainder of the experiment.

### *IV.3.4. End-point Quantification of Intracellular Calcium Levels*

End-point analysis of intracellular calcium was performed using the Fluo-4 NW calcium assay kit (Molecular Probes). Molt-4 cells were harvested by low-speed centrifugation (200 x G, 5 minutes) and re-suspended in assay buffer (Hank's balanced salt solution supplemented with 20 mM HEPES). The cells were plated in 96-well plates at a density of 125,000 cells/well. Cells were incubated at 37 $^{o}$C for one hour to allow the cells to settle, and were then suspended in Fluo-4 NW dye solution supplemented with 5 mM probenecid. Cells were incubated at 37 $^{o}$C for 30 minutes and at room temperature

for 30 minutes to allow for sufficient dye loading. Fluorescence was measured immediately following the addition of graded concentrations of small molecules, and every 10 minutes for 1 hour. For experiments in which EGTA pretreatment was necessary, all assay buffer used was supplemented with 5 mM EGTA.

### *IV.3.5. Flow Cytometric Analysis of Intracellular Calcium Levels*

Molt-4 cells were harvested by low-speed centrifugation (200 x G, 5 minutes) and re-suspended in Hank's buffered saline solution (HBSS) supplemented with 10 mM HEPES at a density of 1 X $10^6$ cells/mL. Cell suspensions were treated with 3 μM Fluo-4 AM for 15 minutes at 37 $^oC$. Fluorescence intensities were measured in the FL-2 channel using a C6 Accuri Flow Cytometer. After several minutes, small molecules or $CaCl_2$ was added as a solution in assay buffer without removing the sample tube from the cytometer. In experiments performed in the absence of extracellular calcium, calcium free HBSS supplemented with 0.5 mM EGTA was used as the assay buffer. Average fluorescent intensities were determined per second, and are reported here.

### *IV.3.6. Dual Analysis of Intracellular Calcium Levels and Mitochondrial Integrity*

143B.TK- cells were harvested according to the aforementioned procedure, and plated in 35 mm glass-bottomed dishes in growth medium. Cells were incubated overnight, and the following day the medium was aspirated and the cells were covered in 10 mM HEPES supplemented HBSS buffer containing 600 nM TMRE and 3 μM Fluo-4 AM. Cells were incubated for 15 minutes at 37 $^oC$, washed twice with fresh assay buffer, and covered in assay buffer. Images were taken every 5 seconds for 15 minutes at 37 $^oC$,

and small molecules were added as solutions in assay buffer after several minutes to allow the baseline fluorescence to settle. Dishes were not removed from the microscope stage during compound addition. Fluorescence intensities were quantified using the microscope control software, SlideBook.

### *IV.3.7. Isolated Mitochondria Calcium Uptake*

A rat's liver was removed, kept on ice, and submerged in BSS buffer. The liver was cut into small pieces, rinsed several more times with BSS buffer, and transferred to mitochondrial sucrose buffer containing potassium, but no calcium. The liver pieces were homogenized, and centrifuged at 600xG. The supernatant was removed and centrifuged at 7000xG. Pellets were kept at 0 $^{o}$C until immediately before experiments were performed. 3 mL of buffer was added to a cuvette, and absorbance was measured at 540 nm. Mitochondria were diluted into the cuvette, followed by 10 µL of 0.11 M aqueous ATP solution. Test compounds were added followed by consecutive pulses of $CaCl_2$ solution, until mitochondrial integrity was lost. Experiments were performed in duplicate.

### *IV.3.8. Measurement of Calcium Mobilization by Fura-2*

Fura-2 loading solution was prepared by dissolving 50 µg of Fura-2 AM in 25 µL of DMSO, and adding 25 µL of Pluronic-F127 (20% solution in DMSO). CHO-K1 cells were plated in 35 mm dishes with glass cover slips at a density of 50,000 cells per dish in 1 mL of growth media. Cells were allowed to adhere over two days to allow cells to fully attach to the dish, and were subsequently washed with HBSS, and covered in 1 mL of HBSS containing 3 µL of the Fura-2 loading solution (3 µM Fura-2 AM) for 30 minutes

at 37 $^{o}$C. Pre-treatment compounds were added 15 minutes before test compounds, and the ratio of fluorescence intensities at 340 nm and 380 nm were measured by an Olympus IX81 inverted fluorescence microscope.

## IV.4. Experimental Procedures for Chapter III

### *IV.4.1. RoGFP Sensors*

The RoGFP protein contains two engineered cysteine thiols, as first described by Remington et al (RoGFP2).[4] The cDNA encoding the protein was created by introducing four mutations in the mammalian GFP expression vector (pEGFP-N1) (C48S, Q80R, S147C, and Q204C) using a QuikChange Multi Site-directed mutagenesis kit (Strategene). The RoGFP construct was ligated into the VQ Ad5CMV K-NpA adenoviral shuttle vector between the *KpnI* and *NotI* sites; after sequencing and amplification, this plasmid was used to generate a recombinant adenovirus to permit widespread expression in our cells (ViraQuest Inc, North Liberty, Iowa). The resulting redox-sensitive protein has excitation maxima at 400 and 484 nm, with emission at 525 nm. In response to changes in redox conditions, RoGFP exhibits reciprocal changes in intensity at the two excitation maxima,[5] and its ratiometric characteristics render it insensitive to expression levels.[6-8] Although the fluorescence behavior of RoGFP is relatively independent of pH and it does not respond to authentic NO, reduced NADH, or the antioxidant N-acetyl-L-cysteine, its spectrum is slightly affected by reduced glutathione possibly attributable to thiol-disulfide exchange.

RoGFP was expressed in the mitochondrial matrix (Mito-RoGFP) by appending a 48-bp region encoding the mitochondrial targeting sequence from cytochrome oxidase subunit IV, at the 5′ end of the coding sequence. This construct was then ligated into the VQ Ad5CMV K-NpA plasmid between the *KpnI* and *NotI* sites, and used to generate an adenoviral vector.

### *IV.4.2. Measurement of Endogenous Oxidation Level*

Cell lines were maintained according to general procedures described above. Cells were harvested and plated in 96-well plates at a density of 25,000 cells per well in 100 μL of culture media, and allowed to attach overnight at 37 $^{o}$C. The following day, cells were covered in 100 μL of fresh media containing 2 μL of viral stock solution (200 PFU/well; either Mito-RoGFP or Cyto-RoGFP) and incubated for an additional 24 hours. Cells were then washed twice with HBSS, and fluorescence was measured at the excitation wavelengths 400 nm and 485 nm, using the emission wavelength of 525 nm in both cases. Cells were then covered in HBSS containing 5 mM of DTT or 5 mM $^{t}$Bu-hydroperoxide for 15 minutes, and fluorescence was measured again. Percent oxidation levels were calculated from the ratio of fluorescence intensities at both excitation wavelengths.

**IV.5: References**


1) Kuznedelov, K.; Minakhin, L.; Severinov, K. Preparation and characterization of recombinant Thermus aquaticus RNA polymerase. *Methods Enzymol.* **2003**, 370, 94-108.

2) Korzheva, N.; Mustaev, A.; Kozlov, M.; Malhotra, A.; Nikiforov, V.; Goldfarb, A.; Darst, S.A. A structural model of transcription elongation. *Science*, **2000**, 289 (5479), 619-625.

3) Hurdle, J.G.; Heathcott, A.E.; Yang, L.; Yan, B.; Lee, R.E. Reutericyclin and related analogues kill stationary phase Clostridium difficile at achievable colonic concentrations. *J. Antimicrob. Chemother.* **2011**, 66 (8), 1773-1776.

4) Dooley, C.T.; Dore, T.M.; Hanson, G.T.; Jackson, W.C.; Remington, S.J.; Tsien, R.Y. Imaging dynamic redox changes in mammalian cells with green fluorescent protein indicators. *J. Biol. Chem.* **2004**, 279, 22284–22293.

5) Hanson, G.T.; Aggeler, R.; Oglesbee, D.; Cannon, M.; Capaldi, R.A.; Tsien, R.Y.; Remington, S.J. Investigating mitochondrial redox potential with redox-sensitive green fluorescent protein indicators. *J. Biol. Chem.* **2004**, 279, 13044–13053.

6) Cannon, M.B.; James Remington, S. Redox-sensitive green fluorescent protein: probes for dynamic intracellular redox responses. A review. *Methods Mol. Biol.* **2009**; 476, 50–64.

7) Lohman, J.R.; Remington, S.J. Development of a family of redox-sensitive green fluorescent protein indicators for use in relatively oxidizing subcellular environments. *Biochemistry*. **2008**, 47, 8678–8688.

8) Jiang, K.; Schwarzer, C.; Lally, E.; Zhang, S.; Ruzin, S.; Machen, T.; Remington, S.J.; Feldman, L. Expression and characterization of a redox-sensing green fluorescent protein (reduction-oxidation-sensitive green fluorescent protein) in Arabidopsis. *Plant Physiol.* **2006**. 141, 397–403.